DOCTORAL DISSERTATION

Development of Photoinitiated Polymer Conjugation Reactions based on [2+2] Cycloadditions of Functionalized Polymers

Doctoral dissertation submitted to obtain the degree of doctor of Science: Chemistry, to be defended by:

Matthias H. Conradi

Promoter: Prof. Dr Thomas Junkers
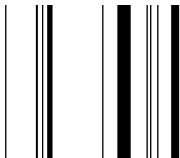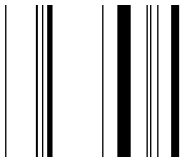
Chairman	Prof. Dr. Karin Coninx, UHasselt
Promoter	Prof. Dr. Thomas Junkers, UHasselt
Members of the jury	Prof. Dr. Dirk Vanderzande, UHasselt
	Dr. Anitha Ethirajan, UHasselt
	Prof. Dr. Hans Heuts, UAntwerpen & TU/e
	Prof. Dr. Christophe Detrembleur, ULg

Table of contents

Chapter 1

1. General introduction

1.1 From a definition to a new concept

Since the first discovery and demonstration of the existence of polymers by H. Staudinger in the early 20th century many important discoveries have been made in the field of macromolecular chemistry.[1] Based on his work it was discovered that rubber and other polymeric substances e.g. starch, cellulose and polystyrene are long chains of short molecular repeating units linked by covalent bonds (**Fig. 1.1**). By this proposal a modern definition of macromolecules was established.

(1)

(2)
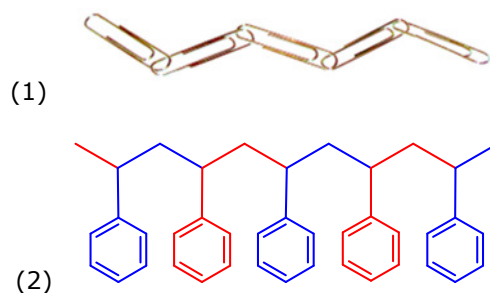
Fig. 1.1: (1): The linked paper clips are a simplified model of a polymer based on the definition by Staudinger. (2): An artificial polymer consisting of styrene units linked together in a head-to-tail fashion.

1.1.1 Architecture, dictator of physical properties
The architecture of a polymer influences its physical properties. The composition can control the e.g. melting point, solubility and critical solution temperatures. A well-known everyday example to illustrate the impact of the topology (i.e. branching, network) is starch. This highly branched natural polymer can incorporate huge amounts of water and increase its viscosity to yield a tasty pudding.

A common plastic bag and a climbing rope are commercial examples on how architecture can influences the physical properties of two materials made of the same monomer units, ethylene. Ordinary plastic bags are made of low-density polyethylene (LD-PE) while climbing ropes and also bullet-proof vests are high performance materials which are made of ultra-high-molecular-weight polyethylene (UHMW-PE, Dyneema[®]).[2,3] The high performance materials are

made via a controlled process (coordination polymerization)[4,5] yielding a very low degree of branching and ultra-high M_w which improves the physical properties such as e.g. tensile and impact strength completely.

Composition

homopolymer   statistical

block coploymer   periodic   gradient

Topology

linear

cyclic   star   graft   network   hyperbranched

Functionality

macromonomer   end functional

multifunctional   side functional   telechelic
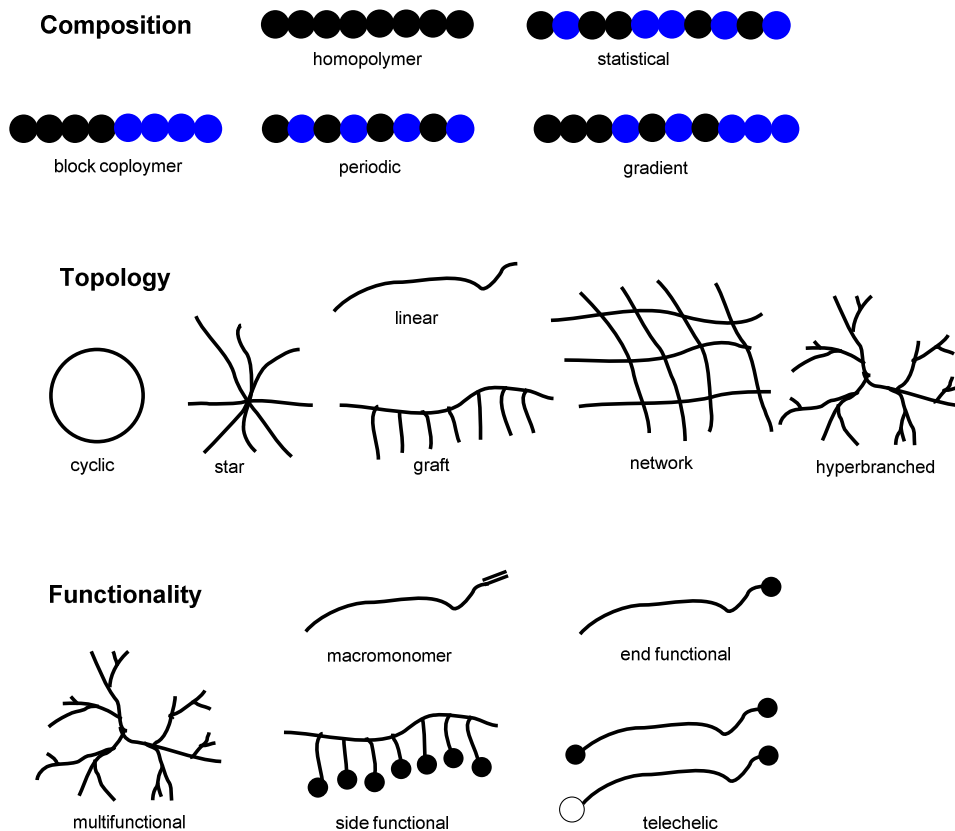
Fig. 1.2: Overview of the three main aspects of polymer architecture: Composition, topology and functionality.

1.1.2 Free radical polymerization

Polymers are an essential piece of our life. There are amounts of polymer-based materials with an unimaginably broad application range. It starts in the morning while brushing your teeth with a toothbrush, continues at your wardrobe which contains a water-repellent jacket made of a polymer coating and ends in your cozy well isolated house. A large quantity of these materials is made by radical polymerization of bulk polymers, e.g. polystyrene (PS), low-density polyethylene (LD-PE) and Plexiglas® (PMMA).[6]

Since Staudinger's definition, many different modes performing free radical polymerization (FRP) were invented, e.g. bulk polymerization,[7] solution polymerization,[7] suspension polymerization[8,9] and (mini-/micro-)emulsion polymerization.[10] FRP methods consist in essence of three different steps: initiation, propagation and termination (**Fig. 1.3**).[7,11] In practice, transfer reactions are not negligible.

Initiation:

$$\text{initiator} \longrightarrow 2\ \overset{\bullet}{I} \xrightarrow{\quad M \quad} 2\ I{-}\overset{\bullet}{M}$$

Propagation:

$$I{-}\overset{\bullet}{P_n} \xrightarrow{\quad M \quad} I{-}\overset{\bullet}{P_{n+1}}$$

Termination:

by disproportionation

$$I{-}\overset{\bullet}{P_n}\ +\ \overset{\bullet}{P_m}{-}I \longrightarrow I{-}P_n{-}H\ +\ I{-}\overset{=}{P_m}$$

by combination

$$I{-}\overset{\bullet}{P_n}\ +\ \overset{\bullet}{P_m}{-}I \longrightarrow I{-}P_{n+m}{-}I$$
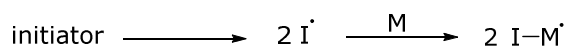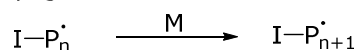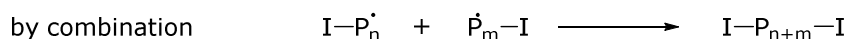
Fig. 1.3: General mechanism of a free radical polymerization

First the initiator is cleaved homolytically, generating two radicals. These initiating radicals add to a monomer. The initiator-monomer radicals can grow by adding more and more monomer units, this process is called propagation. The chains are growing over time quickly. Already at very low conversions are high molecular masses are obtained. FRP belong by definition to the chain-growth polymerization in contrast to step-growth polymerization, which yield high molecular masses at high conversions (see **Fig. 1.4**). By definition a chain-growth polymerization is a polymerization where unsaturated monomers add to the active growing site of a polymer chain one after the other.[12] The average lifetime of a growing radical is usually around one second. Termination occurs in two ways. Either via disproportionation yielding two polymeric chains: one saturated and the other unsaturated or via combination yielding one polymeric chain with the molecular mass equal to the sum of both.[13]
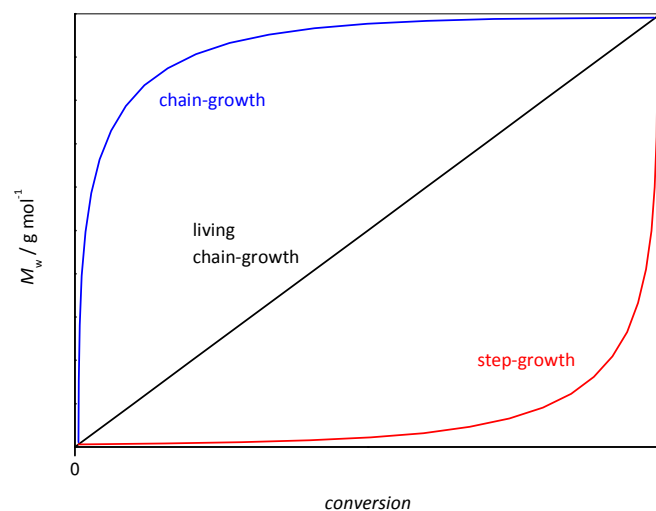
Fig. 1.4: Differences between the three polymerization growth rates.

1.1.3 Controlled radical polymerizations

Within the last 100 years, many inventions have been achieved in the field of macromolecular chemistry. Among those, the invention and development of controlled radical polymerization (CRP) is considered one of the most important breakthroughs in modern techniques. Before the mid 90's, all radical polymerizations were performed in an uncontrolled way, providing only a very limited or even no control over chain length, molecular architecture and end groups. Therefore, more complex polymeric architectures and advanced material properties were inaccessible until the advent of CRP.

The most known CRP methods are nitroxide mediated radical polymerization (NMP)[14], reversible addition-fragmentation chain-transfer polymerization (RAFT)[15] and atom-transfer radical polymerization (ATRP)[16,17]. These types of radical polymerizations are similar in that the control is gained due to the decrease in free radical concentrations, resulting in an overall absence of termination reactions. ATRP and RAFT will be explained in detail because they were applied within this research work.

An example for a standard ATRP is shown in **Fig. 1.5** using a copper(I) halogenate/ ligand-system. This system is characterized by a few main criteria. The ligand is needed to dissolve the copper salt in an organic solvent and to tune the reactivity of the complex. The initiator (R-Br) and the copper(I) bromide-complex react which each other. They form an oxidized copper(II) bromide-species and yield a radical initiator molecule. This radical then can add to a monomer. The deactivation rate r_{deact} is much larger than the activation rate r_{act}, yielding an equilibrium between dormant/ active species and Cu^+/Cu^{2+}. The equilibrium lies on the side of the dormant state. Due to this effect the lifetime of active radicals is very short, often only allowing for addition of a single monomer unit or less before deactivation takes place.[18,19]

General kinetics: $r_{deact} > r_{act} >> r_t$

R-Br + [Cu(I)Br]L $\underset{k_{deact}}{\overset{k_{act}}{\rightleftharpoons}}$ R· k_p + [Cu(II)Br$_2$]L
+ M
k_t
R-Cu(I)Br
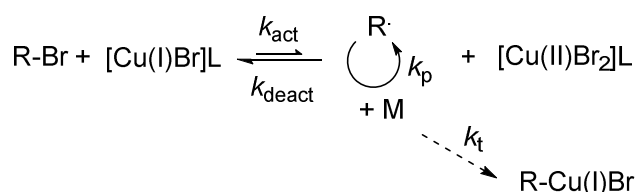
Fig. 1.5: General mechanism of ATRP. On the left-hand side of the reaction scheme is the dormant species and on the right-hand side is the active species.

Another often used CRP technique is RAFT. The example used to explain the RAFT mechanism employs a dithioester as a chain transfer agent (**Fig. 1.6**). In the first step the initiator decomposes to yield free radicals. These radicals add to monomer units forming macroradicals $P_m^\bullet$ (**Fig. 1.6** (I)). In the pre-equilibrium a macroradical adds to the transfer agent. The formed species can continue in two pathways. Both ways proceed via a β–scission; either it undergoes a back reaction or releasing the R-group as a radical (**Fig. 1.6** (II)). Radical $R^\bullet$ can reinitiate by adding new monomer forming a new macroradical $P_n^\bullet$. This leads to the main equilibrium between the propagating chains $P_m^\bullet$ and $P_n^\bullet$. If one propagating chain adds to the transfer agent, β-scission between the carbon and the sulfur atom of the formed intermediate to either side may occur (**Fig. 1.6** (IV)). In this fashion, the propagation probability is equally distributed over all chains and an equilibrium between active and dormant chains is established.

Initiation:

(1)   initiator $\longrightarrow$ 2 I$^\bullet$ $\xrightarrow{M}$ P$_m^\bullet$

Pre-equilibrium:

(2)   P$_m^\bullet$ + [S=C(Z)–S–R] $\underset{k_{\beta,1}}{\overset{k_{ad,1}}{\rightleftharpoons}}$ P$_m$–S–C(Z)$^\bullet$–S–R $\underset{k_{ad,1}}{\overset{k_{\beta,1}}{\rightleftharpoons}}$ P$_m$–S–C(Z)=S + R$^\bullet$

Re-initiation:

(3)   R$^\bullet$ + M $\longrightarrow$ P$_n^\bullet$

Main equilibrium:

(4)   P$_m^\bullet$ + [S=C(Z)–S–P$_n$] $\underset{k_\beta}{\overset{k_{ad}}{\rightleftharpoons}}$ P$_m$–S–C(Z)$^\bullet$–S–P$_n$ $\underset{k_{ad}}{\overset{k_\beta}{\rightleftharpoons}}$ P$_m$–S–C(Z)=S + P$_m^\bullet$
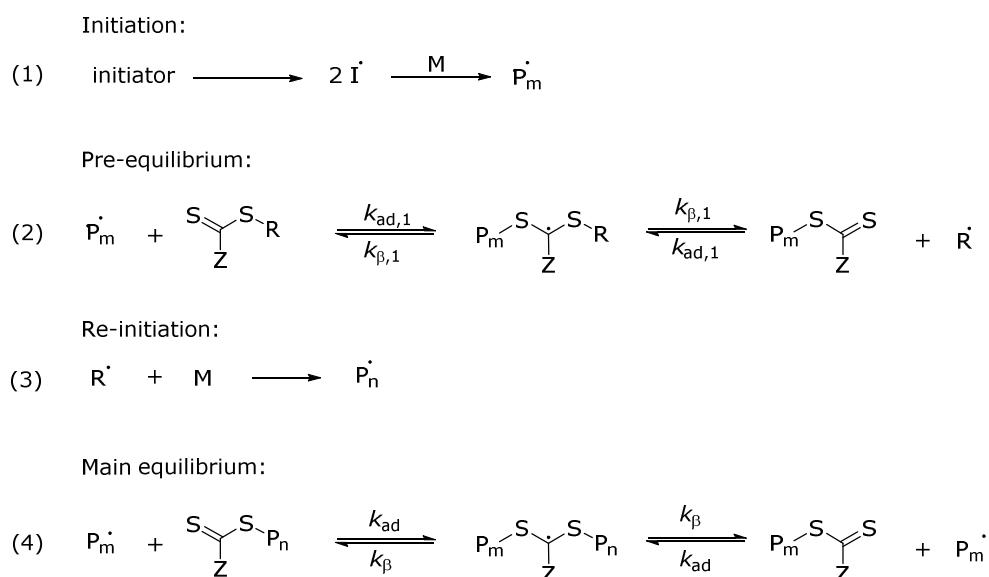
Fig. 1.6: General mechanism of a RAFT polymerization. (1) shows the decomposition of the initiator and formation of radicals. (2) displays the pre-equilibrium. (3) depicts the re-initiation of a second growing chain and (4) displays the main equilibrium which leads to the polymer chain propagation.

In theory, a termination does not play a significant role in CRP ($r_{deact} > r_{act} \gg r_t$), as long as there is monomer it will be added to the active species. When the polymerizations are stopped, the polymer will be present in the dormant form. Later, the polymer can be "fed"' with new monomer and the chain propagation continues when activated. Therefore, CRP methods are also known under the term of living radical polymerization (LRP);[20] even though the term "living" is discouraged to be used. The IUPAC recommended term is reversible-deactivation radical polymerization (RDRP).[20]

1.1.4 Advantages and application of controlled polymers
CRP enables the control of the three main aspects of polymer architecture: Composition, topology and functionality (**Fig. 1.2**). CRP allows creating block-copolymers in the same reaction vessel via adding the second monomer after conversion of the first. It is also possible to synthesize polymeric chains with well-defined end group fidelity, which can later be used, for example as anchor points for surface modification or for labeling of proteins.[21] The topology can be

varied, starting at a star-shaped polymers[22] and ending at a complex structure like (drug-releasing) networks[23], dendrimers[24] or self-assembly systems.[25]

1.2 Concept of *click* chemistry

A further paradigm shift in polymer chemistry occurred in 2001 with the introduction of the *click* concept by Sharpless *et al*.[26] These authors proposed that organic chemists should focus on highly efficient and easy performable reactions, like copper-azide-alkyne cycloaddition (CuAAC, **Fig. 1.7**) or Diels-Alder cycloadditions. The CuAAC is a 1,3-dipolar cycloaddition between an azide and a terminal or internal alkyne to yield a 1,2,3-triazole.[27,28]
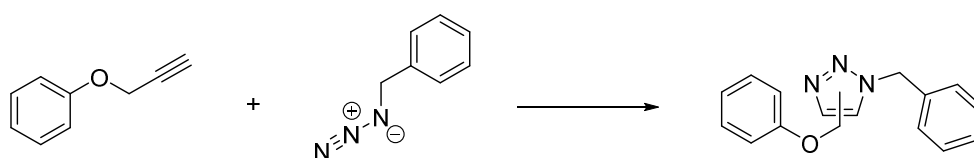
Fig. 1.7: Copper-azide-alkyne cycloaddition, the model case for a *click* reaction as proposed by Sharpless *et al*.[29]

Click chemistry is by definition a rule-set for chemical reactions. It was defined that reactions must be simple, easy to perform, being "springloaded" for a single reactions trajectory (meaning that only one reaction pathway may exist) and that a sufficiently large driving force brings the reaction to high yields within reasonable reaction times. Sharpless proposed these reactions to be called *click* reactions, because they perform so well and simple like putting two LEGO® bricks together (**Fig. 1.8**). There are many high potential reactions whhich applicability is not yet explored entirely.

In polymer chemistry there is a need for reactions with complete conversion at equimolar ratios and simple purification because there is a lack of efficient, simple and cheap purification methods for polymers. Polymers cannot be distilled or separated in an economical way via column chromatography. Reactions between polymers or the modification of them has to fulfill slightly different criteria than published by Sharpless and co-workers. Therefore, the concept of *click* chemistry was adapted to polymer systems in 2011 by Barner-Kowollik *et al*.[30,31]
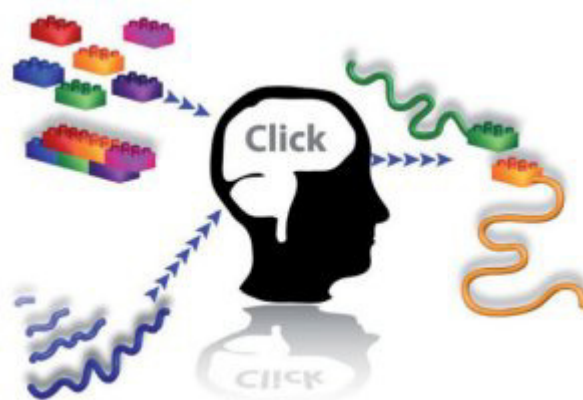
Fig. 1.8: Schematic overview of the *click* chemistry concept. Figure taken from Barner-Kowollik *et al*. 2009.[30]

The general idea behind the *click* concept is to overcome the sequential design of compounds. In a sequential approach one step after the other is done: Out of A follows B and then C, and so on. Several chemical steps have to be done to receive the desired product. By working in a modular approach all chemical points of interest e.g. functional groups are combined and can be tested. This allows a high through-put screening due to improved accessibility of target molecules. The linker between these points of interests is an easily performable reaction which does not need further purification.

The concept of building blocks is beneficial for the synthesis of more complex polymeric architecture and block-copolymers. As described above, the polymer architecture plays a significant part for the material properties and opens the door to advanced materials for the future. Using these reactions it is possible to prepare H-shaped polymers,[32] polymer brushes,[33] surface patterning[34] and particle grafting in a fast and non-elaborate manner. *Click* reactions, considered in polymer chemistry, are CuAAC,[33] RAFT-hetero Diels-Alder (RAFT-HDA),[35] ortho-quinodimethanes[36] and in circumstances thiol-ene.[37]

1.3 Photochemistry and photoreactions

1.3.1 General theoretical background and attributes

The previously mentioned reactions share the need for heat activation. A known exception is the radical thiol-ene reaction in which some concepts use UV-light to form a reactive intermediate that can subsequently lead in conventional *click* reaction.

Photochemical reactions have to be photo-induced to circumvent forbidden π/π -interactions.[38,39] The electronical configuration needed for cycloaddition, is described by the Woodward-Hoffmann rules for pericyclic reactions. The Woodward–Hoffmann rules predict the barrier heights of pericyclic reactions with the requirement of conserved orbital symmetry is. "Allowed" means low energy barrier while "forbidden" means high energy barrier.[40–42] An example based on a [2+2] photo-induced cycloaddition is given in **Fig. 1.9**. A cycloaddition between an aldehyde, in the ground state, and an ethylene molecule cannot happen due to the phase mismatch (**Fig. 1.9** (1)). A photon excites one electron of the aldehyde into a lowest occupied molecular orbital (LUMO, **Fig. 1.9** (2)). The now formed S_1 state's frontier molecular orbitals (FMO) match up and the reaction orbital symmetry is allowed, forming a four-membered ring. Furthermore, the S_1 state can change into a triplet state (T_1) which changes the reaction mechanism but not the event itself.
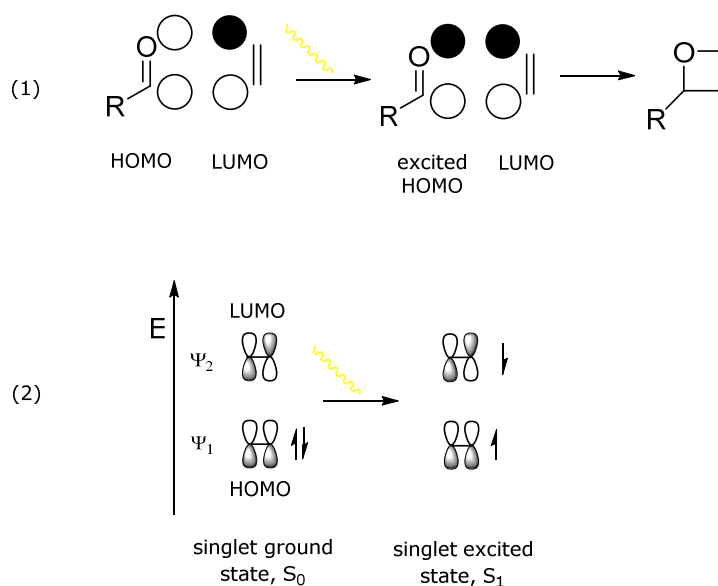
Fig. 1.9: (1) The frontiers orbital mismatch is overcome by a photon excitation yielding a four-membered heterocycle, an oxetane. (2) The energy diagram shows the FMO of the aldehyde compound being excited by a photon and changing to a singlet excited state S_1.

As mentioned before UV-induced reactions are characterized by a phase mismatch of the FMOs at ground state. One electron has to be excited via a photon changing the ground state ($S_{0)}$ to a singlet excited state (S_1), **Fig. 1.10**. This S_1 state can undergo a cycloaddition in a concerted mechanism. The S_1 state is described by two unpaired electrons at different energy levels and spins. Later via vibrational relaxation the system can lose energy (fluorescence) to reach the ground state again. Next to the S_1 state exists a triplet state (T_1), too. It consists of two unpaired electrons at different energy levels with the same spin (**Fig. 1.10**).
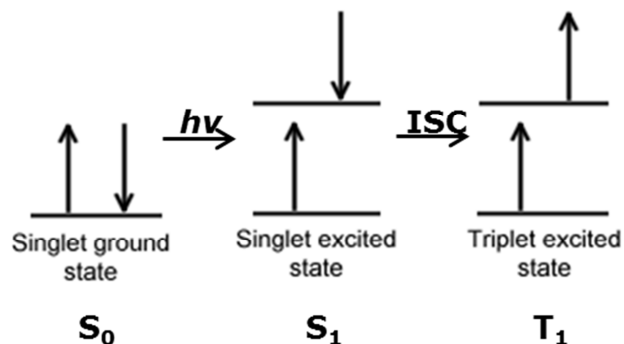
Fig. 1.10: The excitation of a ground state (S_0) of a frontier molecular orbital. First a singlet excited state is formed (S_1). Later a triplet state (T_1) is formed via inter system crossing (ISC). Modified picture taken from Wikipedia.[43]

If the vibrational levels between the S_1 and T_1 are overlapping at a certain energy level the electron can shift its spin yielding a triplet state. This process is called intersystem crossing (ISC)[44], **Fig. 1.11**. The T_1 state can dissipate energy by vibrational relaxation (phosphorescence).
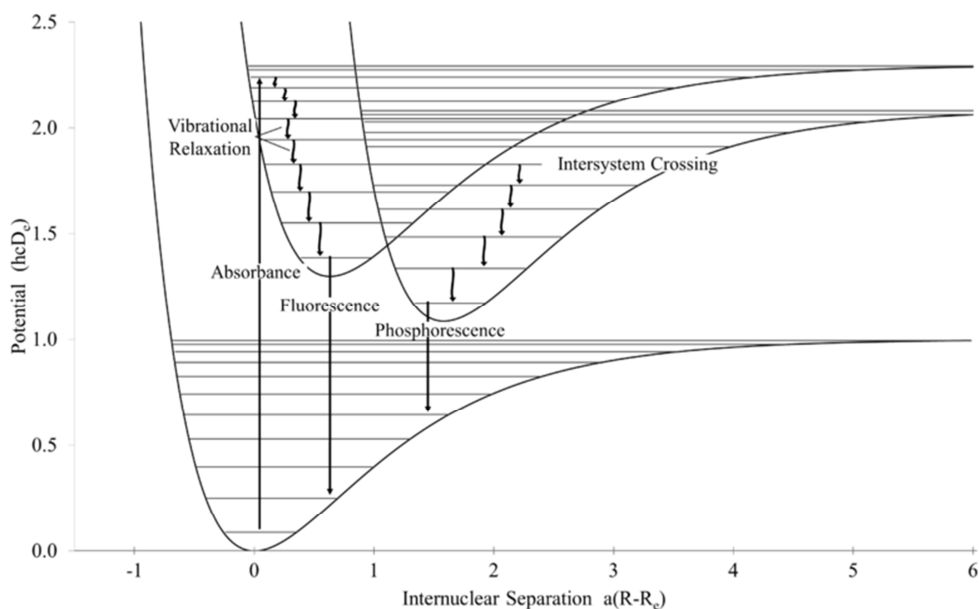
Fig. 1.11: An excited electron can change the state of a singlet excited state to a triplet excited state due to inter system crossing (ISC). Picture taken from Wikipedia.[43]

The T_1 state, also a biradical intermediate, can yield a cycloadduct via a radical mechanism. For a [2+2] photochemical cycloaddition the radical mechanism follows a less strict control of regiochemistry, if there are no bulky groups (e.g. tert. butyl) or other interactions (e.g. hydrogen bonds).[45–48]

The main focus of this thesis is therefore the investigation of truly UV-activated conjugation reactions. [2+2] Cycloadditions are suitable candidates for reaching this goal. Particularly advantageous of photo cycloadditions is the true orthogonality towards "classical" heat-induced reactions. [2+2] Additions can be independently triggered and thus conjugation of different substrates can be achieved in a controlled manner by switching from thermal activation of functional groups to photo-irradiation (**Fig. 1.12**). This is of interest for example, in nanoparticles or in surface modification reactions on natural substrates. Expanding the chemist's toolbox by a light-induced reaction will give the opportunity of truly orthogonal modifications.[49]
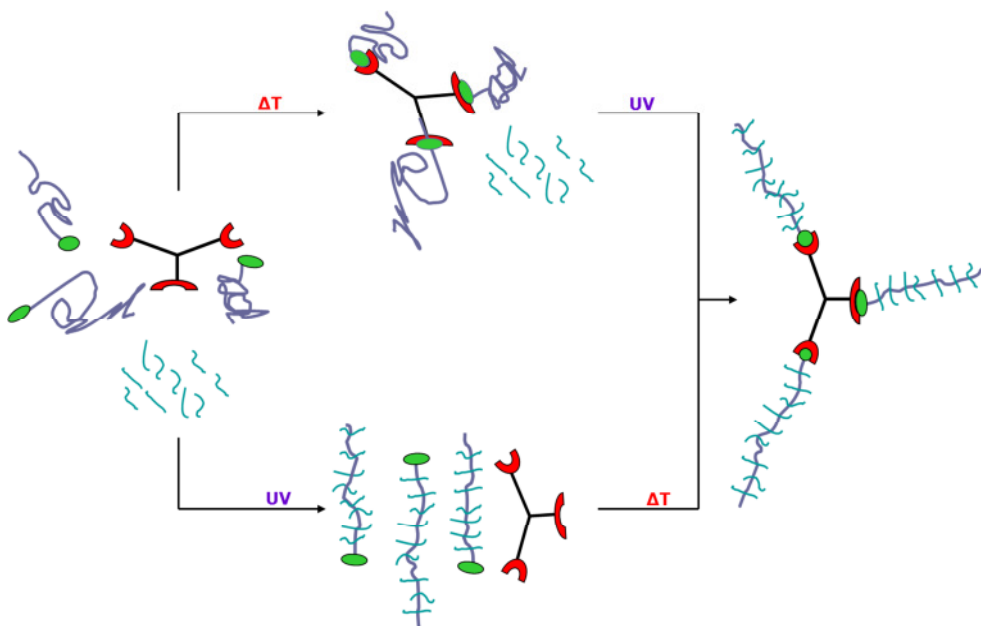
Fig. 1.12: Schematic overview of UV/thermally-orthogonal polymer modification

The cycloaddition's efficiency can further be optimized by several factors:

- The efficiency to excite an electron (light efficiency) can be addressed by different UV-reactor setups.[50,51]
- The right choice of interacting molecules due to the energy difference between HOMO/LUMO-levels.
- The use of photocatalysts[52] which can work as chromophor or a photosensitizer.[53,54]
- Setup of the reaction vessels and light sources

By now, there are several [2+2] photoinduced cycloadditions known (**Fig. 1.13**). In a photoreaction, one electron has to be excited so that the reaction is "allowed" according Woodward-Hoffmann rules. This first step, activation, can be seen as the bottle neck for the following. As depicted in **Fig. 1.13** (1) all the molecules can be activated via UV-light. The needed quencher for completing the cycloaddition is also the same molecule, therefore it is not excluded that a homo-cycloaddition can occur. But one of the required criteria for a stable conjugation reaction is the formation of a homo cycloadduct is neglected. Otherwise, it is not guaranteed that two different molecules react with each other, leading to photo-dimerizations.[55] **Fig. 1.13** (1) displays common photo-induced reactions which are disqualified due to their possible photo-dimerization reaction. Suitable reactions are depicted in **Fig. 1.13** (2), for instance the Paternò-Büchi reaction.[56–58] It is a [2+2] cycloaddition between an aldehyde and an alkene. The needed functionalities are favorable because aldehyde terminated polymers are accessible.[59] Another suitable reaction is an alkene-enone reaction.[52,60]

(1): excited molecule = quencher

2 cinnamate $\xrightarrow{h\nu}$

2 coumarin $\xrightarrow{h\nu}$

2 vinyl $\xrightarrow{h\nu}$

2 maleimde $\xrightarrow{h\nu}$

2 anthracene $\xrightarrow{h\nu}$
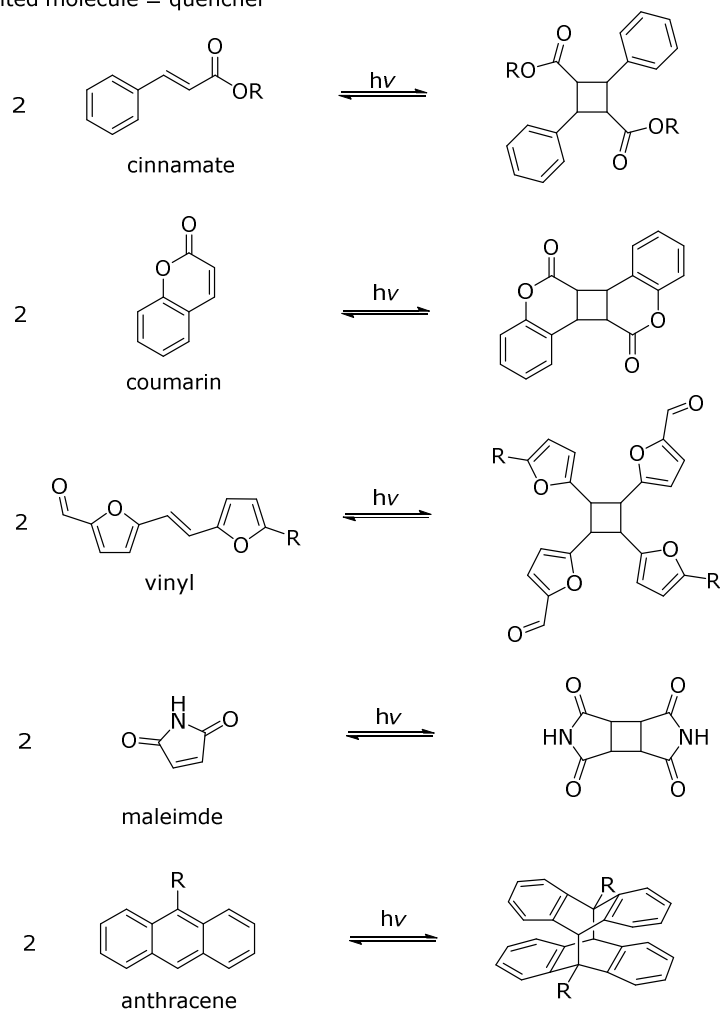
(2): excited molecule ≠ quencher

$\xrightarrow{h\nu}$

$\xrightarrow{h\nu}$
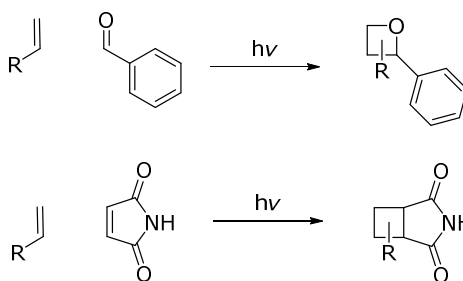
Fig. 1.13: Common photo-reaction separated into photo-dimerizations (1) and hetero photoadditions (2).

1.3.2 Recent progress in the field of polymer conjugation via photochemistry

Up to now, only few research groups deal with photochemical reactions mainly focusing within the field of natural products,[48] thus entailing are regio-and stereospecific control.[51,61–63] Although many of these reactions share the slow reaction kinetics (several days to completion). The group of Booker-Milburn developed 2005 a new reactor concept.[50] They changed the setup from a conventional immersion-well photo reactor to a meso-flow photoreactor. Nevertheless, the research field prioritizes classical natural product design and preparative organic chemistry.

A mentionable study, shown in **Fig. 1.14**, is the use of a visible light photo-catalyst. It changes the reaction conditions by changing the required wavelength from UV to visible light, thus increases reaction rates and enables high yields (> 80%).[52,64]
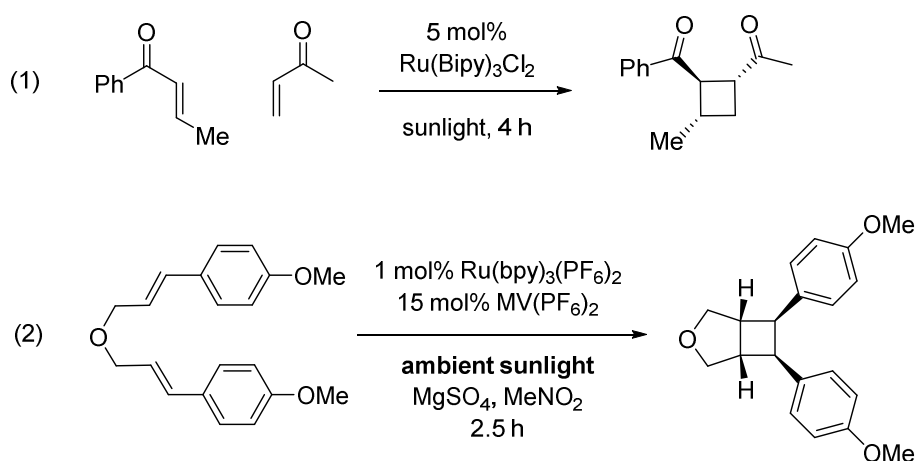
Fig. 1.14: (1) Photo-catalyst catalyzed cycloaddition of α,β-unsaturated ketones. (2) Internal [2+2] cycloaddition at ambient sunlight assisted by a photo-catalyst. Picture taken from Ischay *et al*. 2010.[64]

Also in polymer-related research the issue of polymer conjugation via photochemical reactions is addressed. Gründling *et al*. [65] described a conjugation method of dithioester- and trithiocarbonate-functional RAFT polymers with alkenes in [2+2] cycloadditions (**Fig. 1.15**). The drawback of this reaction is the

very high excess of alkene ($c_{polymer}$:c_{alkene} = 1:1000). The reaction pathway seems to undergo a radical β–cleavage followed by insertion of the alkene.
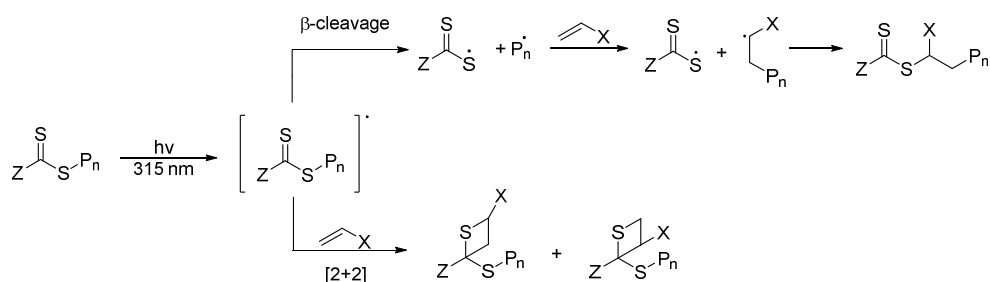
Fig. 1.15: Potential reaction mechanism of UV-light-excited dithioester- and trithiocarbonate-functional RAFT polymers leading mainly to an insertion conjugation of the polymer with an alkene. Picture taken from Gründling *et al*. 2011.[65]

Recently Landfester *et al*.[55] showed that these [2+2] photoinduced cycloadditions can be used for creating networks (**Fig. 1.13**). In this publication, the photo-dimerization of various groups (e.g. cinnamate, coumarins, etc.) at benign conditions was used to crosslink polymeric networks. The networks constitute nanoparticles are suitable for e.g. drug loading. By changing the wavelength the formed four-membered rings were cleaved. This cycle could be repeated several times with little loss of functionality due to degradation. Thereby, they showed a method for making reversible photo-responsive nanoparticles.

Another approach uses UV-light as an activator of precursor molecules (photo-enol). In this case the photons excite the precursor molecule leading to an internal rearrangement which sets free a highly reactive diene, hydroxy-*o*-quinodimethane (**Fig. 1.16**). The diene adds immediately to a present dienophil in an [4+2] Diels-Alder cycloaddition.[34,66,67] An advantage of this reaction is the high reaction rate. The reaction takes place within seconds. However, the precursor molecule decays in the presence of UV-light, the actual conjugation reaction is not a photo cycloaddition but a thermal [4+2] cycloaddition.
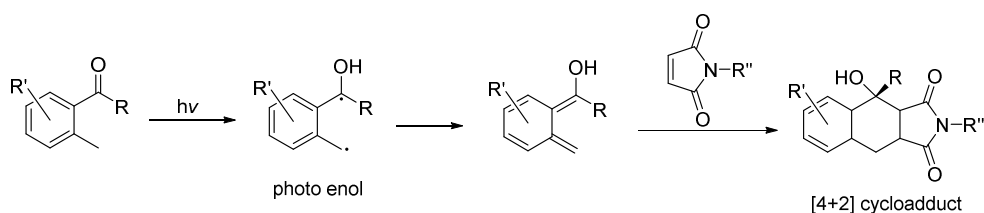
Fig. 1.16: Reaction pathway of the photo-enol polymer conjugation via hydroxyl-*o*-quinodimethane.

1.3.3 UV-induced CRP techniques

Photopolymerization represents a fast growing field in material science, mainly due to the numerous advantages associated to UV irradiation (very fast polymerization, no release of volatile organic compounds (VOC)). For coatings, inks, photoresists or dual-cure systems, the photopolymerization reaction is recognized as particularly interesting and efficient.[68,69]

Beside these above outlined conjugation reactions, (UV-)light can be used to initiate a living polymerization. Hawker et *al*. presented a polymerization using an Ir-complex.[70] The complex, fac-[Ir(ppy)$_3$], works via a photoredox mechanism and equilibrates between Ir^{3+}/Ir^{4+}-species (**Fig. 1.17**). The Ir^{3+}-species is excited by visible light leading to a free radical. It reacts with a standard ATRP-initiator by bromine addition yielding to Ir^{4+}Br and a free radical, which can start a chain propagation with surrounding monomers.
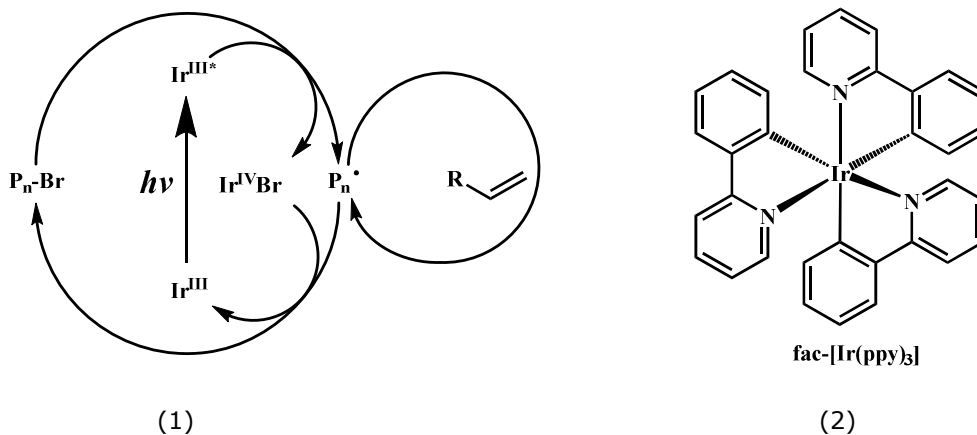
Fig. 1.17: (1): Proposed reaction mechanism of a visible light-mediated living radical polymerization using an iridium-based photoredox catalyst. (2): The photoredox catalyst fac-[Ir(ppy)$_3$] (ppy=2-pyridylphenyl). Pictures taken from Fors *et al*. 2012. [70]

Nitroxide-mediated photopolymerization ("NMP^2") is also a CRP technique enabling classical NMP by UV initiation. The photolysis of alkoxyamines is enhanced with a chromophore attached to the nitroxide moiety which leads to a reversible equilibrium between alkyl radicals and the nitroxide (**Fig. 1.18**).[71] The chromophore is located close to the aminoxyl function (1 or 2 carbons distance) to enhance the intramolecular transfer responsible for the cleavage of the C-O bond.[72] Using this approach the nitroxide workes as a photoiniferter for the polymerization of PBA, resulting in a linear growth of the polymer chains with 80% conv. in 500 s and living character has been evidenced.[71] "NMP^2" is of high importance regarding to many applications such as surface patterning with polymer layers of integrated circuits, data storage devices, miniaturized sensors and many others.[73]
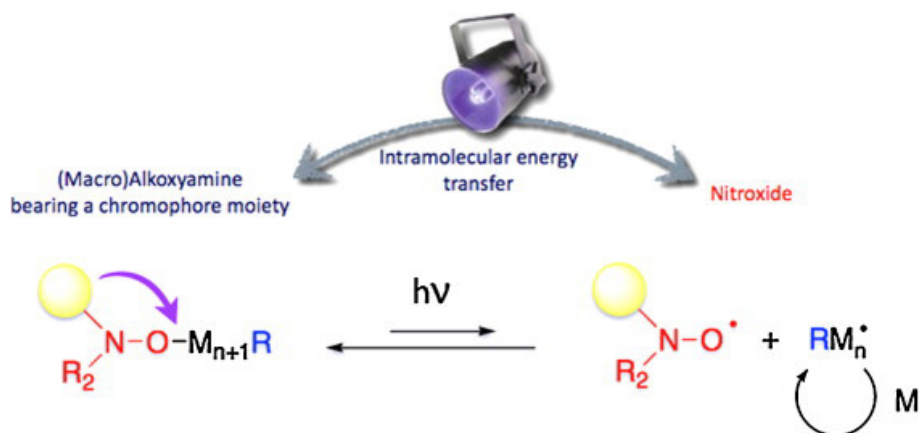
Fig. 1.18: Mechanism of the nitroxide-mediated photopolymerization ("NMP[2]"). Figure taken from Nicolas *et al*. 2013.[74]

To complete the list of photo-induced CRP methods the photo-RAFT polymerization shall be mentioned in a brief example. The group of Bai synthesized a trithiocarbonate RAFT agent (DDMAT) and polymerized MA in the presence of UV-light without using additional photoinitiator (e.g. Irgacure).[75] It yields to well-controlled polymer and a linear tendency of molecular weight evolution (**Fig. 1.19**).
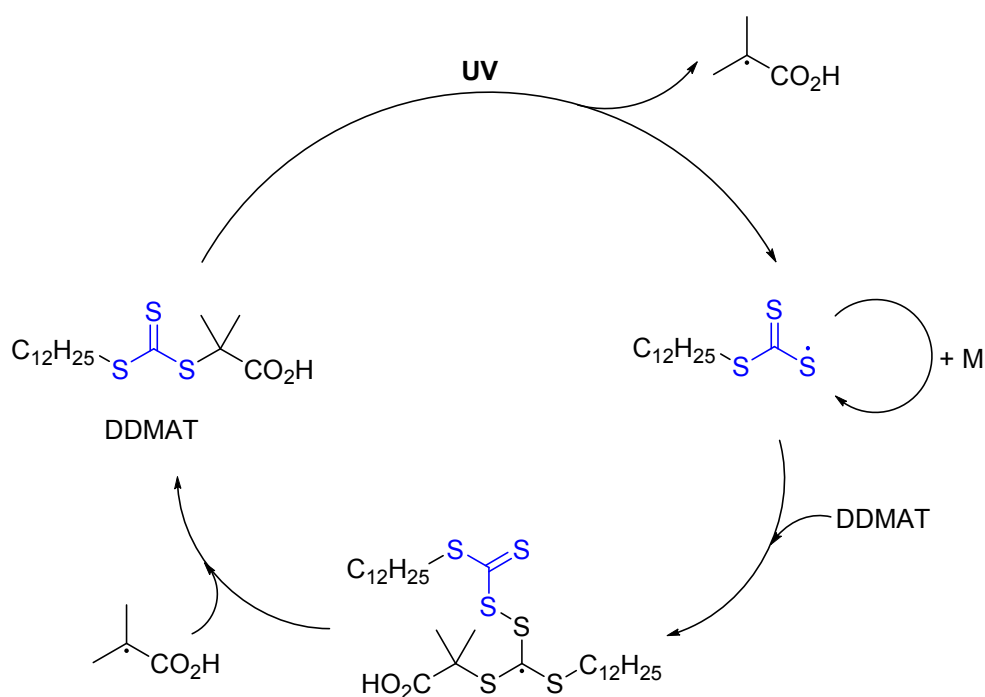
Fig. 1.19: Proposed mechanism for the photo-RAFT polymerization. Modified figure taken from Wang *et al*. 2013.[75]

1.4 Flow chemistry

As mentioned before many photochemical reactions have slow overall reaction kinetics. This lack of speed was improved by Hook *et al*. using a modified flow reactor. Instead of stainless steel tubing UV-light translucent polymer tubing are used.[50] The direct comparison of a flow-type to a batch reactor shows the difference in light take up (**Fig. 1.20**) where as in a flow reactor the light efficiency for excitation of electrons is significant higher than in a stirred batch reactor.
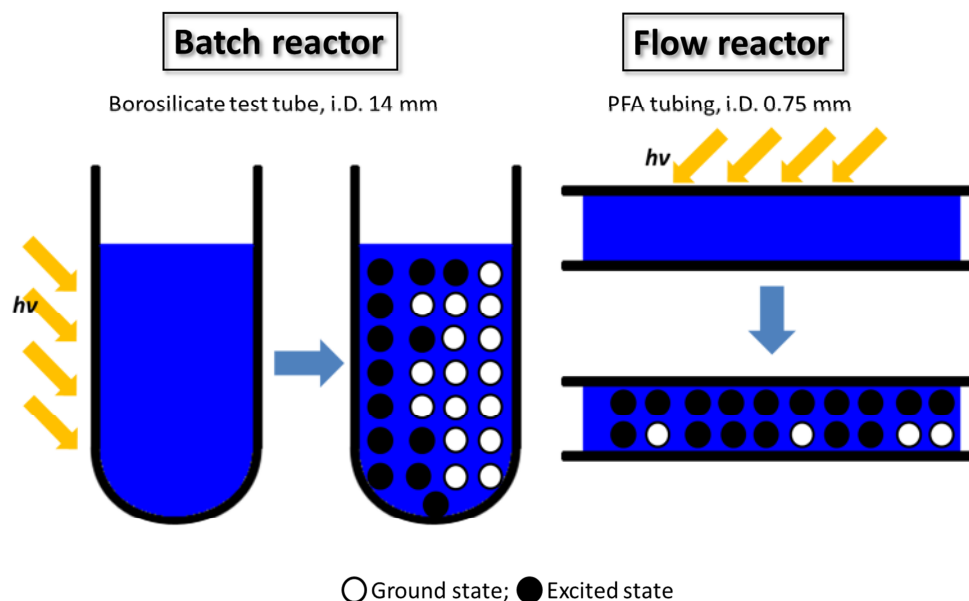
Fig. 1.20: Comparison of the light take up by a batch- and a tube flow-type reactor.[51,76]

Flow chemistry on meso- and microscale has drawn a lot of attention in academic research in the recent years. In comparison to batch processes, continuous synthesis of materials allow fast upscale of production procedures providing high flexibility at the same time. In modern microreactors, a large variety of reactions can be carried out in a broad range of conditions. Furthermore, the high surface-to-volume ratio of the flow meso-/micro-reactor technology (MRT) avoids the disadvantages of classical tubular or batch reactors (**Fig. 1.21**). In classical reactors the formation of punctual hot spots occur, due to poor heat dissipation of highly exothermic reactions.[77] The efficient thermal management in flow microreactors can also be employed to avoid side reactions and quicken up slow reactions by increasing temperature and pressure.[78,79] This fact allows the usage of a wide range of conventional solvents at temperatures above solvent boiling point, but cannot be utilized in classical batch reactor processes under the same reaction conditions.[80] That effects the polymerization of monomers, too. In general, the polymers are of higher definition and increased end group fidelity. Additionally, microreactors allow for a fast and efficient mixing of reaction solutions (**Fig. 1.21**).
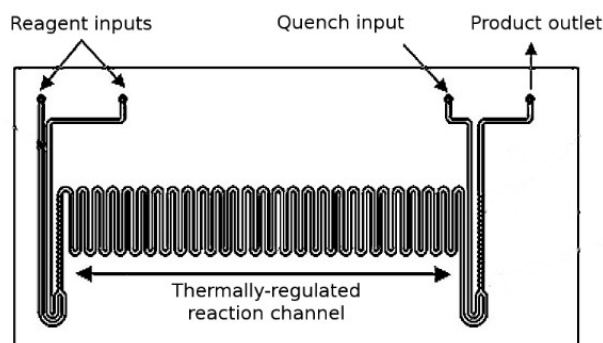
Fig. 1.21: Picture of a Chemtrix BV lab-on-a-chip microflow reactor. Picture taken from Chemtrix BV.[81]

Flow reactors allow for efficient screening of reaction conditions, due to the small scale and simple condition adjustments. Therefore, relatively large amounts of data can be gathered in short time. Here emerge intersecting sets with the concept of *click* chemistry. *Click* chemistry is designed for producing a broad range of molecules in a short time. These amounts of molecules could be quickly tested in (semi-)automatic microreactors and analyzed.

1.5 Aim of research

Many highly efficient reactions for the preparation of defined polymers with a high end group fidelity and assessable architecture are available. The majority of these modification reactions are induced by thermal energy. Therefore, it may cause side reaction with other heat-activated reactions. An possible alternative activation energy source can be (UV-)light. A molecule or polymer adheres functional groups with both these activation pathways and can be modified within two ways in the same pot, one after the other. Furthermore, the photo-induced reaction can be used to couple or graft polymers to surfaces, whereby facilitating surface pattern.

The aim of this PhD research project is the development of a photoinitated polymer conjugation reaction. The most suitable UV-light activated reaction seemed to be a [2+2] cycloaddition, either according to a Paternò-Büchi or an alkene-enone mechanism. To achieve this, the required functional groups had to be synthesized and built in polymeric species.

Suitable candidates were tested, rated and optimized. The optimization was done with variation of reactor setups and the application of catalysts.

The following chapters are written in manuscript style and have been published or submitted to various peer-reviewed journals.

Chapter 2

2. List of abbreviations

ace	aceton
ATRP	atom transfer radical polymerization
BA	benzaldehyde, butyl acrylate
Boc	tert-butyloxycarbonyl
Boc_2O	di-tert-butyldicarbonat
BuA	butyl acrylate
CA	cycloaddition
cat.	catalyst
cel	cellulose
conv.	conversion
Cp	cyclopentadiene
CRP	controlled radical polymerization
CuAAC	copper-catalyzed alkyne-azide cycloaddition
Đ	dispersity
DA	Diels-Alder
DBU	1,8-diazabicyclo[5.4.0]undec-7-ene
DCC	dicyclohexylcarbodiimid
DCM	dichloromethane
DIAD	diisopropyl azodicarboxylate
Di-Cp	dicyclopentadiene
DMF	dimethyl formamide
DP_n	degree polymerization
DVB	divinyl benzaldehyde

EDX	energy dispersive X-ray spectroscopy
ene	alkene
ESI/MS	electro-spray ionization/ mass spectrometry
Et$_2$O	diethyl ether
EtOAc	ethyl acetate
FMO	frontier molecular orbital
FRP	free radical polymerization
FT-IR	Fourier transformation – infrared spectroscopy
GC/MS	gas chromatography/ mass spectrometry
GD	grafting density
GPC	gel permeation chromatography
HDA	hetero Diels-Alder
HOMO	highest occupied molecular orbital
hv	photon
I	initiator
iBoA	isobornyl acrylate
ISC	inter system crossing
k_{deact}/ k_{act}	rate constant for de-/activation reaction
k_p	rate constant for chain propagation
k_t	rate constant for termination reaction
LA	Lewis acid
LD-PE	low density – polyethylene
LEGO	leg godt = play well (engl.)
LRP	living radical polymerization
LUMO	lowest unoccupied molecular orbital

M	monomer
MA	methyl acrylate
Me$_6$TREN	tris[2-(dimethylamino)ethyl]amine
M_n	number-average molecular weight
MO	molecular orbital
MRT	micro-reactor technology
MS	mass spectrometry
M_w	weight-average molecular weight
NEt$_3$	triethylamine
NHS	N-hydroxysuccinimide
NIPAAM	N-isopropyl acrylamide
NMR	nuclear magnetic resonance spectroscopy
NMP	nitroxide-mediated polymerization
NMP^2	nitroxide-mediated photopolymerization
PDI	polydispersity
PE	petrol ether; polyethylene
PEG	polyethylene glycol
Ph$_3$P	triphenylphosphine
PMDETA	N,N,N',N'',N''-Pentamethyldiethylenetriamine
P$_n$	polymer
PS	polystyrene
py	pyridine
r_{act}	reaction rate activation
RAFT	reversible addition-fragmentation chain transfer polymerization
RDRP	reversible-deactivation radical polymerization

r_p	reaction rate for propagation
r_t	reaction rate for termination
S_0	ground state
S_1	singlet excited state
SEC	size exclusion chromatography
SEM	scanning electron microscopy
SET-LRP	single electron transfer – living radical polymerization
T_1	triplet state
TEA	triethylamine
TEM	tunnel electron microscopy
tert.	tertiary
TFA	trifluoroacetic acid
THF	tetrahydrofuran
TLC	thin-layer chromatography
TMS	trimethyl silane
UHMW-PE	ultra-high molecular weight – polyethylene
UV/vis	ultraviolet/ visible light spectroscopy
XPS	X-ray photoelectron spectroscopy

Chapter 3
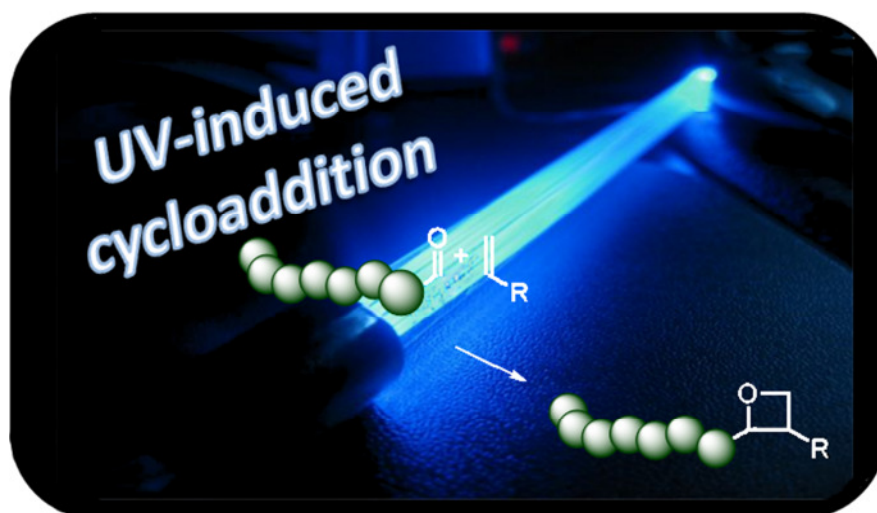
3. Photoinduced conjugation of aldehyde functional polymers with olefins via [2+2]-cycloaddition[*]

3.1 Abstract

Polymer end group modifications via [2+2] Paternò-Büchi reaction were carried out. Polyisobornyl acrylate (PiBoA, 3100 g·mol^{-1}) and polystyrene (PS, 2800 g·mol^{-1}) were synthesized by atom transfer radical polymerization (ATRP) employing aldehyde functional. Good control over the polymerizations was achieved, and materials with high aldehyde end group functionality were obtained. The terminal aldehyde function was reacted with alkenes under UV irradiation in [2+2] cycloaddition reactions. Good yields of the modification reaction was confirmed via NMR and by electrospray ionization mass spectrometry (ESI/MS) analysis and general conversion of the aldehyde function into the respective oxetanes of 90% or higher was observed. With the oxetane, a variety of functional groups were introduced to the polymer chain ranging from multifunctional allyl-compounds to disubstituted alkenes and amino or hydroxyl-functional alkenes. In the photoreaction, the integrity of the bromine endgroup of the ATRP polymers is retained. ATRP chain extensions can be performed after cycloaddition, demonstrating the versatility of this newly introduced polymer modification reaction.

3.2 Introduction

Not only since the introduction of the *click* concept,[26,31] a significant number of studies has been devoted to polymer conjugation and polymer endgroup modifications. Based on (hetero)telechelic polymers,[82] a broad variety of efficient chemistries were developed[30,83–85] that allow conversion of materials for an even broader range of applications. The most prominent reactions in use are the copper catalyzed azid alkyne cycloaddition (CuAAC),[86] thiol-ene and thiol-yne[87] or (hetero) Diels Alder[35,88] reactions. Most of these reactions have, however, in common that they are triggered via thermal activation. Thus, end group conjugations proceed either upon heating or when the reactive compounds are mixed. A control over the reaction in the time domain is hence not given. To date, only few reactions can also be triggered by a light stimulus. The radical chemistry variant of thiol-ene is based on conventional radical initiators.[37] Thus, these reactions can be also started via UV-light or proceed even under sunlight even when no dedicated initiator is added via a self-initiation mechanism.[89]

Another example for a conjugation reaction started by light was recently introduced by Bowman and coworkers, who used the CuAAC reaction, but generated the active copper catalyst in-situ.[90] Also, Barner-Kowollik showed that the light-induced formation of ortho-quinodimethanes can be used to generate a polymeric enophiles that can undergo a classical Diels-Alder conjugation.[36] The above approaches are indeed UV-triggered reactions and the first even allows for a "switch-off" after the light was turned off (with the CuAAC method this can only be achieved by addition of oxidizing agents), the conjugation reaction itself is in those cases, however, not driven by light.

It is evident from the criteria for efficient *click* reactions that cycloadditions (CA) are generally good candidates to perform conjugation reactions; they proceed in high yields on a single reaction trajectory and – in most cases – form stable C-C bonds. While the thermally allowed [2+3] and [2+4] cycloaddition reactions are already largely exploited, almost no example in the polymer field is so far found for photochemically allowed [2+2] CA reactions.[91] Only the team of Barner-Kowollik recently demonstrated that a [2+2]-like reaction can in principle be performed using the dithioester thiocarbonyl bond on a polymer derived by the reversible addition fragmentation transfer polymerization (RAFT) technique.[65] In their study, these authors demonstrated that conjugation of an ene can be achieved under UV-irradiation even though the ene was – due to a rearrangement reaction – not conjugated in the form of a four-membered ring, but rather inserted into the bond.
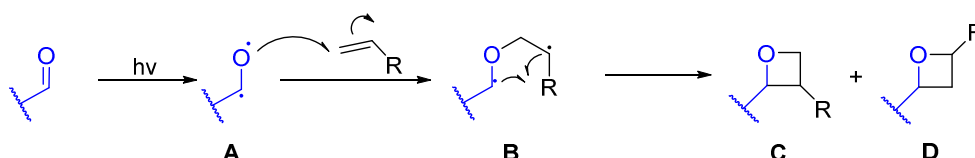
Scheme 3.1: Mechanism of the Paternò-Büchi reaction.

As a starting point in this research project, the alkene-enone and the Paternò-Büchi reaction seem to be the best choice as most data are available on these reactions in literature.[56,91] Generally, the reaction can proceed via two distinct pathways that lead to cyclization. No cyclization can occur from the ground state because of a phase mismatch of the frontier molecular orbitals. If the ground state of the activated compound is promoted to the S_1 state via a photon, then cycloaddition is allowed and can occur in a concerted mechanism. Via intersystem crossing, also a T_1 level can be reached which then is followed by cycloaddition via a biradical intermediate (**Scheme 3.1 A**). Which pathway is predominant is dependent on substituents, solvent and concentration of the reaction partners, but the radical intermediate pathway (**B**) is most commonly

observed, which leads to less predictable regio- and stereoselectivity; a stable C-C bond is however reached in any case. Thus, both reaction pathways are viable routes towards stable conjugations (**C** + **D**).

Many high-yield Paternò-Büchi reactions are found in literature, where ethyl-phenylgloxylate,[92] benzaldehyde, acetophenone or benzophenone have been used as the carbonyl group source to name some prominent examples. Generally, substrates that are electron rich and stabilized via aromatic rings are good choices for such reactions. The part of the alkene quencher can be taken for example by allylic alcohol,[93] oxazole,[62] methyl vinyl ketone,[52] isobutene,[94] 1,2-dicyano ethane,[95] furan(-derivatives)[61] and octene,[96] for which yields in the range of > 70% - 92% were reported.

In here, we want to report on the conjugation of a variety of alkene compounds onto aldehyde-functional polymers that were synthesized via atom transfer radical polymerization (ATRP) by employing a ATRP initiator bearing a benzaldehyde-type functional group.[16] Examples for polystyrene (PS) and polyisobornyl acrylate (PiBoA) are given and the conjugation products carefully analyzed using NMR spectroscopy as well as electrospray ionization mass spectrometry (ESI/MS).

3.3 Results and discussion

To find suitable reaction conditions, first model studies using low-molecular weight compounds were carried out. As expected from theory, best results were obtained with terminal olefins in presence of benzaldehyde. When activated alkenes were used, e.g. an acrylate, cyclization was observed, however the alkene showed a high propensity to react with itself. Ketones, as described in literature as suitable reagents in Paternò-Büchi reactions underwent the desired reactions, with however very slow reaction rates. **Fig. 3.1** depicts the proton NMR spectrum of the cycloaddition product from benzaldehyde and 1-octene. Despite the simple starting materials, a complex spectrum is obtained, which is due to the large number of stereo- and regioisomers that are formed in the reaction. As in the depicted case an excess of octene was used (removed in vacuo after reaction) an almost complete disappearance of the characteristic aldehyde peak close to 10 ppm is observed. Even though a clear assignment is not easily done, the peak region between 2 and 2.5 ppm can be assigned to the protons at the carbon atom opposite to the oxygen in the four-membered ring, the proton region 4-5 ppm to the protons close to the oxygen and the region of 5-6 ppm to the protons adjacent to the aromatic ring. For the formation of the

two different regioisomers (**Scheme 3.1**, part **C**+ **D**), indication is given that the 1,2 disubstituted oxetane is preferentially formed compared to the 1,3 substituted product. An abundant doublet at 5.91 ppm is observed, which can only be assigned to the 1,2 substituted product.[97,98] Despite the large number of isomers, it can be concluded that the oxetane formation out of the aldehyde is almost quantitative, therefore demonstrating that the Paternò-Büchi reaction can serve as a conjugation tool for two individual building blocks.
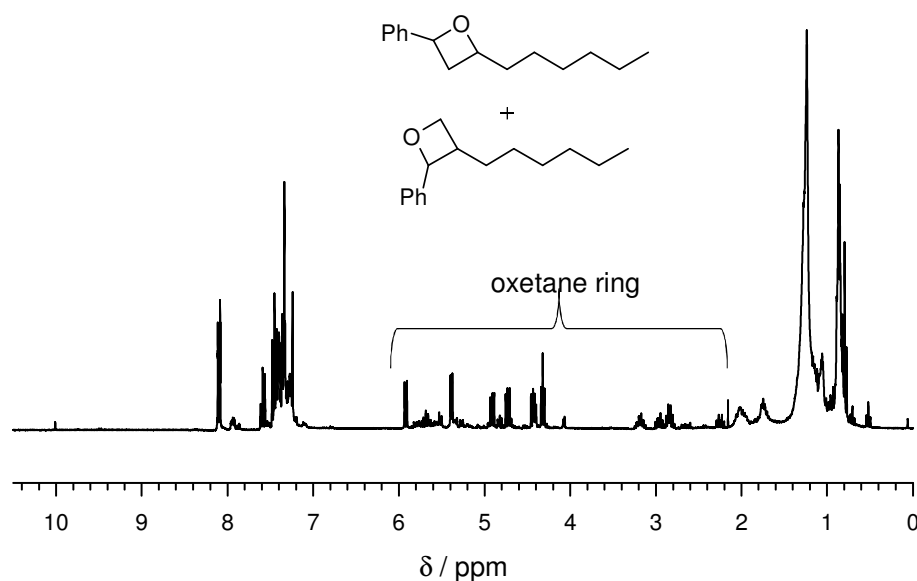
Fig. 3.1: NMR-Spectrum from model studies with benzaldehyde and 1-octene (1:50) after 48 h UV irradiation.

In order to transfer the results from small organic compounds to a polymeric system, several design criteria need to be considered. Generally, high fidelity (hetero) telechelic polymers are required to ensure a complete conjugation of substrates onto polymer chains. Since the carbonyl function is the moiety that is activated by UV-light, higher reaction efficiencies are obtained when the alkene is employed in excess. Hence, for purification reasons, polymers carrying a terminal aldehyde moiety needed to be synthesized to allow for an excess of alkene that can be removed after reaction. A facile route to reach such structures is given via the ATRP process employing an aldehyde-functional initiator (**Scheme 3.2**). A suitable initiator, 4-formylphenyl-2-bromopropanoate (FPBP), carrying a benzaldehyde moiety has been synthesized before by Yagci and his team and no interference of the aldehyde group with the ATRP process was observed.[59]
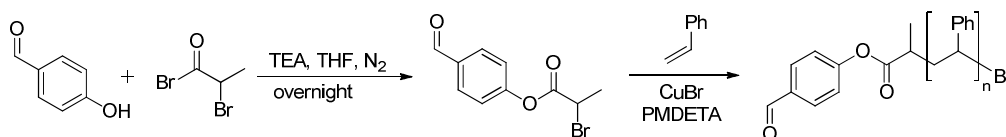
Scheme 3.2: Synthesis of the aldehyde functional ATRP initiator followed by polymerization of styrene.

Two polymers were synthesized employing FPBP. To cover different materials, a polystyrene and a polyisobornyl acrylate was targeted as starting materials for later conjugation reactions. The molecular weights and polydispersities of the residual polymers are collated in **Table 3.1**. Low conversions were chosen to prevent chain termination via chain transfer-to-polymer,[99] which would result in lower end group fidelity. In both cases, a successful ATRP could be carried out. Also MMA was tested with FPBP, however, significant amounts of dead polymer material were observed as side products repeatedly, giving rise to broad molecular weight distributions with low-molecular weight shoulders. It should be noted that NMR analysis revealed a relatively high aldehyde functionality, indicating that the initiator was effective and that by changing the reaction conditions, i.e. the ligand, well-controlled PMMA should be obtainable with FPBP.

Also for the other two polymers, PS and PiBoA, high end group functionalities were obtained. Also, a good match between expected average molecular weight, measured M_n from SEC analysis and from NMR analysis was found. Molecular weights from NMR were deduced by comparison of the characteristic peak of the proton adjacent to the bromine at 4.1 - 4.25 ppm. Functional fidelity was obtained by comparing the peaks of both endgroups. A representative NMR spectrum of the polystyrene sample **II** is shown in **Fig. 3.2**.

Table 3.1: Average molecular weights and functional fidelity of the aldehyde-functional polymers

	Poly.	M_n / g·mol^{-1}	M_w / g·mol^{-1}	$Đ$	conv./ %	$M_{n,NMR}$ / g·mol^{-1}	$M_{n,theo}$ / g·mol^{-1}	End group funct.^{a} /%
I	PiBoA	3100	3600	1.16	13.4	2700	2705	97
II	PS	2770	3080	1.11	20	3380	2930	91

^{a}Calculated by comparing peak integrals of the polymer endgroups
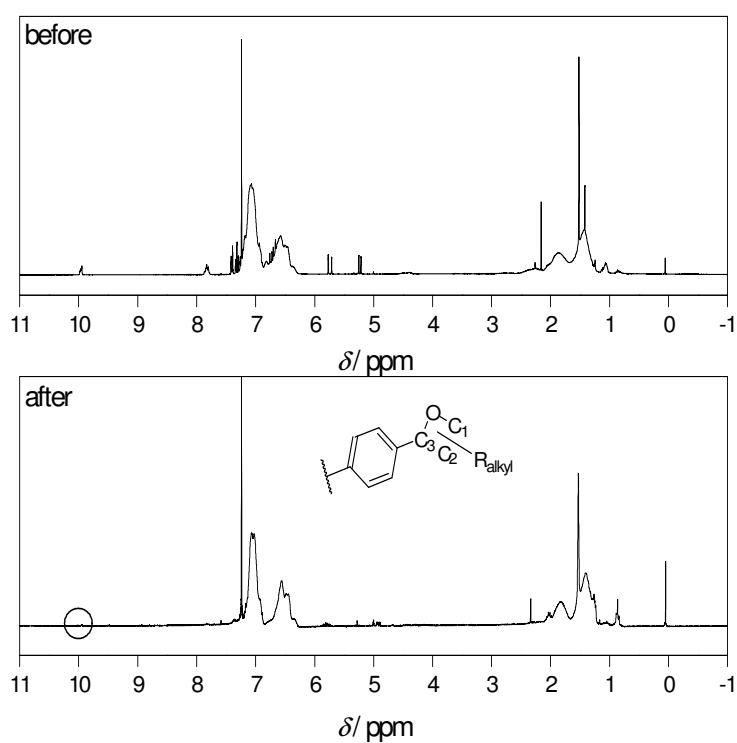
Fig. 3.2: NMR spectra of polystyrene **II** before and after cycloaddition with 1-octene at room temperature (**II** to octene = 1:50).
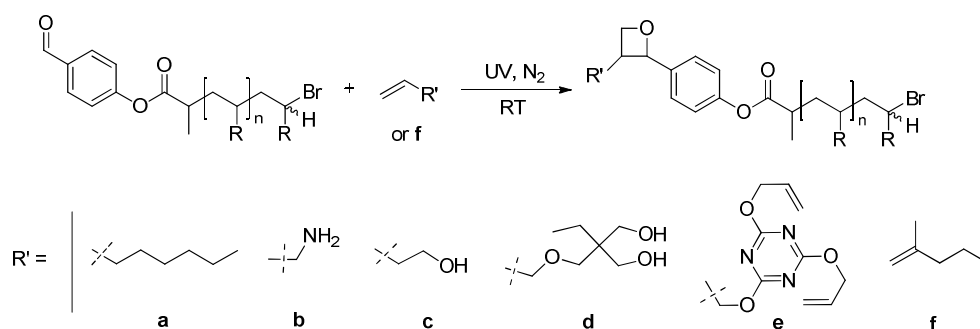
Scheme 3.3: Endgroup modification of the aldehyde-terminal polymers via [2+2] cycloaddition.

Scheme 3.3 depicts the Paternò-Büchi [2+2] reaction of the polymeric substrate. In the scheme, R is a representative for the different polymer types, PS or PiBoA. In a first step, the polymers were all conjugated with 1-octene (**a**). To test for the conjugation efficiency, trials were carried out with varying contents of (**a**) whereby all other reaction conditions were kept constant, that is reaction at room temperature for two days under constant UV irradiation in a degassed toluene solution. The yield of the photoreaction was determined by two different techniques after isolation of the polymer by precipitation. NMR analysis was carried out on all polymers to test for complete disappearance of the aldehyde peak. It should thereby be noted that to stay on the side of caution, a prolonged pulse delay time (12 s) and a larger than normal number of scans was applied in the proton peak acquisition to ensure that a reliable quantitative analysis of the polymer endgroup could be performed. An example for a NMR spectrum of a completely converted aldehyde-functional polymer is also given in the lower part of **Fig. 3.2**. Integration of the aldehyde peak region reveals complete disappearance of the aldehyde signal. At the same time, peaks according to the oxetane appear, which are, however, not abundant enough to allow for accurate integration.

To allow for a better assignment of the products, the polymers obtained from the cycloadditions were subjected to ESI/MS mass analysis to further test the conjugation efficiency. The advantage of a mass spectrometric analysis over the NMR characterization is that both the disappearance of the starting material as well as emergence of the products can be traced in higher detail and with a largely increased accuracy. Also, all different stereoisomers of the formed oxetane are isobaric and hence appear as only one apparent species in the mass spectrum. In view of the present study this is an advantage since the exact configuration of the conjugated moiety is not of relevance. In the upper part of

Fig. 3.3, a representative section of the full mass spectrum is depicted. The peak assignment alongside experimental and theoretical m/z can be found in **Table 3.2**. Several peaks are seen which may practically all be assigned according to the expectations of an ATRP polymerization. The most abundant peak in each monomer repeat unit (i.e. 1735.7 *m/z*) can be assigned to species I (Br-M_7-CHO) as depicted in **Table 3.2**, which is a polymer species consisting of seven monomer units, the aldehyde-functional initiator on one side and a bromine endgroup on the other side. A relatively good match (0.3 Da) between theoretical and experimental mass is found considering the mass spectrometer type used and mass range under observation. The peak pattern of the main peak (and all others) can be adequately simulated when taking the natural abundances of isotopes into account. Other peaks in the spectrum represent double-charged products which can be also assigned to the main ATRP product. Low abundant single-charged species (**III** and **V**) also appear in the spectrum, which can be assigned to potassium adducts of the main product (**III**) and disproportionation products stemming from conventional termination during polymerization (**V**). Occurrence of such termination product is not uncommon for ATRP polymerizations in the observed amounts.[100] Regardless, even though species **V** cannot be reactivated in further ATRP polymerization, it nevertheless carries the desired aldehyde endgroup and can hence be functionalized. Satisfyingly, no side products resulting from transfer to polymer reactions, which are often observed in acrylate polymerizations, are observed in significant concentrations. Thus, all species present in the mass spectrum can in principle be conjugated with alkenes and a complete shift of all peaks should be observable after a successful Paternò-Büchi reaction. Indeed, when inspecting the ESI/MS spectrum of the polymer after conjugation, a more or less complete shift is observed, as indicated in **Fig. 3.3**. The main product, both the single charged as well as the double charged species are shifted according to the mass of octene (112.12 Da and 56.06 Da for the double charged chains, respectively). Only few, very low abundant species are seen in the depicted case. Success of the reaction can thus also be confirmed from the side of the product, where the NMR only confirmed the conversion of the starting material. For the analysis of the product mass spectra, it is important to note that Barner-Kowollik and coworkers, when trying the cycloaddition of RAFT C=S bonds with alkenes obtained products where an insertion rather than a cycloaddition had taken place.[65] Such product is isobaric and can, at least in principle, also contribute to the spectrum in the present case.
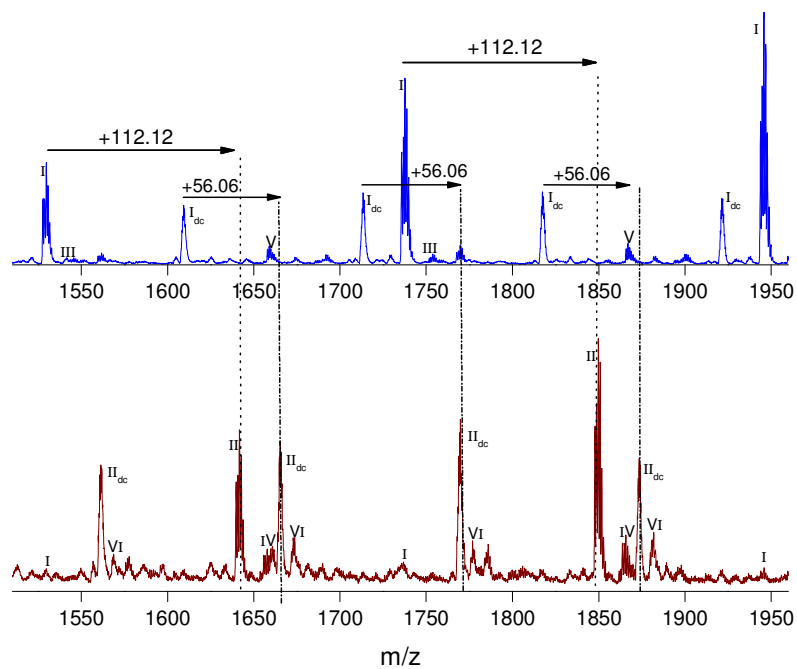
Fig. 3.3: ESI/MS spectrum of polyisobornyl acrylate sample **I** before (top) and after (bottom) conjugation with 1-octene.

Table 3.2: Species identified in the mass spectra as shown in **Fig. 3.3**

Number	Name	Formula	m/z_{exp}	m/z_{theo}	δ
	Na$^+$ adducts				
II	Br-M$_7$-oxe	$C_{109}H_{165}BrO_{17}Na^+$	1847.80	1848.11	0.3
I	Br-M$_7$-CHO	$C_{101}H_{149}BrO_{17}Na^+$	1735.67	1735.99	0.3
V	H-M$_7$-CHO	$C_{101}H_{150}O_{17}Na^+$	1658.73	1658.08	0.6
	K$^+$ adducts				
IV	Br-M$_7$-oxe	$C_{109}H_{165}BrO_{17}K^+$	1863.80	1864.09	0.3
III	Br-M$_7$-CHO	$C_{101}H_{149}BrO_{17}K^+$	1751.73	1751.96	0.2
VI	H-M$_7$-CHO	$C_{101}H_{150}O_{17}K^+$	1673.73*	1674.05	
VI	=-M$_7$-CHO	$C_{101}H_{149}O_{17}K^+$	1673.73*	1672.04	
	Na$_2$$^{2+}$ adducts				
I$_{dc}$	Br-M$_{15}$-CHO	$C_{205}H_{309}BrO_{33}Na_2^{2+}$	1711.93	1712.07	0.1
II$_{dc}$	Br-M$_{15}$-oxe	$C_{213}H_{325}BrO_{33}Na_2^{2+}$	1767.93	1768.14	0.2
VI	H-M$_{15}$-CHO	$C_{205}H_{310}O_{33}Na_2^{2+}$	1673.73*	1673.12	
VI	=-M$_{15}$-CHO	$C_{205}H_{309}O_{33}Na_2^{2+}$	1673.73*	1672.11	

*The monoisotopic peak of the species is overlapped, *m/z* 1673.73 is the maximum of the full peak

Both NMR and ESI/MS are suitable to determine the yield of the reaction. A series of experiments was carried out at constant reaction time with varying amounts of alkene. The results from these experiments are collated in **Table 3.3**. In this table, yields based on NMR, that is disappearance of aldehyde in the product spectrum and yields based on ESI/MS are given. ESI/MS yields were obtained by integration of all single charged species within a representative monomer repeat unit in the mass spectra that are unambiguously assignable to a polymeric species (peaks that show a typical isotopic pattern). Such approach can be taken for acrylates to obtain relative concentrations of all polymer species with different end groups.[101] As one can see from the table, NMR predicts higher yields for the reaction that is observable ion ESI/MS. This may have two reasons; (i) occurrence of side products, which are too low in concentration to be detectable in NMR and (ii) peaks that represent the desired product but have been degraded (e.g., ring-opened) during the ESI process are falsely accounted for. Regardless, the ESI-based yields represent a lower limit and the true yields may lay between both numbers obtained.

Table 3.3: Conjugation efficiencies for aldehyde functional PiBoA **I** with 1-octene

[polymer]/[**a**]	$Yield_{MS}$ /%	$Yield_{NMR}$ /%
1000	90	100
100	90	100
50	85	100
40	44	75
30	32	75
25	29	63
20	33	75
15	25	55

Overall, with decreasing equivalents of alkene present in the reaction mixture a decreasing yield is observed. Close to quantitative conversion of the aldehyde is only seen when at least 50 equivalents are employed at the chosen reaction time of two days. It should be noted that in order to avoid side-reactions, relatively low intensity UV-light was used and therefore long reactions times were chosen to compensate. Higher amounts of alkene in the reaction mixture or higher light intensities will lead to an increase in reaction rate and further refinement of the exact conditions will be required.

After a relatively good correlation between NMR analysis and ESI/MS is established, estimates on the overall quality of the reaction can be made based on NMR analysis alone. This is important to allow for an easy screening of reaction conditions. Also, an even more important, NMR also allows for reaction control in case where no mass spectra can be obtained. ESI/MS is in most cases limited to low molecular weight compounds and polymers with sufficient polarity in order to ionize. Thus, unpolar polymers such as polystyrene can only be analyzed via mass spectrometry with comparatively high effort.[102] In case of the polystyrene (**II**) that was prepared via ATRP with the aldehyde functional polymer, no mass analysis could be carried out. With identical reaction conditions and 50 equivalents of 1-octene, however, were quantitative yields indicated by NMR, thus allowing for the conclusion that also for these types of polymers successfully end group modifications via the [2+2] cycloaddition could be carried out.

In the subsequent step, different alkenes carrying various functional groups were subjected to Paternò-Büchi end group modifications. Largely successful modifications were achieved in case of the functional alkenes depicted in **Scheme 3.3** as well as 2-methyl pentene to also test a 1,1-disubstituted alkene. In all cases, complete conversion of the terminal aldehyde was observed by NMR. Yields based on ESI/MS are given in **Table 3.4**. Satisfying results were obtained in most cases. Somewhat surprisingly, even the disubstituted methyl pentene exhibited very high yields, demonstrating that steric hindrance might not be too high. It may be assumed that with a disubstituted compound, a higher regioselectivity was potentially achieved; however no further characterization was carried out to test for this hypothesis.

Table 3.4: Yields of reaction of polyisobornyl acrylate **I** with various alkenes

Alkene	$C_{C=C}/C_{C=O}$	$yield_{MS}$, %
1-octene (**a**)	1:40	95
allylamine (**b**)	1:50	60
3-buten-1-ol (**c**)	1:50	34
trimethylolpropane allyl ether (**d**)	1:50	88
triallyl cyanurate (**e**)	1:50	86
2-methylpentene (**f**)	1:50	90

It should be noted again that the MS technique most likely leads to an underestimation of the true yield of the reaction. For example, in case of the alcohol **c**, the expected oxetane product peak is clearly the most abundant. However, due to unfavorable signal to noise and presence of many small background peaks, a low yield was numerically deduced. Regardless, yields close to or higher than 90 % are observed (with the exception of **b** and **c**), indicating good success of the end group modifications and demonstrating that the [2+2] photoreaction is relatively tolerant towards other functional groups. This is a very important observation since only with a high functional tolerance applicability of the method to a large number of polymers consisting of functional monomers is given. Especially the cyanurate **e** is therefore of high interest, since it introduces 2 alkenes to the polymer chain, hence allowing for branch point for further modification reactions.

An interesting effect is seen with the analysis of the conjugation product with trimethylolpropane allyl ether **d**. In the mass spectra, peaks according to an internal cyclization of the conjugated molecule appear as the most abundant

species in the mass spectrum. Since such cyclization was not observed when irradiating **d** alone by UV-light (as confirmed by NMR), it can be concluded that this specific peak is a result of a condensation reaction occurring during the ESI process (**Table 3.5** and associated **Fig. 3.4**). Thus, both the product peak as well as the cyclized product together were counted to calculate the yield.

Table 3.5: Peak assignment of the ESI/MS spectrum for the [2+2] cycloaddition using alkene **e** as shown in **Fig. 3.4**.

Number	Name	Formula	m/z_{exp}	m/z_{theo}	δ
I	Br-M_5-oxe	$C_{84}H_{127}BrO_{16}Na^+$	1493.67	1493.82	0.15
II	Br-M_5-oxe^2	$C_{84}H_{125}BrO_{15}Na^+$	1475.60	1475.81	0.21
II$_{dc}$	Br-M_{13}-oxe^2	$C_{188}H_{285}BrO_{31}Na_2^{2+}$	1582.07	1581.98	0.09
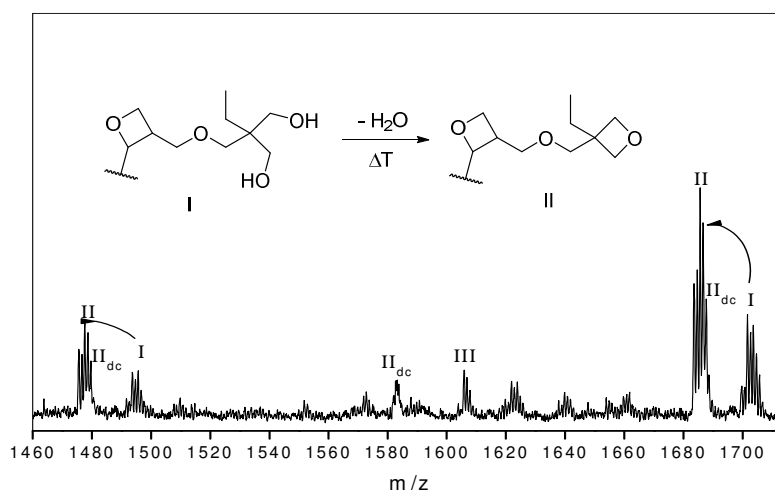
Fig. 3.4: ESI/MS spectra of a PiBoA sample (M_n = 3100, Đ = 1.16) after irradiation of UV-light for 48 h, in presence of trimethylolpropane allyl ether ($C_{CHO}/C_{C=C}$ = 1/50).

Unsatisfying yields are determined for **b** and **c**. As noted above, for **c** this may be attributed to the appearance of many smaller product peaks that cannot be assigned unambiguously, thus reducing the calculated yield of the reaction. For

the amine derivative **b**, less product is observed. Therefore, a peak according to an oxidized version of the expected functional oxetane is seen. Since the reaction is carried out under inert conditions, it is therefore assumed that the oxidation to the substituted hydroxylamine occurs during mass analysis and the conversion of the reaction was calculated based on this peak. The overall yield is, however, still low (60%), and the reaction with the amine must be considered as unsuccessful at this point in time. It should, be stressed again that the presence of unassigned peaks in the spectrum does not necessarily mean that the reaction was unsuccessful. Side reactions after the cycloaddition may occur such as oxetane ring-opening, bromine substitution reactions or further oxidations during the ESI measurement. Further studies as well as analysis with higher resolution mass spectrometry may help to elucidate the exact situation. All ESI/MS spectra and the peak assignment can be found in the supporting information of the article.[103]

The mass spectra described above indicated that the bromine end group is retained in the end group modification and is not disturbed by the UV-light. Therefore, it should be possible to carry out ATRP chain extensions after the photoreaction had taken place. Therefore, the chain-end modified **I** was subjected to further polymerization under ATRP conditions. **Fig. 3.4** depicts the molecular weight distributions before and after the ATRP reaction. The full line represents **I** after successful cycloaddition with 1-octene where all polymer characteristics such as average molecular weight and polydispersity of the original ATRP polymer was retained. The dashed line shows the polymer after chain extension. In the given example, the number average molecular weight increased from 3100 to 4100 g·mol^{-1} and the $Đ$ increased from 1.16 to 1.32. While the extended polymer is hence slightly broader in its distribution than usually achievable in ATRP block polymerizations, it still shows a complete shift of the whole distribution towards higher molecular weights, which is an independent proof for the retention of the active bromine functionality at the polymer chain end.
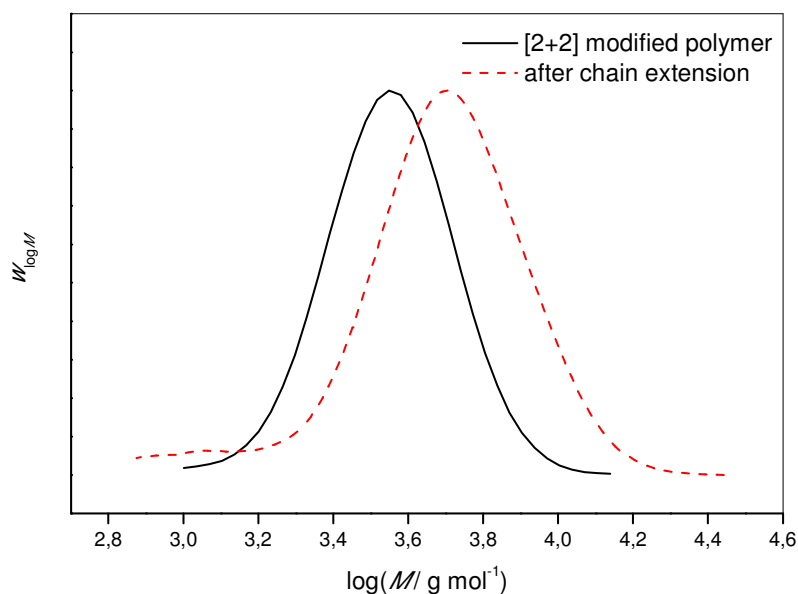
Fig. 3.4: Molecular weight distributions of the chain-end modified polyisobornyl acrylate **I** (solid black line) and chain extended polymer via subsequent ATRP (dashed red line).

It must be noted that the experiments described herein resemble a fundamental study to resolve whether the Paternò-Büchi reaction is suitable as an efficient polymer modification reaction. Compared to typical *Click*-reactions, the photo-cycloaddition may not fulfill the stringent criteria of the *Click* concept as reaction times are generally too high and also relatively large excesses of the alkene compound need to be employed in order to achieve complete conversions of the aldehyde compounds. Nevertheless, the required starting materials are easily obtained at low cost via the route described and reaction conditions may still be further refined to allow for faster reactions and lower excess amounts of alkene. Overall, the Paternò-Büchi cycloaddition has a distinct synthetic potential: A relatively high tolerance towards other functional groups is achieved and thus secondary functionalities can be introduced at the chain end under relatively mild reaction conditions. Combinations of the cycloaddition with other efficient modification reactions or ATRP block polymerizations can be made, giving rise to interesting synthesis pathways towards more complex macromolecular architectures. It should hereby be also noted that the oxetane ring that is formed in the cycloaddition can potentially be ring-opened and hence serve as a secondary conjugation point in the polymer.

3.4 Conclusion

The successful implementation of UV-induced Paternò-Büchi cycloaddition of alkenes onto aldehyde-functional polymers was demonstrated. A polyisobornyl acrylate as well as a polystyrene derivative, both carrying a terminal aldehyde endgroup were synthesized utilizing an aldehyde-functional ATRP initiator. The efficiency of the CA reaction was tested via NMR and ESI/MS analysis and for the conjugation of 1-octene, conversions of 90-100% were obtained after mild UV irradiation for two days at room temperature, when 50 equivalents of the alkene were used. Via this modification reaction, different functional groups were introduced ranging from multifunctional allyl-compounds to disubstituted alkenes and amino or hydroxyl-functional alkenes. In the photoreaction, the integrity of the bromine end group of the ATRP polymers is unchanged and subsequent ATRP chain extensions can be performed after the cycloaddition, demonstrating the versatility of this newly-introduced polymer modification reaction.

Chapter 4
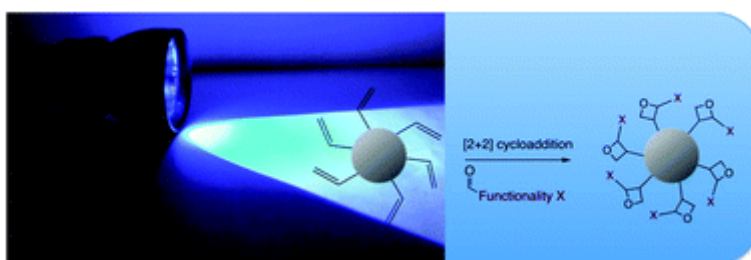
4. UV-induced functionalization of poly (divinylbenzene) nanoparticles via efficient [2+2] photocycloadditions[†]

4.1 Abstract

The efficient functionalization of poly(divinyl)benzene (polyDVB) nanoparticles via Paternò-Büchi type [2+2] photocycloadditions is described in this chapter. Initially polyDVB nanoparticles with high density of alkene groups on the surface are synthesized via radical miniemulsion polymerization. Subsequently, UV-induced [2+2] photocycloadditions with different functionalized aldehydes have been performed on the surface under mild and catalyst-free conditions. In order to show the versatility and the accessibility towards incorporation of different functionalities with this strategy, surface modifications were carried out with ATRP-initiators and NHS esters for bioconjugation, respectively. Finally, these photofunctionalized nanoparticles were grafted with poly(butyl acrylate) or with gold-labelled antibodies to proof the success of the reactions. PolyDVB nanoparticles before and after photofunctionalization were characterized with X-ray photoelectron spectroscopy (XPS), electron microscopy (SEM and TEM) and ATR-FTIR spectroscopy. The results show that the photoconjugation route is highly efficient and grafting densities of 4 to 5 molecules per nm^2 on the entire surface of the particles can be achieved.

4.2 Introduction

Functional nanoparticles have attracted tremendous interest with continually gaining prominence in a wide variety of fields ranging from nanomedicine, surface coatings, optoelectronics to classical materials design.[104–106] The application of novel functional nanomaterials in different disciplines has been paralleled by attempts to develop efficient, low cost/effort protocols of synthesis. In this context, (surface) functionalization of polymer nanoparticles has seen significant progress in recent years in the realms of drug delivery, bioimaging, biotechnology, pharmaceutics, functional coatings and biomimetic templates to name just a few examples.[107–110] Functionalization of polymer nanoparticles is achieved either directly via one-pot fabrication or by employing postmodification strategies in which functionalization is achieved after particle formation in a subsequent reaction step.

To date a large variety of materials have been developed with various surface functionalities, whereby for most systems optimization of the synthesis protocol is required depending on the desired functionality to be incorporated (one-pot strategy). Thereby, immense interest has been laid on surface functional groups that specifically allow facile attachment of biomolecules for targeted drug delivery systems. Optimization of such one-pot protocols are not trivial and thus the development of a basic synthetic platform that allows simple postmodification of nanomaterials with various types of substrates is highly desirable. In such manner the processes of nanoparticle formation, optimization and surface functionalization can be separated from each other. In that respect, *click* chemistry[26,31] has led to a paradigm shift in designing suitable synthesis routes.[30] By incorporation of a *click*-able groups to the interface of nanoparticles, virtually any conjugate can be formed hence allowing for introduction of any surface functionality that may be desirable.

Among the different heterophase polymerization routes, the miniemulsion technique has attained a fortified position in the fabrication of nanoparticles as it offers flexibility in design and synthesis of nanoparticles: tailor-made materials with vastly different physical properties are accessible in a minimum amount of time and effort.[111] At the same time, surface functionalities can be introduced via functional monomers, control agents or surfactants. In-situ functionalization is hindered by issues concerning the hydrophilicity of compounds. Classical postmodification procedures on the other hand are associated with the need to use catalysts or higher temperatures for ligation reactions, which can lead to contamination of particles, tedious washing procedures and likewise insufficient grafting density. The development of a versatile chemistry tool for nanoparticle surface functionalization that give access to good surface coverage as well as to mild (and preferably catalyst-free) reaction conditions is thus of great interest and would mark a significant improvement in the field. Light induced reactions are suitable to reach such aim. Light-induced reactions allow for mild reaction conditions (room temperature or below) and introduce a further orthogonality to the system. In principle, light of different wavelengths can trigger independent reactions and reactions can be switched between a thermal activation and photochemical modification. To date, only few phototriggered chemical ligation reactions are reported for surface modifications. Popik *et al.* described the photochemical dehydratation of 3-hydroxy-2-naphtalenemethanol derivatives which undergo hetero Diels-Alder cycloadditions,[112,113] or Michael additions with a surface thiol[114] and photochemical decarboxylation of cyclopropenone derivatives followed by a cycloaddition with azides.[115] Barner-Kowollik described light triggered chemical reaction based on nitrile imine-ene 1,3-dipolar cycloadditions[116] or a Diels-Alder reactions of *o*-quinodimethanes[117] or oxime ligation with hydroxylamines derivates after phototriggered deprotection of a *o*-nitrobenzyl acetal.[118] In all these reactions, the UV-light is used as an activator

to create the starting product, the conjugation reaction itself always relies on thermal activation.

In here, we demonstrate how a [2+2] photocycloaddition,[91] namely the Paternò-Büchi reaction between an alkene and an aldehyde,[56] can be employed to reach the aim of not only efficiently functionalizing nanoparticles, but also allow for temporal control over the reaction. Reactions only occur where the sample is illuminated and reactions immediately stop when the light source is switched off. Nanoparticles containing alkene groups in high density are readily available from miniemulsion polymerization of divinylbenzene (DVB), a low-cost, commercially available crosslinker monomer. Aldehyde counterparts are also easily available. The Paternò-Büchi reaction is largely tolerant to a wide range of functional groups, thus allowing for introduction of diverse functionalities such as halogens, esters, alcohols or amines.[76,103] The conjugation point that is formed upon reaction consists of an oxetane ring, and thus creates a stable C-C bond. Ligation is thus not reversible. [2+2] cycloadditions are known as synthetic tools in photochemistry since decades,[91] but are not extensively applied in synthetic organic chemistry due to limitations in stereoselectivity.

We have recently demonstrated as outlined in **Ch. 3**, that the Paternò-Büchi reaction is an excellent tool for polymer modifications.[103] Quantitative conversion of polymer chain ends with various functional alkenes was achieved. In principle, polyDVB particles with their pendant unreacted double bonds at the particle surface should be likewise accessible to [2+2] cycloadditions. The approach we describe in here is straight forward and simple. Particles are made following a standardized protocol and are subsequently subjected to the photo-grafting reaction after washing the samples. Due to the high density of unsaturated groups at the surface, high grafting densities with the aldehyde compound can in principle be achieved without subjecting the particles to thermal stress or without the need to use a catalyst. Additionally, due to the UV activation, functionalization occurs strictly on the particles surface, thus the approach is in principle also efficient from an economical point of view as no functional material is trapped inside the particles.

4.3 Results and discussion

4.3.1 Preparation of acrylate-loaded polyDVB nanoparticles

To demonstrate that the proposed method is indeed capable of covering the surface of DVB-made nanoparticles efficiently and with high grafting density, we have decorated particles with the aldehydes **1** and **2** that carry either a functional group suitable to act as a polymerization initiator in an atom transfer radical polymerization (ATRP)[16] or an N-Hydroxysuccinimide ester for subsequent bioconjugation. In subsequent steps, grafting with poly(butyl acrylate) (P(BA)) and a protein, respectively, is then performed. Particles before and after reaction are characterized in depth, especially on the P(BA) grafted particles to provide a concise picture on the efficiency of the UV reaction. It should be stressed that the grafting as well as the bioconjugation – while being themselves also highly efficient – are the only tools to demonstrate the versatility of the approach and to assess the grafting density on the particles surface that can be obtained in the UV reaction step. Also other functional aldehyde moieties are available, hence presenting a wide variety of obtainable surface functional groups. Further, it should be noted that Landfester et al. demonstrated recently that photoresponsive nanoparticles can be generated by exploitation of photo-induced cycloadditions.[55] Under influence of UV-light (> 250 nm), nitrocinnamate undergoes a photocrosslinking reaction and results in interparticle crosslinking, which can be reversed by illumination with wavelengths < 250 nm. While such system allows for versatile switching of the system, its chemistry should not be confused with the current approach, where the [2+2] reaction is used for modular particle design. In the latter case, a higher specificity and also much higher efficiency of the reaction is required in order to achieve satisfactory surface coverages.
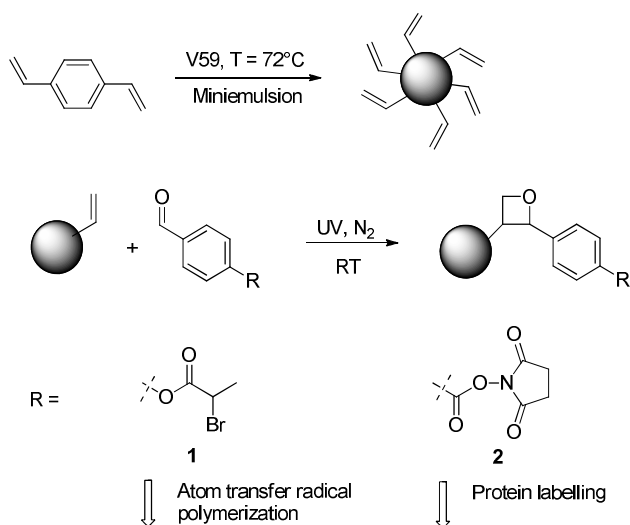
Scheme 4.1: Reaction scheme illustrating the photoconjugation of aldehydes **1** and **2**.

PolyDVB particles were synthesized from miniemulsion adapting the protocol given by Choi *et al.*[119] In our work, we employed an oil-soluble initiator for the particle synthesis under otherwise similar reaction conditions. The particles studied here were obtained after 30 minutes polymerization followed by washing to remove any unreacted monomer and the surfactant. The solid content of the dispersion determined after the reaction was 14.5 % and of the washed dispersion 5.9 % (after multiple centrifugation and redispersion). The average diameter of the nanoparticles, determined by TEM, was 110 nm ± 30 nm. The number average diameter obtained from dynamic light scattering (washed dispersion in water) was 134 ± 5 nm (dispersity = 0.19). These values are in good agreement with literature.[91] For microspheres it is known that the surface layer consists of lightly crosslinked polyDVB with a high concentration of residual vinyl groups,[120] which allow direct grafting.[121] Previously, DVB crosslinked particles have been employed as substrates for ATRP polymerization.[122] It should be noted that free vinyl groups will not only be present on the particles surface, but in principle also inside the particles, where they will, however, not be accessible to UV reactions.

First, the synthesized DVB particles were subjected to UV modification with aldehyde **1** to achieve introduction of the ATRP initiator moiety followed by polymerization (**Scheme 4.1**). After each reaction step, the spherical shape of the particles was retained and no visible change in size was observable in TEM

or SEM (**Fig. 4.1**). The TEM-images of core polyDVB particles with longer polymerization times, respectively 1 and 3 hours, point towards a particle size increases with longer polymerization times.
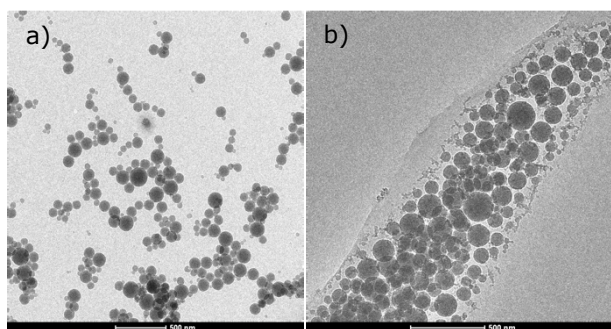
Fig. 4.1: TEM images of core polyDVB particles after a) 1 h of polymerization and b) 3 h of polymerization.

The presence of the functional groups was confirmed via energy-dispersive x-ray (EDX) (**Fig. 4.2**). Before polymerization, bromine functionalities on the particle surfaces were clearly visible (from the ATRP initiator) alongside a strong carbon peak, which is expected for polyDVB particles. The silicon and the oxygen peaks in the spectrum originate from the substrate on which the sample was dropcasted. After ATRP, the same peaks are observable as in **Fig. 4.2**.
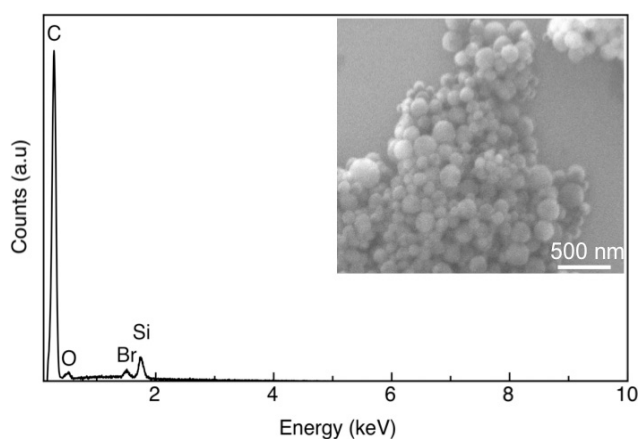
Fig. 4.2: Energy-dispersive X-ray (EDX) spectra and SEM images obtained for the particles grafted with the ATRP initiator.

Independent confirmation was given by analysis of the samples from ATR-FTIR (**Fig. 4.3**). It shows the ATR-FTIR spectra of the polyDVB nanoparticles before and after surface functionalization (introduction of ATRP initiator and grafting-from of pBA chains). The black spectrum represents the core polyDVB particles synthesized via mini emulsion. After the UV-treatment, when the [2+2] cycloaddition of 4-formylphenyl 2-bromopropanoate is performed (green spectrum) on the particle surface, a decrease in intensity for C=C the peak positions is observed. After ATRP polymerization with butyl acrylate, a clear C=O peak appears in the red spectrum.
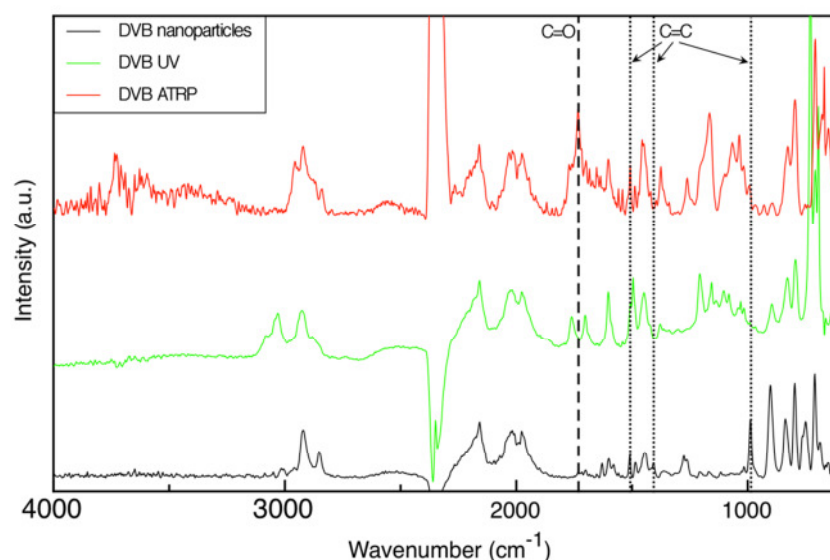
Fig. 4.3: ATR-FTIR spectra of unmodified core polyDVB particles (black), UV-treated polyDVB particles (green) and ATRP-treated polyDVB particles (red).

Before UV conjugation, peaks associated with double bonds were clearly visible in the spectra (1628 cm^{-1}, 1405 cm^{-1} and 990 cm^{-1}; vibrations associated with in- and out-plane deformation motions), which disappear completely after grafting of the aldehyde, indicating that all double bonds have been consumed (it should be noted that in principle also [2+2] additions between two neighboring double bonds can occur as a side reaction). At the same time, the appearance of the carbonyl peak after UV reaction indicates the presence of the initiator moiety. Further, after polymerization, a relatively strong signal in the carbonyl region was observed (1728 cm^{-1}), thereby also confirming the attachment of polyacrylate chains.

4.3.2 Determination of the grafting density and chain length

The chain length of the ATRP polymers was preliminarily determined via the sacrificial initiator method. Polymerizations were carried out under addition of a small concentration of free initiator in solution. After reaction, the soluble polymer chains were isolated from the particles and analyzed via size exclusion chromatography. A number-average molecular weight of 3000 g·mol^{-1} was deduced for the free chains. This value can be used as an approximation of the chain length of grafts, but should be strictly seen as an upper limit for their length since free chains in solution are in principle more accessible to chain growth compared to surface-bonded grafts. A first method to calculate the grafting density of the polymer chains on to the core DVB nanoparticles is based on the weight increase of the nanoparticles after the ATRP grafting. Presuming that the average molecular weight of the grafted polymer is similar to the one of the free polymer in solution as shown by Barsbay *et al*. for RAFT polymerization,[123] a number of 2.01×10^{20} chains per gram nanoparticle can be deduced. Assuming perfect spherical shape of the particles (which should be a justifiable postulate for this calculation) and a density of 1.18 g·cm^{-3} a total surface of the particles of $4.62 \cdot \times 10^{19}$ nm^2·g^{-1} is obtained, which then yields a grafting density of 4.3 chains per nm^2. This grafting density (GD) is significantly higher compared to in many other protocols for nano- and microparticle functionalization. For polyDVB microspheres, grafting densities between 1.6 and 2 chains per nm^2 had previously been reported.[121] Higher grafting densities (4-7 chains per nm^2), were also obtained by Nebhani *et al*. via thermally induced Diels-Alder grafting-to techniques.[124]

An alternative method to obtain the grafting density of the nanospheres is the use of elemental analysis (EA), which allows to monitor the functionalization after each step based on the oxygen content. The oxygen content increased to 3.3% after photo-functionalization and to 12.65% after ATRP grafting, leading to a GD of 7.4 and 3.6 chains per nm^2 respectively (the value of 7.4 certainly marks an upper limit and taking error margins into account, also a GD of about 5 may be reasonable (see supporting information of the associate publication for details[125]). The decrease in grafting density after ATRP indicated that not all of the immobilized initiator is consumed during the polymerization, most likely due to steric hindrance. Regardless, taking into account that different batches of nanoparticles were used for the determination of grafting densities, almost excellent agreement between the gravimetric analysis and the elemental analysis is found (4.3 and 3.6 chains per nm^2).

The sacrificial initiator method is relatively imprecise: Due to steric factors, chains on the surfaces may only grow to shorter size as compared to free chains

in solution. The determined grafting density herein is inversely dependent on the chain length; assumption of shorter chains will increase the apparent grafting density. In case of the nanoparticles synthesized via the miniemulsion route, the upper limit of grafting density is defined by the amount of unsaturated group for conjugation as well as space available; rough calculation of the space demand of **1** via MM2 force field calculations shows that a maximum of 4-6 units per nm^2 may be expected.

To further support the high grafting density, X-ray photoelectron spectroscopy (XPS) with its inherent surface sensitivity has been exploited to study the chemical state of the samples within the near-surface region. **Fig. 4.4** depicts the C 1s core level spectrum for the unmodified DVB particles revealing essentially two characteristic spectral features (bottom curve). While the main peak at a binding energy of 285 eV can be assigned to C-C/C-H bonds within the polymer, a weaker spectral feature is noticeable at 291.7 eV (see magnified view) representing a characteristic shake-up peak arising from aromatic ring π orbitals (π→π*). This shake-up feature is typical for a polymer with a significant degree of aromaticity.[126] In case of the UV treated sample, the appearance of an additional shoulder can be recognized at binding energies of around 289.5 eV which can be attributed to O-C=O groups[127] thereby giving direct evidence for the successful coupling of the ATRP initiator to the nanoparticle surface. The presence of the initiator is also confirmed by the detection of bromine using the Br 3d core doublet around 70.3 eV as probe.
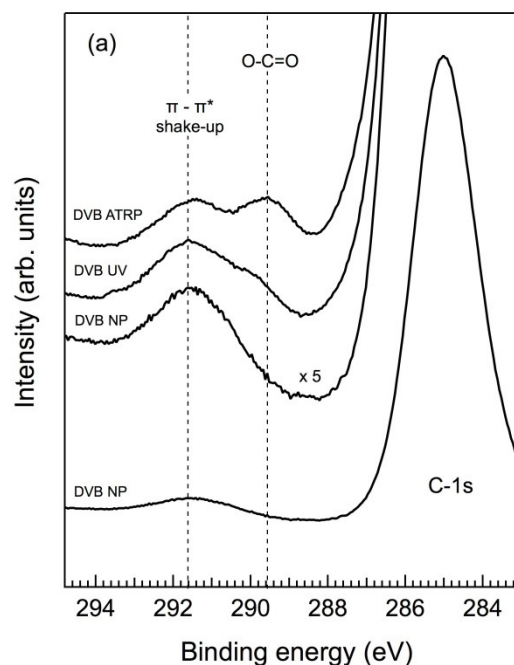
Fig. 4.4: XPS characterization showing the C 1s binding energy range of particles before UV reaction, after ATRP initiator introduction and after ATRP reaction. The upper 3 spectra are magnified by a factor of 5 for better view.

After the polymerization step, the sample exhibits a clear increase in the spectral weight at 289.5 eV, thereby proving an increase in the number of O-C=O groups at the nanoparticle surface corresponding to the growing polymer chains.

In order to estimate the density of initiator molecules at the particle surface, the main C 1s line (representing, to first approximation, the polymer particle) as well as the Br 3d core level spectrum both acquired after UV treatment were integrated using a Shirley-type of background. In a second step, the Br:C intensity ratio was used as input for a core-shell model simulation (**Table 4.1**).

Table 4.1: Quantification of core level peak intensities (corrected for photoionization cross sections) for the different sample stages as expressed by the intensity ratios between the Br 3d signal and the C 1s main line.

Status of reaction	$I_{Br3d} / I_{C1s\_C-C/C-H}$
before UV reaction	0
after UV reaction	0.0045
after polymerization	0.0042

Taking mean free path values of 3.3 nm for C 1s electrons travelling through the polymer particle and its shell and 3.6 nm for Br 3d photoelectrons while passing through the shell, the layer thickness of the initiator moiety on the particles surface as well as the density of molecules per nm^2 can be derived (see supporting information of the associate publication for details[125]). This way, an effective layer thickness of 1.6 ± 0.2 nm can be extracted, which corresponds to 4.7 ± 0.7 grafted molecules per nm^2. This latter value agrees very well with the results mentioned before, thereby confirming a very high surface coverage close to the theoretical limit and, consequently, proving the high efficiency of the UV-induced [2+2] reaction. Most surface functionalization techniques allow only for significantly lower grafting densities. Similar grafting densities were, however, also obtained from one-step synthesis of surface functionalized polymer nanoparticles via the miniemulsion technique using a functional comonomer and nanocapsules from interfacial polymerization reactions.[128,129]

4.3.3 Photochemical induced immobilization of gold–labeled antibodies

In the next step, also **2** was used towards the [2+2] cycloaddition onto the polyDVB particles to highlight the versatility of the approach. As indicated by ATR-FTIR (**Fig. 4.5**) the NHS group also can be efficiently incorporated via the UV reaction, giving rise to a large number of reaction sites. The ATR-FTIR spectra displays the changes of the polyDVB nanoparticles before and after surface functionalization (introduction of NHS ester). The black ATR-FTIR spectrum represents the core polyDVB particles without any surface functionalization. The green ATR-FTIR spectrum represents the N-succinimidyl-*p*-formylbenzoate (NHS-aldehyde). After the UV-induced cycloaddition of the NHS-aldehyde to the core polyDVB nanoparticles, the red ATR-FTIR shows successful surface modification.
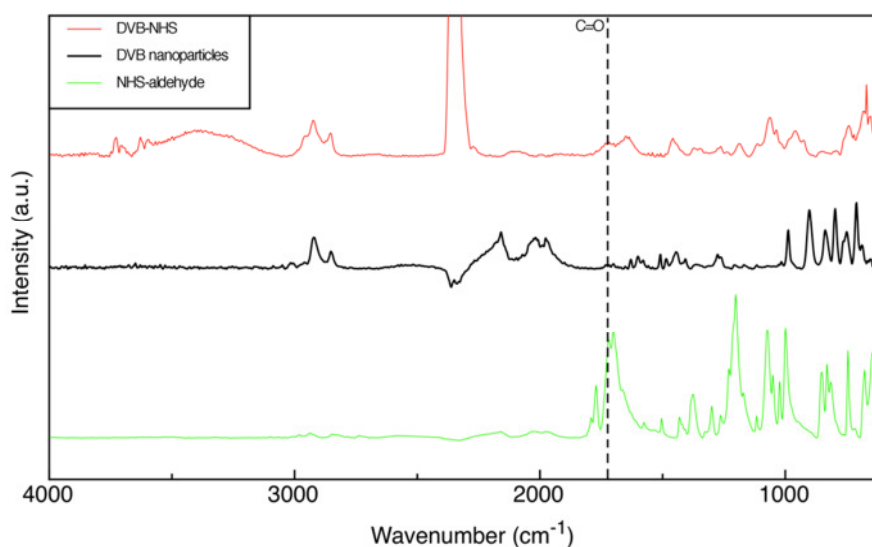
Fig. 4.5: ATR-FTIR spectra of N-succinimidyl-p-formylbenzoate (NHS-aldehyde) (green), unmodified polyDVB particles (black) and polyDVB particles functionalized with N-succinimidyl-p-formylbenzoate after UV-treatment (red).

The activated NHS group served as a versatile conjugation point for a large number of biomolecules. It is noteworthy to add that for bioconjugation a high grafting density is often not required to achieve a certain function. As a proof of principle, Goat anti-Mouse IgG (H+L) gold-labeled antibodies were band to the particles. The gold label allows facile detection of the grafts on the particle surface via TEM (**Fig. 4.6**). Firm attachment of gold labels, distributed over the particles surfaces, was observed, unambiguously confirming a successful attachment of the biomolecules. Not all particles are covered with gold labels, which can be attributed to a large number of NHS groups being still unreacted. Important is that all gold particles appear to be tightly bound to the particles, demonstrating that the added IgG have effectively reacted with the nanoparticles. It should be reiterated that the low coverage with gold labels in **Fig. 4.6** is the consequence of using only a small amount of protein for bioconjugation in our experiment. This can be easily increased than allowing higher coverages by employing larger concentrations of the protein during grafting. Preliminary results on the bioconjugation clearly showed an increased amount of surface-attached gold labels with increasing the protein amount in the reaction. Also, each gold label is attached to a larger number of proteins and hence the density of gold labels cannot be linearly extrapolated to the number of protein grafts on the surface. It must be stressed that the bioconjugation experiments were carried out to demonstrate the versatility of the photografting technique, but not to achieve maximum grafting densities, even though no

reason exist to doubt that the grafting density achieved in the photoreaction is significantly lower than for the ATRP initiator. Regardless, the activity of the NHS groups on the particles surface was clearly confirmed and an overall good distribution of the labels over the whole sample was achieved.
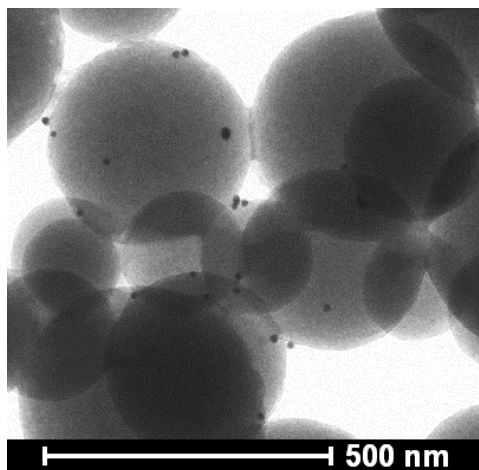
Fig. 4.6: TEM image of polyDVB particles after UV conjugation with NHS-aldehyde followed by gold-labeled antibody coupling.

4.4 Conclusion

In summary, we demonstrated that PolyDVB particles made from miniemulsion in combination with the UV-triggered Paternò-Büchi-type [2+2] cycloaddition provides a facile platform for the decoration of particle surfaces with different functional moieties under mild and catalyst-free reaction conditions. Surface functionalization with bromine functional ATRP-initiators as well as NHS esters for bioconjugation was successfully performed, but also other functionalities should be accessible using the same strategy. The ability to graft pBA from the ATRP initiator moieties as well as the attachment of gold labeled proteins was confirmed via ATR-FTIR, EDX, TEM and XPS measurements. The photoconjugation route is highly efficient and grafting densities of 4 to 5 molecules per nm^2 on the entire surface of the particles are achievable.

Chapter 5
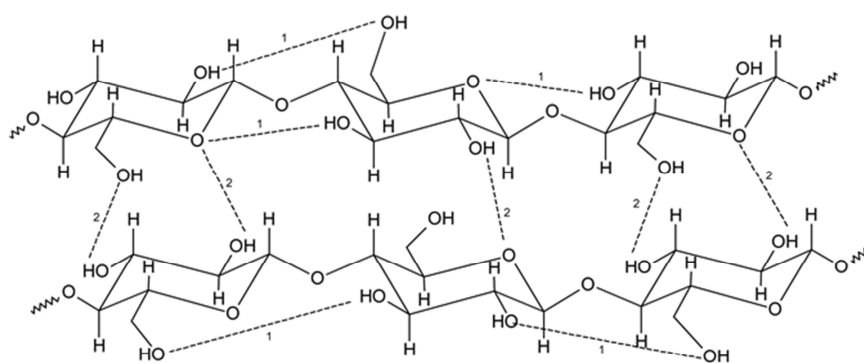
5. Application of the [2+2] Paternò-Büchi cycloaddition for cellulose surface modification[‡]

5.1 Introduction

In the recent research, preparation of thermo-responsive material is rather popular; due to its bright prospects for the preparation of controlled cell detachment systems[130,131] and drug-carrier-complexes.[132,133] An artificial material with a high potential is PNIPAAM (poly(N-isopropyl acrylamide)).[134] Its astonishing abilities, like an LCST of 32°C,[135] makes it a thermo-responsive system, that switches its hydrophilicity to hydrophobicity.[136] The chosen natural carrier material was cellulose. It is a non-harmful material that is cheap, while being mechanically and thermally relatively stable.[137,138] The thermo-responsive complex is built by the combination of cellulose and an artificial polymer. For an advanced material with thermo-responsive application some features, like a high versatility is needed and hence there exists a need for modification of the natural base layer.[139] On the other hand synthetic polymers are far more flexible and can be treated with harsher conditions for modification (e.g. end group modification). The novel idea of this research project is to combine cheap non-toxic base layer cellulose with an artificial polymer via a photochemical reaction.[103,140]

In the first steps the cellulose was modified using a classical chemical approach. The modification steps: (i) activation, (ii) tosylation and (iii) nucleophilic substitution were confirmed by attenuated total reflectance infrared (ATR-IR) spectroscopy. The attachment of the polymer involves a photochemical [2+2] cycloaddition also known as the Paternò-Büchi reaction.[56] This reaction is known to work well between an alkene and a ketone or aldehyde. This cycloaddition was already applied for polymer end group modification[103] and surface grafting of nanoparticles.[140] The photoreaction involves excitation of the carbonyl group by UV-light with a wavelength smaller than 300 nm. If the excited electrons are quenched by an alkene a cycloaddition occurs, yielding an oxetane.

The advantage of this approach is that the polymer can be grafted site and region specific to the cellulose substrate. Comparable work was done by Böhm *et al*. They synthesized a statistical free radical co-polymer with MMA and MA-benzophenone. The benzophenone modified polymer was grafted region

---

[‡] Conradi, M.; Junkers, T.; manuscript for publication in preparation.

unspecific to a base layer.[141] Using a mask while being illuminated the approach can be used for patterning. This technique can be applied vice versa immobilizing the benzophenone to the cellulose and grafting the polymer again region unspecific to it.[142]

In here presented work, we first show how to prepare aldehyde modified cellulose (cel-CHO). Followed by testing the [2+2] cycloaddition with cel-CHO and small model alkenes, then alkene end group functionalized polymers were synthesized and the photoreaction was tested on polymers and cellulose sheets. So far, only one approach introduced by Barner-Kowollik and co-workers is site specific.[143] It couples NMP-polymers to a surface-immobilized photoactive benzoyl derivative (similar to Irgacure® 2959).

5.2 Results and discussion

5.2.1 Preparation of aldehyde functionalized cellulose

In the first step the photoactive cellulose was prepared by grafting an aldehyde, here benzaldehyde derivative, to the cellulose surface. This group can be excited under irradiation of UV-light and forms an cycloadduct, oxetane, with an alkene.[103,140] Before approaching any reaction involving cellulose surface modification, the cellulose (cel-OH) has to be activated (cel-OH*). As cellulose source served normal filter paper (Whatman no. 5). The activation breaks the hydrogen bonds in the network; this can be done by immersing the sheets into sodium hydroxide solution (10%) for 18 hours (see **Scheme 5.1**). Afterwards the cel-OH* was washed with neutral ethanol. The contact angle of unmodified cellulose is 0° because the drop is soaked in. The pretreated cellulose shows swelling compared to untreated cellulose. The swelling is a result of the breaking intermolecular bonds between cellulose chains. In this condition the hydroxyl groups are more accessible for further modifications.
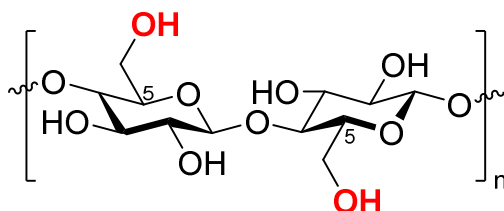
Scheme 5.1: Chemical structure of cellulose (cel-OH) with the most active hydroxyl groups at C6 position.

The activated hydroxyl groups at position C6 of the cellulose (cel-OH*) were tosylated with *p*-toluene sulfonic acid chloride in dry pyridine yielding cellulose (cel-OTs) with good leaving groups suitable for further modification reactions (see **Scheme 5.2**). The purification was done by thoroughly washing the filter paper with THF.
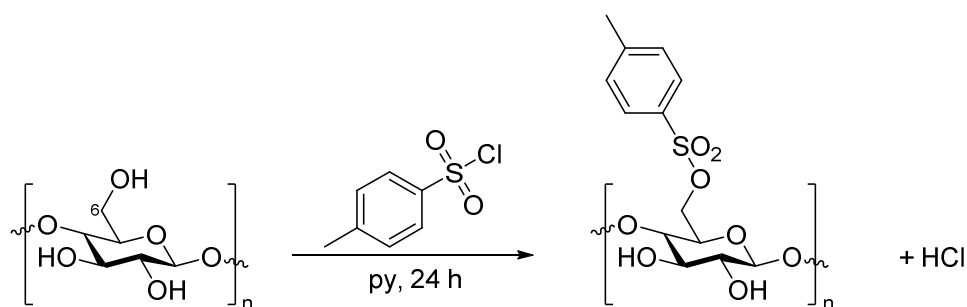
Scheme 5.2: Tosylation of the C6 hydroxyl group of basic activated cellulose in dry pyridine.

The progress of the tosylation was monitored by ATR-IR of the dried cellulose sheets (see **Fig. 5.1**). The modification could be followed qualitative by recording new signal in IR for cel-OTs. v_{max}(ATR)/cm^{-1}: 2950 – 2850, 1380 (-CH$_3$); 3100 – 3000, 1700 – 1500, 840 – 810 (C=C), 860 – 680 cm^{-1} (=CH) and 1420 – 1330, 1200 – 1145 (-SO$_2$O-). The cel-OTs showed a hydrophobic behavior underlined by an average contact angle towards water of 110°.
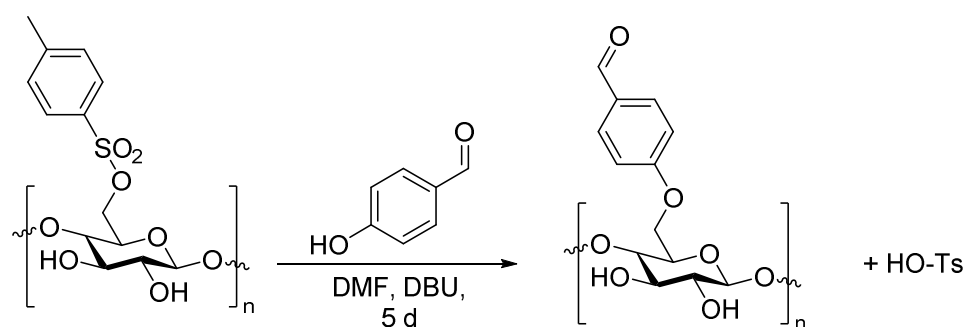
Scheme 5.3: Schematic overview of the Williamson ether synthesis using 4-hydroxybenzaldehyde as the benzaldehyde source.

The tosylate group is prone to nucleophiles and therefore a good leaving group. The tosylate functionality was removed via Williamson ether synthesis applying the nucleophile, 4-hydroxybenzaldehyde, yielding cel-CHO. The reaction was catalyzed using DBU (1,8-Diazabicyclo[5.4.0]undec-7-ene) as a steric hindered base promoted by the polar aprotic solvent DMF (see **Scheme 5.3**). Pre-experiments showed that using inorganic bases, like sodium hydroxide in water or elevated temperature accelerate the hydrolysis of the cellulose sheets. In that case only filter paper slurry was obtained. To reduce the physical stress to cellulose the reactions were carried out by stirring gently on an orbital shaker. The work-up was done by thoroughly washing the filter paper with THF. The exchange of the tosylate functionality was verified by ATR-IR showing the aldehyde signal at 1685 cm^{-1} (see **Fig. 5.1**). Due to the exchange of the tosylate group by a similar hydrophobic benzaldehyde derivative the average contact angle (a) of the cellulose did not change significantly ($a \approx 119°$, see **Table 5.1**).

Table 5.1: Overview of the contact angle of water towards the different cellulose modifications.

Cellulose modification	Contact angle α
Cel-OH	0°
Cel-OH*	0°
Cel-OTs	≈ 110°
Cel-CHO	≈ 119°
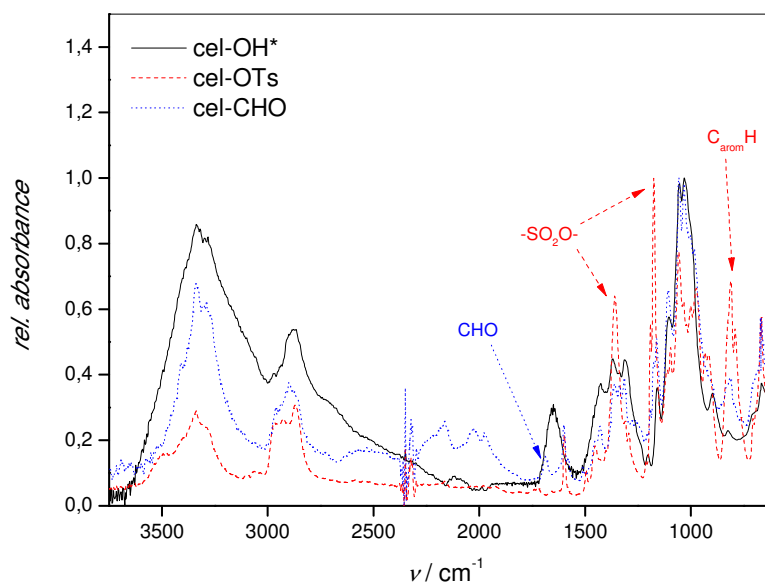
Fig. 5.1: Infrared spectra of modified cellulose at different modification states, measured by ATR-IR.

5.2.2 Cycloaddition with small molecules

Before attaching a polymer via photo reaction to the modified cellulose, the reaction was tested with three small molecules, here triallylcyanurate, trimethylolpropane allyl ether (TMPAE) and allyl chloroacetate. The first two molecules were chosen because they do not comprise aldehyde functionalities, making the detection of conversion by ATR-IR easier. The aldehyde functionality was visible at about 1680 cm^{-1} in the spectrum from cel-CHO (**Fig. 5.2**). The reduction of this signal intensity, present in both graphs, indicates the conversion in a Paternò-Büchi cycloaddition.
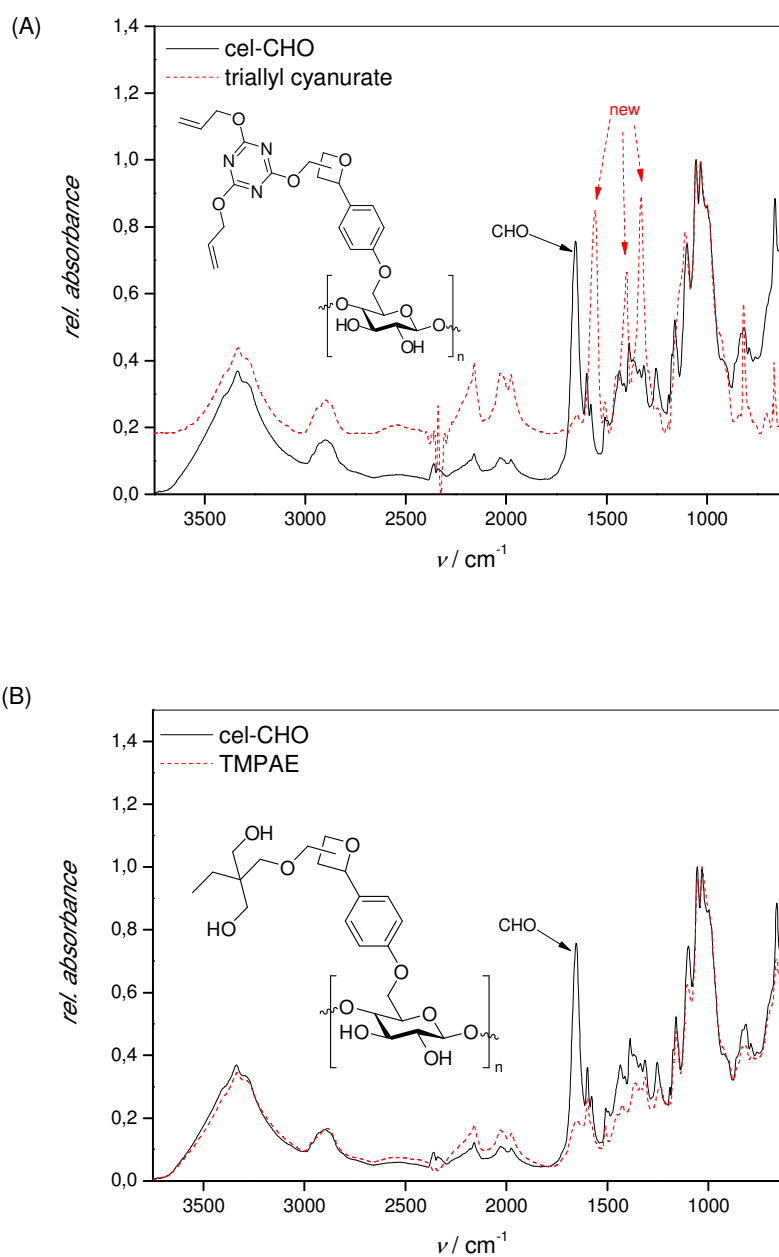
Fig. 5.2: (A) Overlay IR spectrum from cel-triallyl cyanurate formed by cycloaddition and the IR spectrum from cel-CHO. (B) Overlay IR spectrum from cel-TMPAE formed by cycloaddition and IR spectrum from cel-CHO.

The cycloaddition between cel-CHO and allyl chloroacetate can be detected by a chloride signal in the IR spectrum, expected about 785-540 cm^{-1}. A small signal can be observed in the cycloaddition sample at about 930 cm^{-1}. Due to a small shift in the IR spectrum it can be assume that this is associated with the chloride (**Fig. 5.3**). Another indication is the reduction of the aldehyde signal, indicating carbonyl conversion.
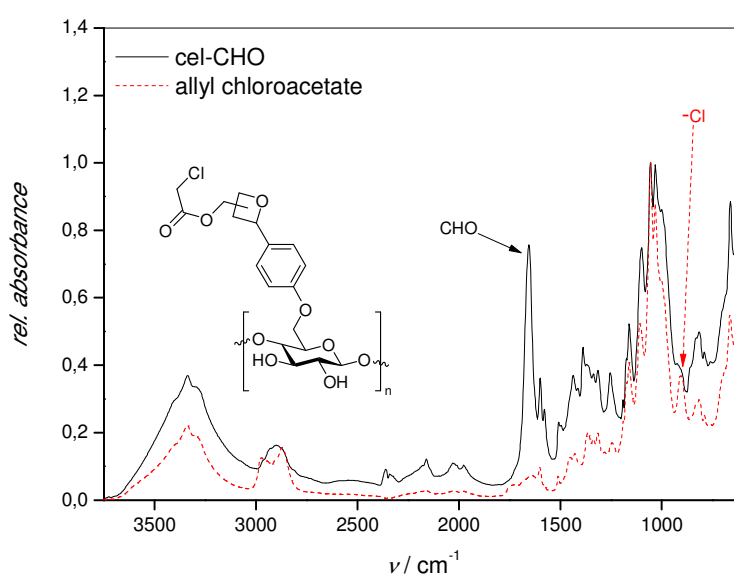
Fig. 5.3: Overlay IR spectrum from cel-allyl chloroacetate formed by cycloaddition and the IR spectrum from cel-CHO.

5.2.3 Synthesis of allyl end group functionalized polymers

After it was proven that the cycloaddition works for small molecules on the cellulose surface, the reaction was tested on polymers and cel-CHO for surface modification. An alkene end-group functionalized polymer was synthesized as shown in **Scheme 5.4**. The RAFT agent DoPAT was treated in a DCC coupling with 3-butenol to obtain the specific RAFT agent (allylDoPAT). In the second step allylDoPAT/AIBN were used to polymerize BA and NIPAAM for synthesizing the required allyl end group functionalized acrylate polymers. Using the ratios (BA/allylDoPAT/AIBN = 100/1/0.05) yielded 4.30 g PBA (M_n = 6990 g mol^{-1} and Đ = 1.12) and using the ratios (NIPAAM/allylDoPAT/AIBN = 75/1/0.1) 1.68 g PNIPAAM (M_n = 9500 g mol^{-1} and Đ = 1.16).
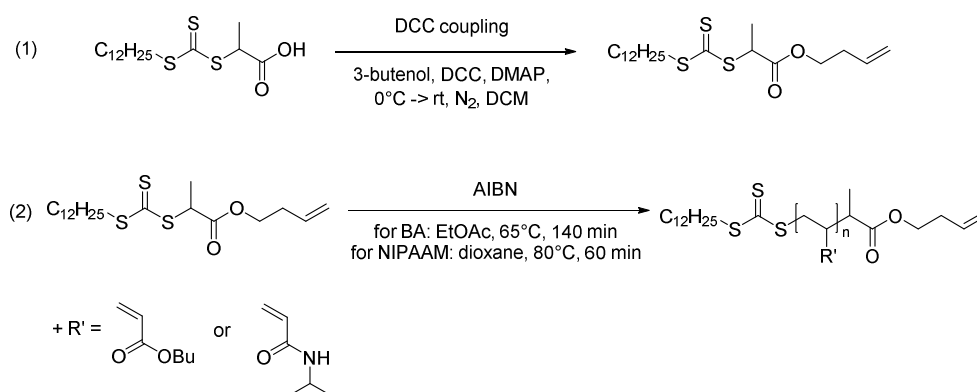
Scheme 5.4: (1) Synthesis of allylDoPAT via DCC coupling starting from 3-butenol and DoPAT. (2) RAFT polymerization of the functionalized agent with acrylic monomers.

The polymer characterization was attempted via NMR but due to their large molecular mass the allyl end group was not clearly detectable. A prove of principle was achieved by making a PBA with M_n = 2030 g mol^{-1} ($Đ$ = 1.21). In this specific sample the allyl group was detected by ^{1}H-NMR because after precipitation all signals related to the alkene group of the monomer and the acidic proton from DoPAT were absent. The allyl group was visible via multiplets at 5.76, 5.07 and 4.81 ppm. Further, the only single charge product in ESI/MS was [allyl-(BA)$_x$-trithioester]Na$^+$ (see **Table 5.2**). Therefore it was assumed that the larger polymers had the same end groups.

Table 5.2: Experimental and theoretical m/z values for the peaks detected of the PBA (M_n = 2030 g mol^{-1}).

Species	DP_n	Ion	m/z_{theory}	m/z_{exp}	$Δ$ / Da
allyl-(BA)$_x$-tri thioester	10	Na$^+$	1708.0143	1708.03	0.02
allyl-(BA)$_x$-tri thioester	24	Na$^{2+}_2$	1762.0879	1762.11	0.02

5.2.4 Cycloaddition between modified cellulose and allyl functionalized acrylic polymers

After the preparation of the allyl functionalized polymers and the aldehyde modified cellulose the cycloaddition was tested (see **Scheme 5.5**). The cellulose sheets were immersed in acetonitrile mixed with 25 mg of the polymer, 0.1 mg photosensitizer TXS and were deoxygenated for 15 min by purging with nitrogen. The vials were placed in a Multilamp reactor (12 × 15 W) and were irradiated for 48 hours.
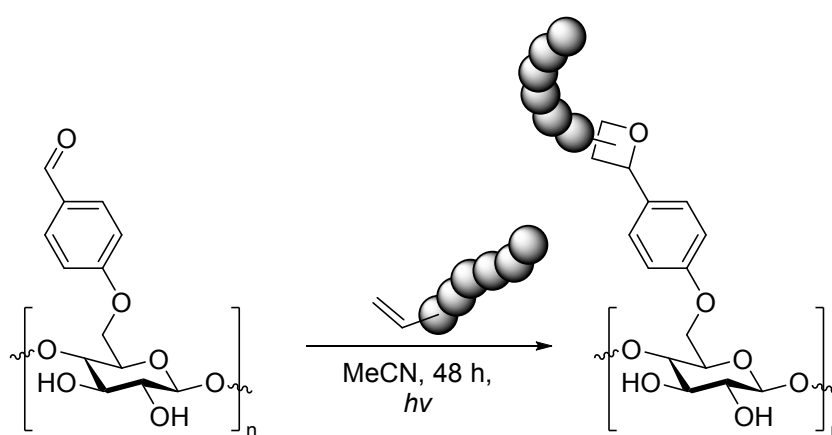
Scheme 5.5: [2+2] cycloaddition between aldehyde functionalized cellulose and alkene started by UV-light irradiation.

The appearance of a new IR-signal at 1731 cm^{-1} was related to the ester group of the polyacrylate backbone (see **Fig. 5.4**). To verify the exact positioning of the absorption band, unmodified cel-OH was dip-coated with PBA (cel-OH w/ BPA), then washed three-times with THF while the formerly present 1731 cm^{-1} peak disappeared, and later irradiated for 2 days (see **Table 5.3** for contact angles).

Table 5.3: Overview of the contact angles of water towards the different cellulose modifications steps.

Cellulose modification	Contact angle α
Cel-OH	0°
Cel-OH w/ PBA	≈ 114°
Cel-OH w/ PBA; washed	0°
Cel-OH w/ PBA; washed; UV	0°
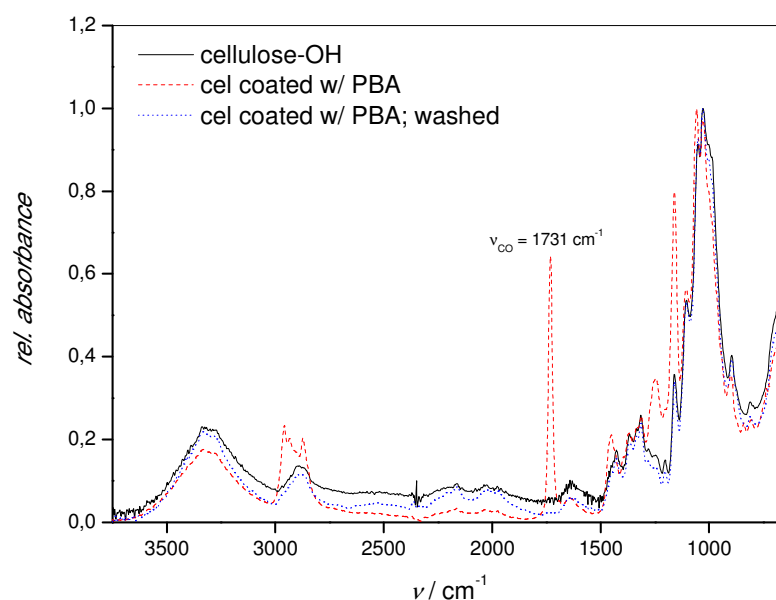
Fig. 5.4: Overlay of IR spectra unmodified; cellulose (cel-OH), PBA dip coated cellulose (red dashed line) and washed thoroughly cellulose sheet (blue dotted line).

The photo cycloaddition was tested with PBA, using 25 mg of polymer and one cel-CHO sheet (0.5 cm × 0.5 cm) in acetonitrile under oxygen-free conditions. After 48 hours the reaction was stopped and ATR-IR as well as contact angle were measured. The contact angle did not change significantly, 103.5° – 116.5° (see **Fig. 5.5**). RAFT polymers, especially the transfer agent, are prone to photocatalyzed reactions.[65] Therefore an additional experiment (blank test) was performed to assure that only the allyl group reacted under UV-light with the

cellulose. Random PBA polymerized via conventional DoPAT without any alkene functionality was treated with hexylamine to remove the potential photoactive RAFT group. The sample solution changed from colored to clear, verifying the destruction of the trithioester. Then the cel-CHO and acetonitrile were added. The solution was irradiated for 48 h under nitrogen atmosphere. In infrared spectroscopy a clear peak associated to an ester carbonyl group was detected in the sample with allyl-PBA (see **Fig. 5.6**, red dashed line). The blank test (blue dotted line) did not show a carbonyl signal originated from esters. A small absorption band can be detected but also in the cel-CHO sample. Surprisingly, the aldehyde signal was reduced, too. Maybe this is due to a photo degradation of the aldehyde group.

T = rt
α = 0°

T = rt
α = 116°
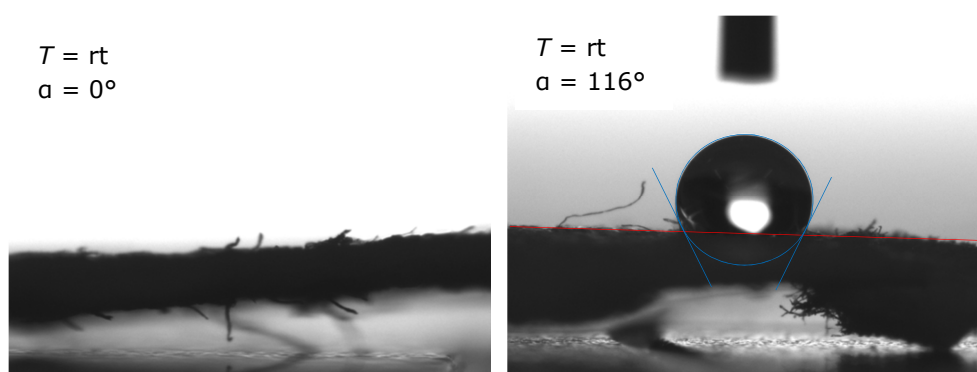
Fig. 5.5: Left: Unmodified cel-OH at room temperature. Right: Modified cellulose cel-[2+2]-PBA showing hydrophobic behavior.
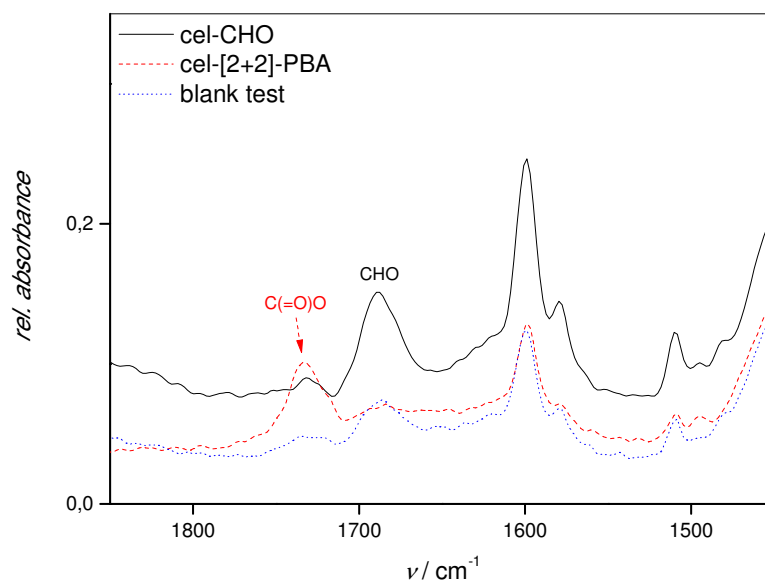
Fig. 5.6: Overlay of IR spectrum from cel-[2+2]-PBA formed by cycloaddition and the IR spectrum from cel-CHO. Clearly detectable is the disappearance of CHO (1680 cm^{-1}) and appearance of the polymer related signal (1731 cm^{-1}).

PNIPAAM is a potential substrate for advanced thermo-responsive materials, due to its LCST close to the human body temperature. Therefore, cel-CHO (0.5 cm × 0.5 cm), the allyl end group functionalized PNIPAAM (25 mg) dissolved in MeCN was irradiated for 2 days under N$_2$ atmosphere (see **Fig. 5.7**). Judging from the infrared spectrum it remained unclear, if the reaction was successful due to an uncomplete loss of the CHO signal. The new detectable signals (v_{C-N} = 1280-1220 cm^{-1} and v_{N-H} = 3500-3000 cm^{-1}; 1650-1560 cm^{-1}) are in the same region as the carbonyl group from the 4-hydroxy benzaldehyde or the hydroxyl groups of the cellulose.
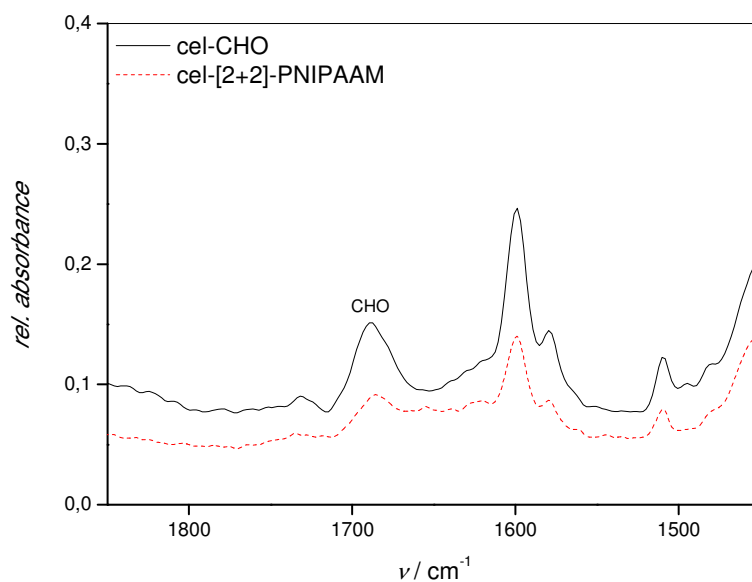
Fig. 5.7: Overlay IR spectrum from cel-[2+2]-PNIPAAM formed by cycloaddition and the IR spectrum from cel-CHO. The CHO signal (1680 cm^{-1}) decreased but is still visible.

To confirm the results of the experiment of the photo-grafting of PNIPAAM, temperature depending contact angle measurements were taken (see **Fig. 5.8**). At room temperature the cellulose sample showed an angle of 0°, meaning the cellulose surface is hydrophilic due to swollen PNIPAAM. Afterwards, the sample was stored for 5 min in a circulating air oven (T = 80°C) and the contact angle was calculated at a temperature of 40-50°C. The sample revealed a contact angle of 80° and 93° at two different spots. By these results, it was proven that the PNIPAAM is grafted to the cellulose base layer via [2+2] photo cycloaddition.

T = rt
α = 0°
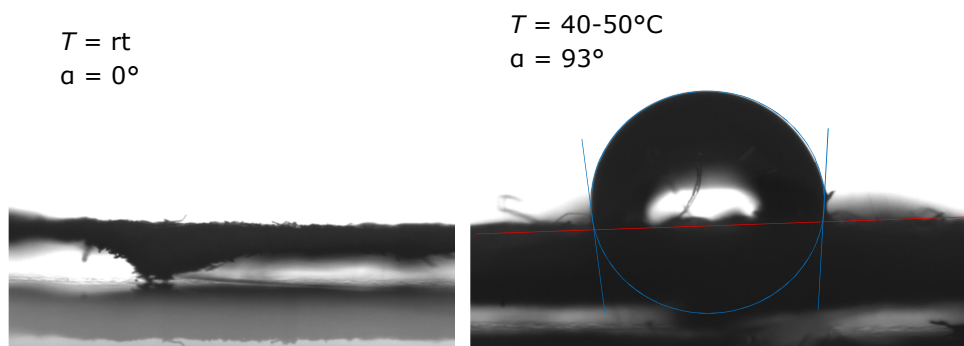
T = 40-50°C
α = 93°

Fig. 5.8: Left: Cel-[2+2]-PNIPAAM at room temperature. Right: Same cellulose sheet at approximately 40-50°C showing hydrophobic behavior.

5.3 Conclusion

The in here presented experiments show that the established Paternò-Büchi [2+2] cycloaddition is a powerful tool for polymer grafting onto natural substrates like cellulose. The cellulose was modified in a 3-step process to obtain the desired surface functionality and coupled to small model compounds. Additionally, the needed acrylate polymers were synthesized using controlled radical polymerization technique (RAFT). At last, the allyl functionalized polymers were coupled to the cellulose. This was proven by ATR-IR and contact angle measurements performed in the sessile drop mode with water. The PNIPAAM grafted cellulose showed the expected temperature depending response towards hydrophobicity.

Chapter 6
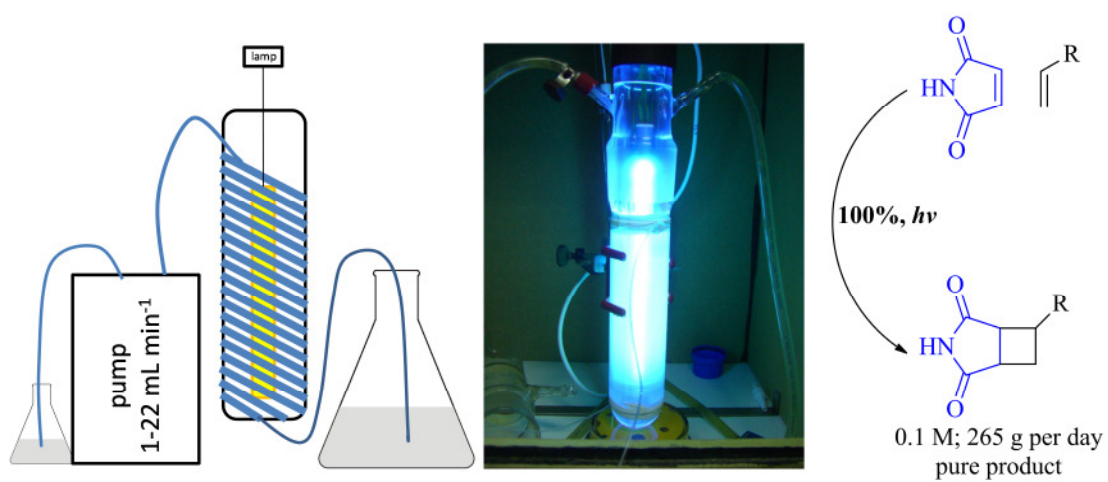
0.1 M; 265 g per day
pure product

6. Efficient [2+2] photocycloadditions under equimolar conditions by employing a continuous UV-flow reactor[§]

6.1 Abstract

The [2+2] photocycloaddition between maleimide and various alkenes was optimized in a simple custom-made UV-flow reactor. While complete maleimide conversion is only achieved with excesses of at least 10 eq. of alkene and reaction times of 12-24 h in batch, complete reactions with yields in the range > 98% could be obtained in 5 min in the flow reactor under strictly equimolar conditions. Functional alkenes carrying allyl, alcohol, amine and ether moieties were successfully conjugated in good yields under optimized reaction conditions. As it is demonstrated, the reaction gains in flow practically all characteristics of a high-efficient reaction following the *click*-concept with the exception of stereoselectivity, making the process highly valuable for upscaled synthesis of maleimide conjugates.

6.2 Introduction

Photo-induced [2+2] cycloadditions, e.g. the Paternò-Büchi or alkene-enone reactions have been in use in organic chemistry for many years.[56,60] [2+2] cycloadditions are a useful tool in conjugation reactions and have in the past been used extensively for the preparation of natural products or drugs.[48] Compared to thermal cycloadditions, photochemical [2+2] reactions have the advantage of yielding complex four-membered carbon-rings, a common structure element in natural products,[61,91,144] in one synthetic step. Especially maleimides are suitable substrates for photoadditions and at the same time are useful building blocks in the synthesis of natural products because they can be readily alkylated using the Mitsunobu reaction. [145,146] Also they are known as key functionalities in polymer conjugation reactions, which allows to use them directly in *click*-like approaches for macromolecular reactions.[35,88] Another advantage of photocycloadditions is true orthogonality towards 'classical' heat-induced reactions. [2+2] additions can be independently triggered and thus conjugation of different substrates can be achieved in a controlled manner by switching from thermal activation of functional groups to photo irradiation. This is of interest for example in surface modification reactions on natural substrates or for example nanoparticles.[125]

Photoreactions on the other hand tend to suffer from disadvantages with respect to reaction performance. In many cases UV batch reactions require long reaction times of up to days to reach acceptable yields.[103] The long reaction times are mainly a reason of low light efficiency.[51,147,148] The excitation of the ground state is needed to create a reactive intermediate which can be quenched by an alkene yielding the [2+2] cycloadduct. It should be noted that the mechanism is assumed to proceed through an exciplex.[149–151] Reaction yields (per time interval) can, however, be greatly improved when changing the reaction mode from batch to a flow chemistry setup.[50,79,152–155] Reduction of reaction times down to few to tens of minutes became achievable in different translucent tubular reactors for various cycloadditions, demonstrating the power of flow (micro-)reactor technologies. One of the main reasons for low yields in batch reactors is the distance of the sample to the UV-source, which is greatly reducible in flow reactors. Additionally, due to the narrow reaction channels in a flow reactor more effective light absorption is realized due to the small pathlengths that need to be considered in Lambert-Beer-law, thus resulting in much higher light efficiencies. Flow reactors allow for a more uniform irradiation profile of the reaction solution compared to decreasing light intensities with increasing beam penetration length of a voluminous sample.[63,156–158] Also, flow reactions have the advantage that the reaction – once optimized – can be up-scaled without much effort allowing for production of significant amounts of product in relatively short reaction times.

Thermal cycloadditions, such as [4+2] Diels-Alder or [3+2] dipolar cycloadditions[28,159–163] have gained increased attention in the recent years due to the concept of *click* chemistry, which was introduced by Sharpless in 2001.[26] Especially the copper catalyzed azide-alkyne cycloaddition (CuAAC) has become a prime example for simple conjugation reactions of building blocks and has rapidly gained prominence in the field of drug design, polymer materials and bioconjugation to name only few examples. Photocycloadditions have in principle the same potential to be used as *click*-like reactions. Indeed, compared to the CuAAC reaction they even feature the advantage of requiring no catalyst. Also, the substrates used in [2+2] reactions are orthogonal to many functional groups and can hence be used broadly in different areas. Functional alkenes are well known from certain click reactions already such as Diels-Alder or base-catalyzed thiol-ene conjugations. In order to fulfill the requirements of a *click* reaction, equimolarity is a crucial condition *sine qua non*,[31] at least in the field of materials chemistry. Following Sharpless definition, a *click* reaction should be wide in scope, modular, preferentially proceed under physiological condition, follow a single reaction trajectory and be chemoselective. Stereochemistry plays a major role in the field of natural products or drug design, but is only of limited interest in other areas. For example, in the field of polymer chemistry stereoselectiviness plays often only a minor role since the primary aim of *click* chemistry is there stable C-C bond formation and fast completion of the

reaction. Depending of the application the stereo- and regioselectivity can be neglected. [2+2] cycloadditions adhere practically all above rules with the exception of stereoselectivity. These reactions can proceed with tolerance to various substrates and functionalities, is orthogonal to many other processes and can be performed under mild reaction conditions. Disadvantages of this kind of reactions, which exclude them from the class of *click*-reaction in conventional cases, are however the low efficiency of the reactions (long reaction times) as well as the necessity to use large excesses of one compound to reach high yields (violation of the eqimolarity requirement). To date, all [2+2] cycloadditions, performed in batch or in flow, require excesses of one compound (usually the ene since this acts as a quencher for the excited state).

The in here presented work demonstrates how the light efficiency can be improved for a photo-induced [2+2] alkene-enone cycloaddition by using a self-made tubular flow UV-reactor. Fast reactions in the order of few minutes can be achieved, even under strictly equimolar reaction conditions and thus under conditions where virtually no purification of the product is required. Under flow, the reaction exhibits all required characteristics of a *click*-like reaction (with respect to the field of polymer materials development)[31], a fact that has not been acknowledged before and which makes it an interesting synthetic tool not only in the realm of drug design, but also materials chemistry, for example block-copolymers formation or nanoparticle modification (flow chemistry may on first glance be problematic to use in heterogenic reaction conditions. Clogging of the tubing can, however, be prevented).[164]

6.3 Results and discussion

6.3.1 Optimization of a photo cycloaddition in batch

6.3.1.1 Minimum required enone:alkene-ratio
First, the batch reaction of a [2+2] cycloaddition between an alkene and an enone (for mechanism see **Scheme 6.1**) is compared with the flow process. Maleimide (MI) was chosen as a versatile enone compound. The absorption maximum of maleimide lies at 275 nm and can hence be excited by UV-light with moderate wavelengths. For simplicity, octene (**2**) was used as alkene counterpart in the conjugation reaction since it can easily be removed after the reaction when employed in excess or if the reaction was incomplete. Later, also other alkene components, namely allylamine (**3**), 3-butenol (**4**), triallyl cycanurate (**5**), 2-methylpentene (**6**) and allyl ethyl ether (**7**) were used in the reaction to test for functional tolerance of the reaction. So far the only described reaction between maleimide and an alkene was presented by Booker-Milburn *et al*. performing a related reaction in lower performances than achieving complete

conversion using a flow-reactor.[165,166] In the beginning, the reaction between maleimide and octene was performed in a multilamp reactor MLU 18 (Photochemical Reactors Ltd., UK; mercury vapor lamp, UV broadband, λ_{max} = 254 nm) to determine the required excess of quencher (octene) for allowing a complete maleimide conversion in the photoreaction. For tabulated results see **Table 6.1**. The experiments showed that an excess of at least 10 equivalents is needed to obtain the desired [2+2] adduct (**2**) in a range of good 90% yield (within an acceptable reaction time of 24 h). Furthermore, the reaction can be monitored by FT-IR because of the decrease the maleimide signal at 3220 cm^{-1} (**Fig. 6.1**). To compare, in previous Paternò-Büchi cycloadditions of benzaldehyde and octene 20 equivalents of octene and 48 h reaction time were required to reach similar conversions.[103]
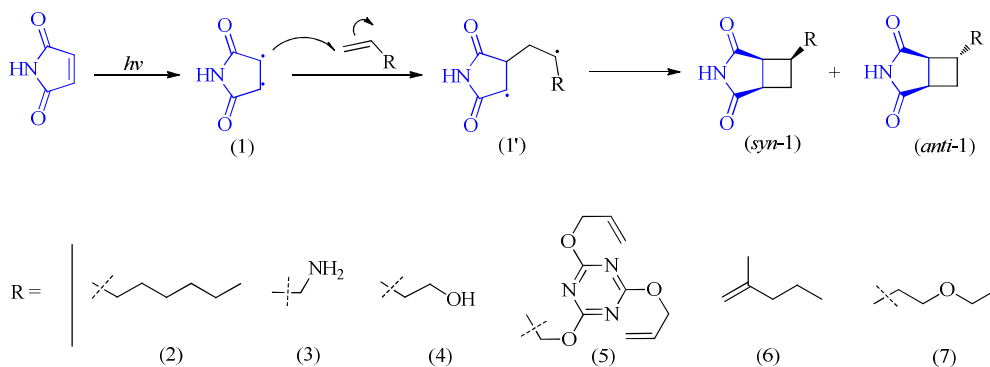
Scheme 6.1: First row: Mechanism of the alkene-enone [2+2] cycloaddition yielding to two diastereomers.[149] Second row: Overview of the tested alkene compounds in the UV-cyclization.

Alternatively, the same batch reaction was performed in an immersion well photoreactor (Photochemical Reactors Ltd., UK) with a 16 W lamp with an emission peak at 254 nm. Similar results were obtained as for the other reactor (data not shown).
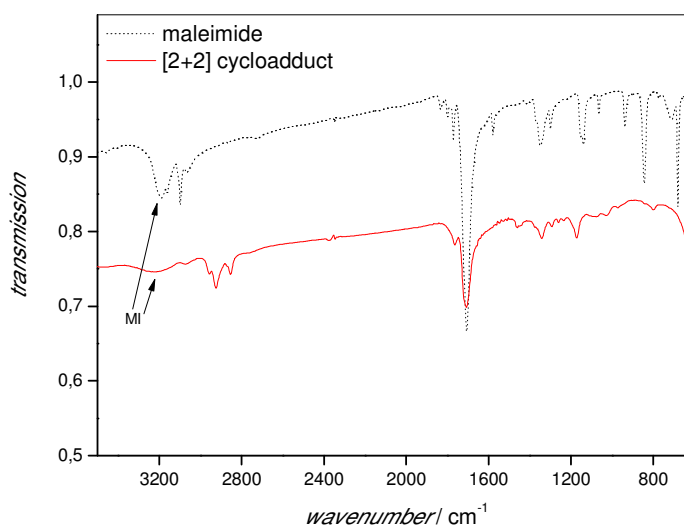
Fig. 6.1: Overlay of IR spectrum of [2+2] cycloadduct and maleimide

Table 6.1: Influence of the excess of octene towards the cycloaddition with maleimide (1.0 equiv., 0.104 M in ethyl acetate solution).[a]

Entry	X_{MI} / % [b]	$X_{[2+2]adduct}$ / % [b]
5.0 equiv	38	62
10.0 equiv	8	92
15.0 equiv	9	91
20.0 eqiuv.	6	94

[a]The reaction solutions were degassed by N_2 purging and irradiated for 24 h.

[b]Yields determined by GC/MS.

6.3.1.2 Minimum required reaction time for a batch reaction

After determination of the minimum excess of alkene required, the kinetics of the reaction were studied in both reactors. Yield-time correlations are plotted in **Fig. 6.2**. As seen, the yield drops significant at reaction times below 8 h for the multilamp reactor and 12 h for the immersion well photoreactor. The difference between both reactors can be most likely explained by the different light intensities and differences in the light spectrum of the light sources. The multilamp reactor illuminates the sample with 6 × 15 W (254 nm) while the

immersion well reactor irradiates only with 1 x 16 W (254 nm). Yet, both reactors showed consistent results, exemplifying that both wavelength regions can be used for activation of the cycloaddition. It should be noted, that when using a higher light intensity (400 W at 360 nm) in the immersion well reactor, reactants and products underwent decomposition after already moderate reaction times, thus increasing the light intensity did not necessarily lead to improved reaction yields or reaction times.
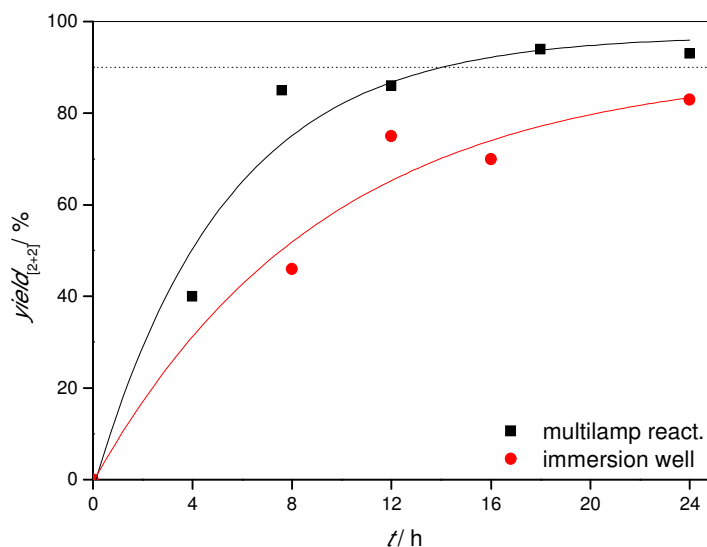
Fig. 6.2: Time/yield-dependence for the [2+2] cycloaddition between maleimide (0.104 M) and octene (10 equiv) in ethyl acetate solution. All yields were determined by GC/MS.

From the batch reactions it is hence evident that c*lick*-like conditions cannot be reached. Reaction times are rather long (in principle not in contradiction with the definition by Sharpless, but of course generally not favorable) and the required tenfold excess of the ene compound makes the reaction uneconomical in most cases. Thus, in the next step we performed the reaction in a flow reactor to improve the performance of the reaction.[153]

6.3.2 Continuous reactor system

6.3.2.1 Comparison between batch and flow mode
The flow UV-reactor was installed as described:[50] The commercial quartz cooling mantle of the immersion well photoreactor was wrapped tightly with a non-airpermeable fluoropolymer (PFA) tubing, tempered at 15°C and connected to a peristaltic pump. As UV sources two different lamps were available (16 W, λ_{max} = 254 nm and 400 W, λ_{max} = 365 nm). More information, that is detailed descriptions of the setup alongside photos, can be found in **Ch. 10.2**.

The benefit of such setup is that the reaction mixture is as close as possible to the UV-lamp and due to the small inner diameter (I.D. 0.75 mm) of the tubing the whole solution is irradiated homogeneously. Even though only one layer of tubing was wrapped around the reactor, 25 m tubing (V = 11 mL) could be accommodated offering a much bigger surface area compared to a round-bottom flask of the same volume.

Similar to the batch process the molar ration between maleimide and octene required to obtain of full maleimide conversion was determined. Therefore, 1 equiv. maleimide was mixed with decreasing equivalents of octene to check for the minimum amount before the yields drop below acceptable numbers (**Fig. 6.3**).
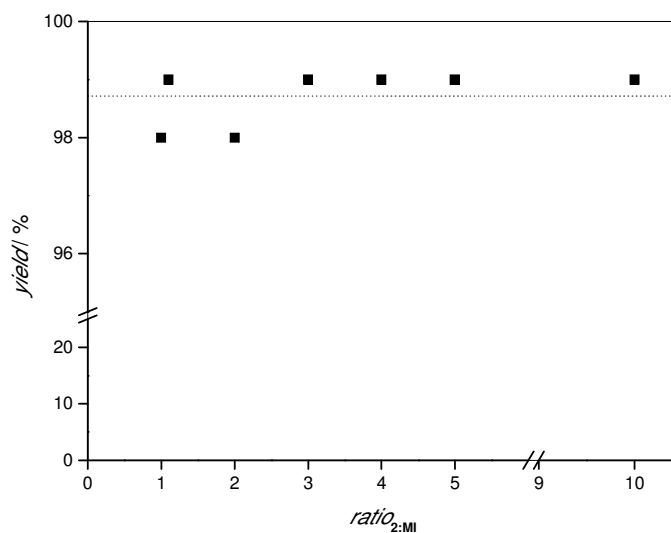
Fig. 6.3: Influence of the octene excess towards the yield of cycloadduct at reaction of 0.01 M maleimide with 1-10 equiv. octene and an irradiation time of 10 min using a 16 W low pressure UV-lamp. All yields were determined by GC/MS.

In all tested ratios, excellent maleimide conversions were observed already after 2.5 minutes at even better results than in the optimized batch reaction. Even in a 1:1-ratio the yields were almost complete, varying between 98 and 100% conversion of the [2+2]-adduct. Yields were determined via GC/MS analysis to simplify product characterization (**Fig. 6.4**), but were also cross-checked via NMR analysis.
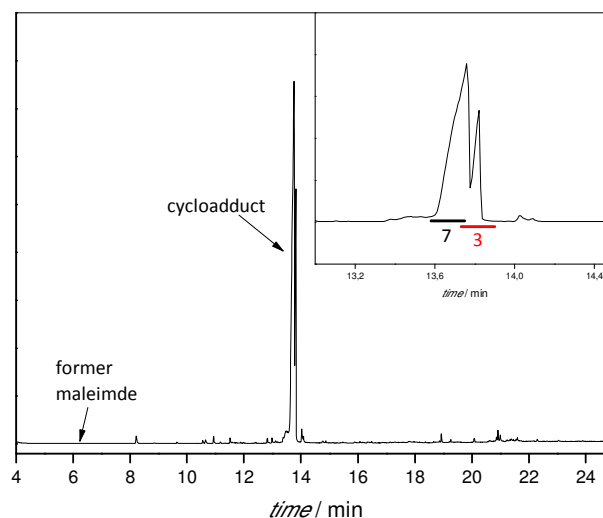
Fig. 6.4: GC/MS spectrum of [2+2] cycloadduct of maleimide and 1-octene. Diastereoisomere ratio is about 7:3.

6.3.2.2 Determination of the limits of the flow reactor (residence time and concentration)

From the above observation it can be already concluded that the reaction yields a stable compound, proceeding on only one reaction trajectory, allows for complete conversions and can be carried out strictly under a 1:1 ratio at ambient conditions. Otherwise lower yields would be the direct consequence. Therefore, it already fulfills five of the *click* criteria conceived by Sharpless *et al*.[26,31] Compared to the batch mode an enormous acceleration was observed, in line with literature observations. Taking the differences in octane excesses not into accound, a rate acceleration by a factor of more than 100 is achieved. In an attempt to further optimize the reaction, additional kinetic trials were carried out. The minimal residence time in the reactor was determined to 2 min to achieve a yield above 95% for the 16 W UV lamp (**Fig. 6.5**). If the residence time in the flow reactor was shorter the reaction was not complete. Further improvement of the reaction can be achieved when the light source is changed for a 400 W medium-pressure UV-lamp (operating at 365 nm), for which the minimum residence times can be decreased to 1.25 min. Similar to the lower power lamp the yield of the cycloadduct dropped below 90% starting from 1 min of residence time. It should be noted additionally, that the gain in efficiency with the 400 W light source is not only reaction time, but also reactant concentration that can be converted. For the kinetic study, also the sample concentration was increased tenfold to 0.1 mol·L^{-1}, thus with the higher light intensity, a largely

improved throughput of material and thus total amount of product per time interval was obtained.
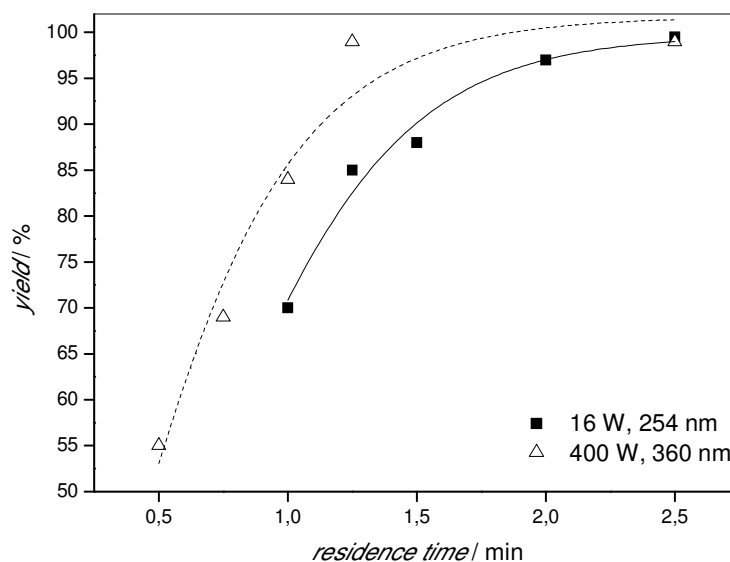
Fig. 6.5: Yield/residence time dependence for the ■ 16 W; 254 nm lamp (0.01 M Maleimide, 0.01 M octene in ethyl acetate solution) and the Δ 400 W; 365 nm lamp (0.1 M Maleimide 0.1 M, 0.1 M octene in acetonitrile solution).

As shown in **Table 6.2**, increasing the concentration to 0.1 M leads to unsatisfying 6% [2+2] adduct conversion after 2.5 minutes. By changing to the more polar solvent acetonitrile the yield could be increased to moderate 23% which is, however, still unsatisfactory. Replacing the 16 W lamp by the much stronger 400 W lamp, however, allowed again for complete conversions even with 0.1 M solutions. As described above, the 400 W lamp thus not only leads to faster reactions, but also for much higher concentrations of reactants to be processed. It should be noted that the concentration is a relatively crucial parameter for assessing the potential for upscale of the process. The concentration of the reactants is directly proportional to the amount of product accessible in a given time interval. With the reaction time of 1.25 min and 0.1 M solutions, 184 mg·min^{-1} of product can be produced in the self-made laboratory flow reactor, which accumulates to 265 g·day^{-1} and thus a multiple of what is accessible in the same reaction time in the batch process. Since upscaling is an implicit criterion in the *click* philosophy, this feature of the flow reaction should certainly not be neglected.

Table 6.2: Influence of the lamp power for high concentrated sample solutions at equimolar amounts of reactants.[a]

c / mol L^{-1}	Solvent	Lamp	Yield / %
0.01	ethyl acetate	16 W (254 nm)	99[b,c]
0.1	ethyl acetate	16 W (254 nm)	6[c]
0.1	acetonitrile	16 W (254 nm)	23[c]
0.1	acetonitrile	400 W (365 nm)	99[b,c]

[a]The reaction solutions were degassed by N_2 purging and irradiated for 2.5 min.

[b]Yields determined by GC/MS.

[c]Yields determined by NMR.

6.3.2.3 Application of the photocycloaddition with various alkenes

The practical last requirement for a *click* reaction is wide scope. Only if the reaction is truly orthogonal (thus also tolerant to a significant number of other functional groups), it can find application in a broader sense. The [2+2] cycloaddition hence needs to be tolerant towards other functional groups (similar to a Paternò-Büchi reaction) and be applicable for other alkene derivatives.[103] Therefore, four functional alkenes bearing amine, alcohol or further alkenes moieties were tested towards the photocycloaddition (**Scheme 6.1**). The reaction with allylamine (**3**) was accomplished in a high yield of 98% proving that the maleimide ring is stable towards nucleophilic attack for short exposure times (**Table 6.3.**). The cycloaddition between maleimide and 3-butenol (**4**) allowed for high yields of 84% at somewhat longer residence times (t_{res} = 5 min), which might still be seen as an acceptable outcome certainly when compared to the batch process. Interestingly, the cycloaddition with triallyl cyanurate (**5**) yielded a single modified [2+2] cycloadduct with a reasonable yield of 73%, which can be improved 94 % by using the 400 W lamp (also at the increased 0.1 mol·L^{-1} concentration as in the previous experiments) rather than the 16 W counterpart. The two other allyl functions stayed intact (in principle, they could undergo crosslinking) offering further conjugation points, which plays a vital role for e.g. dendrimer synthesis. Also, double attachments of maleimide potentially occur and might explain the slightly lower yield of the reaction. Another reason for the slightly reduced yields of the reaction (with the 16 W lamp) in case of compound (**4**) and (**5**) may be a reduced light efficiency yield being operational is in these cases, which can be solved in principle by employing longer reaction times or again by using a high power lamp for irradiation. A steric demanding methyl substituted alkene like 2-methylpentene (**6**) gave a complete conversion (>99 %) even with the 16 W lamp after 2.5 minutes and is thus the most efficient alkene tested in the setup so far. The addition of the methyl group may have a positive inductive effect and thus

increase reactivity. Finally, also an allyl ethyl ether (**7**) was tested to screen further functionalities (allyl ethers are interesting moieties since they can be used as bridges to introduce allyl groups to a large number of compounds. The allyl ether had the lowest reactivity in the experiments, yet with the extended reaction time of 5 min while also using the 400 W lamp, almost full conversion could be obtained. Thus, the flow cycloaddition can be utilized in presence of various functional groups. Amines, alcohols and ethers seem to be tolerated. Additionally, esters should in principle be stable as well, since the maleimide does not undergo reactions with itself under the conditions used in our study; studies on the Paternò-Büchi reaction underpin that [2+2] cycloadditions are in principle tolerant to esters and halogens.[125] Further, also styrene was tested as a model compound for the flow reaction, however only limited conversion (50%) of styrene into product was observed. Potential problems associated with styrene might be the ability of this substance to undergo polymerization, which necessarily lowers the maximum yields.

Table 6.3: Overview of the yields of different alkenes reacted with maleimide. 1:1 ratio of alkene:enone, 0.01 M in acetonitrile.[a,b,c]

Alkene	Yield / %	
	t_{res} = 2.5 min	t_{res} = 5 min
allylamine	98[a]	---
3-butenol	50[a]	84[a]
triallyl cyanurate	73[a] / 94[b]	71[a]
2-methylpentene	>99[a]	---
allyl ethyl ether	70[b]	94[b]

The reaction solutions were degassed by nitrogen purging and irradiated:

[a]16 W lamp (λ = 254 nm); [b]Using a 400 W lamp (λ = 360 nm)

[c]Yields determined by ^{1}H-NMR.

6.4 Conclusion

By using a custom-made UV-flow reactor, the UV-induced [2+2] cycloaddition could be optimized. Very high reaction yields were obtained in short reaction times. The reaction between an alkene and maleimide, which requires large alkene excesses in batch reactions was performed under strictly equimolar reactant ratios in flow, which is a very important factor in materials synthesis, where separation of starting materials from products can be a substantial issue. Thus, the cycloaddition reaction, which under normal reaction conditions is far from being classified as a very efficient reaction, comes very close to fulfill the strict criteria of a *'click'* reaction as defined by Sharpless and others (with the exception of stereoselectivity). Thus, it could be shown that flow chemistry can – at least in the presented case – allow efficiency gains in reactivity that push a reaction from a mere synthetic tool towards *click*-like conditions. Rate enhancements of more than a factor of 100 could be observed, making the cycloaddition a very powerful tool for molecule conjugation. Products could be obtained in very high yields directly, making further purification unnecessary. High intensity UV lamps increased the yield of the reaction significantly, while the choice of peak wavelength (254 vs. 365 nm) seems to be of minor influence. Reactions were carried out at ambient reaction conditions and various alkenes carrying alcohol, ether, amine of vinyl functions could also successfully be attached to the maleimide. The application of flow chemistry makes this [2+2] cycloaddition an example for a highly-efficient photo-induced process.

The described procedure is thus a (further) prime example of how the efficiency of a UV-induced reaction can be improved by orders of magnitude by using simple flow chemistry. It is important to note that such flow setup is comparatively cheap and simple to assemble. While the batch reaction usually allows only for synthesis of small amounts of product, the flow reactor as described herein could directly be used to produce more than 250 g of product per day, which can still be increased by parallelization or extension of the reactor volume without essentially the need of re-optimization.

Chapter 7
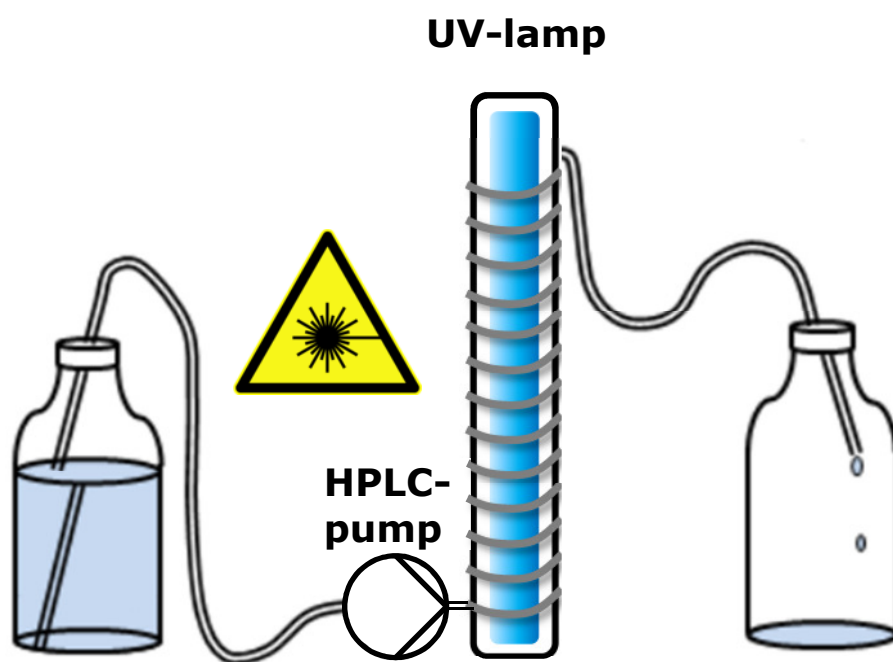
7. Fast and efficient photoinduced alkene-enone cycloaddition for polymer modification by applying UV-flow reactor technology[**]

7.1 Abstract

The alkene-enone [2+2] photocycloaddition reaction between polymer-bound maleimide and functional alkenes has been tested in a UV-flow reactor, demonstrating a very high efficiency of the reaction. As a test reaction, polymer end group modifications were carried out on maleimide-functional poly(butyl acrylate). The polymer was prepared by atom transfer radical polymerization (ATRP) using a N-hydroxysuccinimide-functionalized initiator, followed by an exchange reaction of the activated ester with a maleimide amine linker. Good control over the polymerization and successful exchange of the end group under mild reaction conditions was confirmed by electrospray ionization mass spectrometry (ESI/MS). The terminal maleimide group was then reacted quantitatively with alkenes in a custom-made tubular UV-flow reactor within a minute reaction time. This significant acceleration of the reaction was achieved by employing a photosensitizer in combination with the flow reactor technique. Via the cycloaddition a variety of functional groups can be introduced to the polymer chain ranging from multifunctional allyl-compounds to hydroxyl-functional alkenes, demonstrating the general versatility and high potential of the approach for polymer modification reactions.

7.2 Introduction

Photo-induced [2+2] cycloadditions are a well-known synthetic tool in organic chemistry.[56,60] Via this class of reactions, simple access is given to four membered (heteroatom) ring structures. Different varieties of [2+2] reactions have been extensively applied for the preparation of natural products or drug design[48] where four-membered ring structure are a common leitmotif.[61,91,144] Next to total synthesis, the scope of [2+2] reactions is extended by using them also as conjugation tools to couple two building blocks to each other. In previous studies, we have shown that the Paterò-Büchi reaction (between a terminal aldehyde and a vinyl compound) can be a useful tool for polymer end group modification[103] as well as for dense surface grafting of nanoparticles.[140] Conjugation proceeds in batch mode under high efficiency, however – as a general limitation – quite large excesses of the vinyl compound (> 10 eq) have to be used alongside extended UV illumination times (> 15 h), which limits the applicability of the reaction for material design purposes. In order to optimize

---

[2+2] reactions as conjugation tools, different substrates were tested with good results for maleimide (derivates) in alkene-enone photocycloadditions. Maleimides are easily excited to a triplet state via UV irradiation and can thus serve as excellent conjugation moieties (see **Scheme 7.1**).
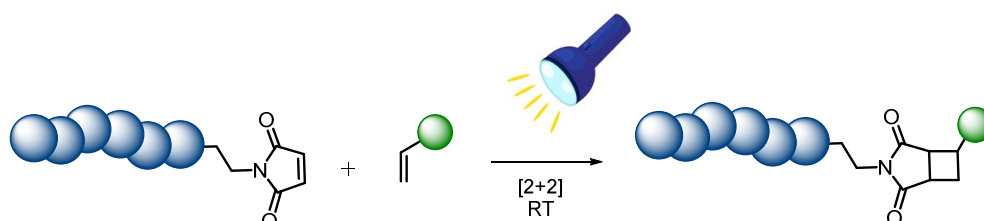
Scheme 7.1: Alkene-enone maleimide [2+2] cycloaddition as a conjugation tool in polymer synthesis

Maleimides are also known as key functionalities in polymer conjugation reactions, namely in thiol-ene and Diels-Alder conjugations, thus two of the most prominent *click*-type approaches used in macromolecular chemistry.[26,31,35,88,159,167,168] Another advantage of photo cycloadditions is its orthogonality towards 'classical' heat-induced reactions.[85,169] [2+2] Additions can hence be independently triggered and different ligation reactions towards maleimide-containing substrates can be achieved in a controlled manner by switching from thermal activation to photo irradiation, allowing a 'dual use' of the functionalities.

In many cases photo reactions suffer from long reaction times; several hours to days are not uncommon to form a desired product in high yields. The long reaction times derives mainly from low light efficiencies, which is often due to too strong light absorption (leading to light intensity gradients) or inefficient energy redistribution.[51,147,148] Generally, for [2+2] cycloadditions to proceed, the first step is the excitation of the ground state of a UV-absorbing ene to create a reactive intermediate which can be quenched by a second alkene, yielding the [2+2] cycloadduct. It is assumed that the mechanism proceeds through an exciplex.[149–151] It should be noted that different stereo- and regioisomers can be obtained in the reaction, which poses a certain limitation for its use in natural product synthesis. For pure conjugation reactions –the formation of stable C-C linkages as often required in polymer reactions – play regio- and stereo selectivity a minor role. In such case, only the yield per time is a limitation, which can be greatly improved when changing the reaction mode from batch to a flow chemistry approach.[50,79,152–155]

By applying the alkene-enone [2+2] cycloaddition between a variety of alkenes and maleimide in a continuous UV-flow reactor, we demonstrated that the reaction rate was increased from days to minutes at equimolar reagent ratios while still allowing for complete conversion to the [2+2] cycloadduct. Hence reaction conditions were met that come in terms of efficiency at least close to classical *click* conjugation reactions.[76] For the flow process, a relatively simple custom-made UV-flow reactor consisting of thin translucent PFA tubing wrapped around a quartz cooling mantle containing a high-power UV-light source was employed. Efficiencies in such reactors are generally increased due to the small optical path lengths that need to be passed, which is followed by a homogeneous excitation in the whole reaction medium. UV-initiated/triggered reactions in this manner are sped up significantly, be it in the realm of polymer synthesis or in the realm of organic chemistry.[170,171] Also, flow reactions have the advantage that the optimized reaction can be up-scaled without too much effort.[172]

In here we demonstrate how the [2+2] alkene-enone cycloaddition between alkenes and maleimides is translated from a small molecule reaction – as we had previously described – to a polymeric system, i.e. poly(butyl acrylate), PBA, substrates. We will introduce a novel synthesis route towards maleimide functional polymers from a combination of controlled polymerization and activated ester transformation. The so-obtained polymers were tested towards their performance in photocycloadditions in a custom-made continuous UV-flow reactor.[50] As we showed, [2+2] photoconjugations between polymer and a variety of alkenes proceed fast (in the order of few minutes) under these conditions, whereby the photo stability of compounds and reaction rates were largely improved by applying an aromatic photosensitizer.[52,53,148] Efficiencies close to that of UV-induced thiol-ene conjugations were achieved. The flow reactor was operated under stable conditions without clogging of the reactor lines, giving direct access to a scalable process. More than a synthesis method for end-functional polymer materials, the demonstrated photoreaction can be seen as a proof that this type of reactions proceeds quickly and in high yields if reaction conditions are chosen carefully. [2+2] Cycloadditions can serve as a highly useful tool in polymer reactions for a variety of modification reactions.

7.3 Results and discussion

The flow reaction of maleimide with vinyl components had been demonstrated in our previous study, we hence focused in this work directly on polymers bearing maleimide end groups to extend the scope of the reaction. As a model polymer PBA was chosen. To allow the use of ESI/MS as characterization tool, end group functional PBA has been modified in the following. The in here presented

reactions are examples for the wide scope of the alkene-enone cycloaddition. They should proceed with similar results on other polymer types and on polymers with multiple maleimide functions.

7.3.1 Preparation of a maleimide-functional PBA

Preparation of maleimide-functional polymers – even though being highly valuable materials as noted above – is not very straight forward. Polymerization of maleimide-functional initiators via reversible deactivation radical polymerization leads to fast copolymerization of the maleimide into the backbone. The result is then a crosslinked polymer network in place of linear maleimide-functional chains. To overcome this problem, maleimide initiators are classically protected in Diels-Alder reactions with furan prior to polymerization. After polymerization, the furan is then removed via thermal treatment of the polymer in a retro Diels-Alder reaction. While generally successful, this approach is not without problems since high temperatures may be harmful to some polymers and lead to endgroup-degradation if not carried out with care. We thus opted to use an alternative pathway by employing an activated ester strategy. Isolatable activated esters, such as pentafluoro phenyl groups[173] can be used in versatile fashion to introduce a variety of functional groups in polymer substrates by simple exchange reactions. Being mostly used in biochemistry, also N-hydroxy succinimide (NHS) esters are well known functions to serve this purpose. NHS esters act, when build into a polymer, as a place holder that is easily exchanged by any amine after polymerization forming a stable amide linkage. Under ambient conditions, exchange reactions are usually quickly and quantitative.

In a first step we synthesized a NHS-functional ATRP initiator by reacting NHS with 2-bromopropanoyl bromide, yielding 2,5-dioxopyrrolidin-1-yl 2-bromopropanoate, (for structure see **Scheme 7.2** (1)). In the second step, the so-obtained initiator was used in conventional ATRP under standard reaction conditions (**Scheme 7.2** (2)), yielding well defined polymers (M_n = 1300 g mol^{-1}, $Đ$ = 1.18) with a high end group fidelity. Notably, polymers were synthesized with low molecular weight on purpose in order to enable mass spectrometry analysis for tracing end group reactions, which is complicated with higher molecular weights. Polymers with higher molecular weights could though also be synthesized without problems.
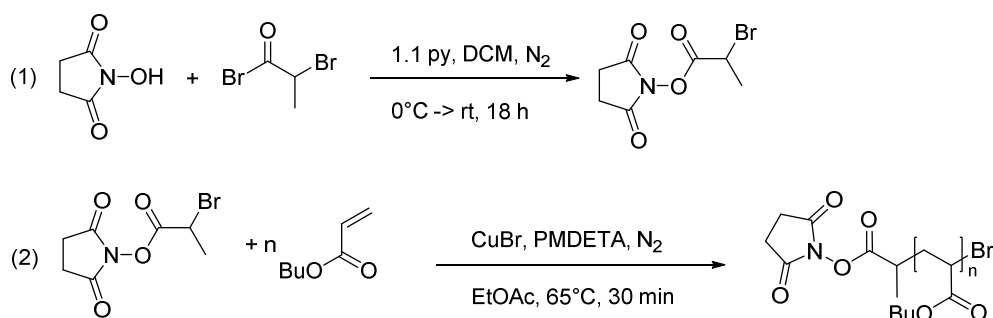
Scheme 7.2: (1) Synthesis of the NHS bearing ATRP initiator. (2) Controlled polymerization employing the initiator.

To add a maleimide functionality to the NHS end-functional polymer, a maleimide linked to a (primary) amine is required since a direct exchange between NHS and maleimide is unsuccessful. The amino group of aminoethanol was boc-protected, followed by linking the maleimide via a Mitsunobu reaction to allow a high reaction efficiencies. Deprotection is in the last step performed via trifluoroacetic acid (TFA) solution yielding the associated TFA salt as a white powder. The NMR data can be found in the Supporting Information S2 of the corresponding paper.[174]

7.3.2 Preparation of maleimide functionalized polymer
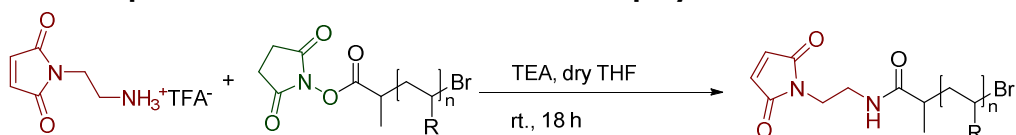
Scheme 7.3: Introduction of maleimide endgroup to the NHS-activated polymer endgroup.

To exchange the NHS ester with the maleimide linker, reactions had to be performed in basic environments to free the amine from the TFA salt (see **Scheme 7.3**), for which TEA was used. Success of the reaction was approved by ESI/MS. Inspection of the mass spectra given in **Fig. 7.1** demonstrates that the end group exchange was successful. The most significant peaks in the spectrum can be clearly assigned. Experimental as well as theoretical *m/z* are summarized in **Table 1**. All NHS-related peaks (A_{Br}) have almost quantitatively disappeared

from the spectrum and the main product is the desired maleimide-functional product $\boldsymbol{B_{Br}}$. The only mentionable side products observed, is a species that is isobaric formally with a maleimide dimerization reaction product between the maleimide amine linker and maleimide functional polymer ($\boldsymbol{C_{Br}}$). This species could, however, also simply be a physical adduct that forms during the ESI process (as is indicated by absence of an analogue $\boldsymbol{C'_{Br}}$ species). Regardless, $\boldsymbol{C_{Br}}$ occurs in acceptable low abundances and does not interfere with the following reaction steps and indeed disappears in the following reaction steps (see discussion below). In small quantities, also some proton-terminated (but yet maleimide-functional) polymer is observed which originates from disproportion products that formed during the ATRP process ($\boldsymbol{B_H}$). Tthe spectrum displays a relatively large number of peaks due to the ammonium salt [$C_4H_2NO_2$-$(CH_2)_2$-NH_3^+; elemental formula $C_6H_9N_2O_2^+$] being able to act as a counter ion, thus doubling the number of peaks visible in the spectrum. Unassignable, low abundant peaks might stem from different counterions.

In summary, the NHS synthesis route allows to synthesize maleimide-functional polymers with overall good success. Both the synthesis of the ATRP initiator as well as the maleimide ammonium linker are simple to prepare in significant quantities. Polymerization in presence of a NHS ester is largely unproblematic and proceeds under the usual reaction conditions, as demonstrated for a number of systems before.[175–178] The exchange of the NHS ester by the maleimide linker proceeds efficiently, whereby access is given by rather mild reaction conditions compared to the (retro) Diels-Alder method. Such amine exchange reactions usually are carried out on much shorter time-scale, which is in the present case hindered by the TFA salt. If the amine would be set free from the salt prior to the reaction, reaction times could probably be reduced to tens of minutes, which in the present case was, however, not required.
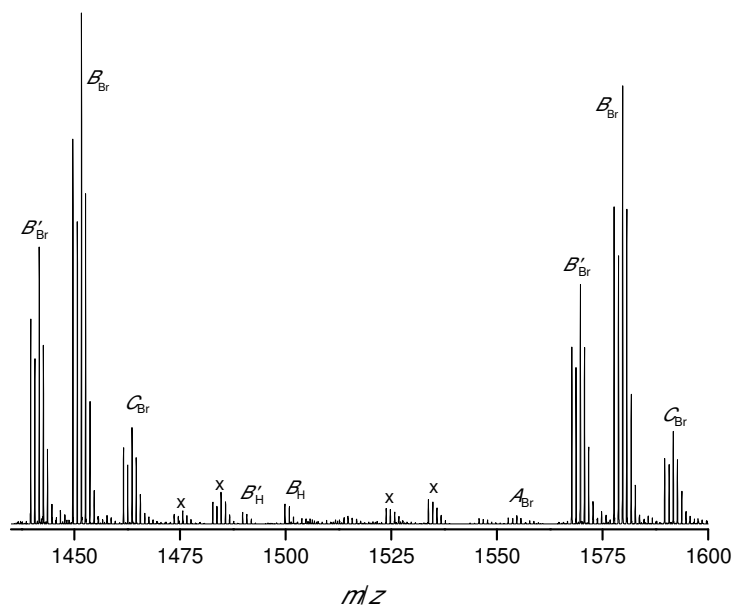
Fig. 7.1: NHS end group exchange of PBA end groups by maleimide linker as monitored by high-resolution ESI/MS. Peaks marked with "x" could not be assigned to any species.

Table 7.1: Experimental and theoretical *m/z* values for the peaks identified in the spectrum given in **Fig. 7.1**. Main products are marked in bold.

Symbol	End group 1	End group 2	*DP*	Ion	m/z_{theory}	m/z_{exp}
A_{Br}	NHS	Br	9	Na$^+$	1552.790	1552.791
B_{Br}	**maleimide**	**Br**	**9**	**Na$^+$**	**1577.822**	**1577.822**
B_H	maleimide	H	10	Na$^+$	1499.911	1499.916
B'_{Br}	**maleimide**	**Br**	**8**	**C$_6$H$_9$N$_2$O$_2^+$**	**1567.815**	**1567.820**
B'_H	maleimide	H	9	C$_6$H$_9$N$_2$O$_2^+$	1489.904	1489.909
C_{Br}	**'dimer'**	**Br**	**8**	**Na$^+$**	**1589.797**	**1589.797**

7.3.3 Alkene-enone cycloaddition

With the precursor maleimide-functional polymers at hand, polymer modification in the [2+2] ene-enone reaction were targeted. Therefore, reactions were carried out in a UV batch reactor, according to our previous study on Paternò-Büchi conjugations.[103] Reactions in batch were successful with comparable efficiencies (long reaction times, large excess of alkene) as observed before. We then proceeded quickly to the UV-flow reactor.[76] The reaction efficiency of the [2+2] cycloaddition was mapped for the reaction of the PBA-malemide with a small model compound (see **Scheme 7.4**). 2-Methyl pentene **1** and 1-octene **2** were used to optimize conditions. Since pure maleimide alkene-enone cycloadditions proceeded in flow within few minutes, the reaction was tested at a wavelength of 254 nm (16 W) for short timespans (1-8 min, regulated by adjusting the flow rate). Acetonitrile was chosen as a solvent due to its inertness and low UV-absorption profile. PBA-maleimide ($c = 8 \cdot 10^{-4}$ mol L^{-1}, M_n = 1300 g mol^{-1}) and alkene (10 eq) in acetonitrile solution were irradiated at 4 °C. Under these conditions, no reaction with octene was observed, while the reaction with the secondary alkene, 2-methyl pentene yielded 45% cycloadduct. Increase in yield by choosing higher reaction times failed due to the onset of polymer degradation. The full ESI/MS spectra of the degrading materials can be found in the according paper.[174]

These results are in contrast to our previous findings based on small model molecules. A shift in maleimide absorption to form the triplet state cannot explain the reason the loss in reactivity since the polymer displays an almost unchanged UV absorption at 275 nm for the maleimide when bound to the polymer. On the other hand, a reduction of reaction efficiency can be expected when switching from small molecules to polymer systems, because the polymer chain can sterically shield the end group or absorbs light. To enforce the reaction, the flow experiments were repeated employing a stronger UV-lamp (400 W) with higher light emission wavelength (λ = 365 nm) to avoid potential absorption of light by the acrylate polymer itself. With the 400 W light source, residence times above two minutes resulted in heavy degradation of the polymer, as evidenced by mass spectrometry and THF-SEC.
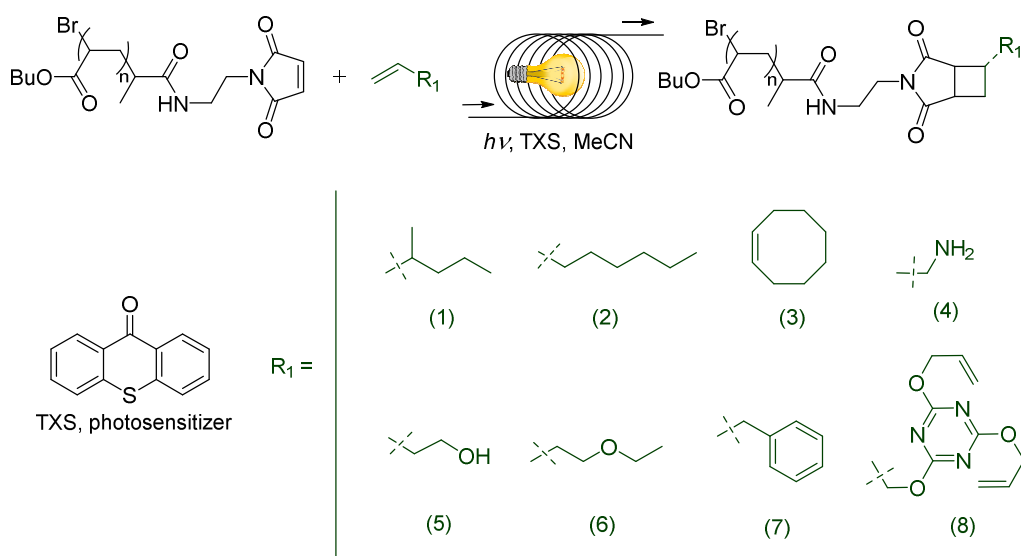
Scheme 7.4: [2+2] photo-induced alkene-enone polymer cycloaddition in flow in presence of the thioxanthone photosensitizer TXS.

The reaction time was reduced to the residence time where no degradation was yet, or at least not clearly observed (1.1 min, flow rate of 10 mL·min⁻¹). With thioxanthone (TXS, λ_{max} = 378 nm), known to act as a photosensitizer for alkene-enone cycloadditions[53] further experiments were performed at this short residence time (note that low residence times are equivalent to high flow rates and fast synthesis of materials at large scale). TXS absorbs light efficiently and transfers the energy to the maleimide.[52] The UV-Vis spectra of the PBA-maleimide and TXS can be found elsewhere.[174] Again, the use of TXS was tested towards the conjugation of the primary and secondary alkene **1** and **2**. The concentration of TXS varied from zero to 10 mol% according to the polymer alongside a 10-fold excess of alkene (polymer concentrations are typically low, 8·10⁻⁴ mol L⁻¹, thus TXS concentrations as well as alkene concentrations were still in an adequate level. As evident from **Table 7.2**, the yield of reaction increased significantly from zero and 50% to almost quantitative conversion for both alkenes. The usage of the same TXS concentration in a batch [2+2] cycloaddition did not result in significant yields on the time scale (1 h, yield = 23%). The acceleration of the reaction is a result of the combined action of TXS and the flow processing, not just of one of both.

Table 7.2: Conjugation yields (conversion of maleimide) for the UV-cycloaddition of PBA-maleimide at $c_{PBA} = 8 \cdot 10^{-4}$ mol·L^{-1} in presence of a ten-time excess of alkene under variation of the photosensitizer concentration TXS at a fixed residence time of 1.1 min in the UV-flow reactor.

mol%$_{TXS}$	yield$_{[2+2]}$ /%	
	octene	2-methyl pentene
0	≈ 49*	55*
10^{-3}	-	48*
10^{-2}	-	35.0
10^{-1}	53.4	41,8
1	71.4	69.4
10	> 95	> 95

*Polymer degradation observed

Interestingly, presence of small amounts of sensitizer did not lead to quantitative conversion, but still significantly reduces the occurrence of photodegradation. TXS served a double purpose in the reaction as photocatalyst, but also in preventing unwanted side reactions. From roughly 0.1 mol% on, increasing yields were observed for the [2+2] cycloaddition, also allowing to couple 1-octene, which showed no activity in the flow reactor before. Reaching 10 mol% of TXS compared to polymer, practically quantitative conversion to the desired product was observed. The difference between the reaction with and without TXS is depicted in **Fig. 7.2** for the less active 1-octene as reaction partner. ESI/MS spectra with 0 and with 10 mol% were overlapped, showing clearly the degradation that occurs in absence of TXS and the almost pristine end group distribution that is achieved in presence of it. A list of m/z for the individual peaks is given in **Table 7.3**. Peaks in the spectra that were unassignable (degradation products) are marked with a cross. The according data of the mass spectrum for the secondary alkene is in general comparable and shows less degradation products.[174]

Interestingly, the species **C_{Br}** that (seemingly) was present after the (non-UV) reaction of the NHS-functional PBA, practically vanished after the reaction in presence of TXS, indicating a measurement artifact. However, if it was a physically present species, its disappearance can be explained. As was demonstrated before,[55] maleimdies also form dimers in a photocycloaddition. These reactions are reversible when irradiated at wavelengths below 250 nm. A study of Horie *et al*. examined the formation of maleic anhydride photo-dimers

in a microreactor and found that by installing a pyrex glas filter (UV cut-off at 280 nm) in front of the UV lamp avoids photosplitting.[164] Thus, in our setup, photosplitting – here then a desired reaction – can take place. Regarding polymer dimerization, we detected a slight increase in molecular weight after the flow reaction from 1300 g·mol⁻¹ up to 1750 g·mol⁻¹ with, however, unchanged polydispersity. A doubling of molecular weight was not observed and the change may be attributed to the limited reproducibility of SEC as well as to the fact that a changed endgroup does at such short chain lengths significantly alter the hydrodynamic volume. Additionally, ESI/MS did not show any species affiliated to a maleimide polymer dimer of two polymer chains; neither single nor double charged. It is hypothesized that – should a dimer be formed during the flow reaction – immediate cleavage of the maleimide dimer but not the desired alkene-enone product occurs due to the presence of high-energy light (< 250 nm). Absence of dimerization products was observed in all reactions carried out.
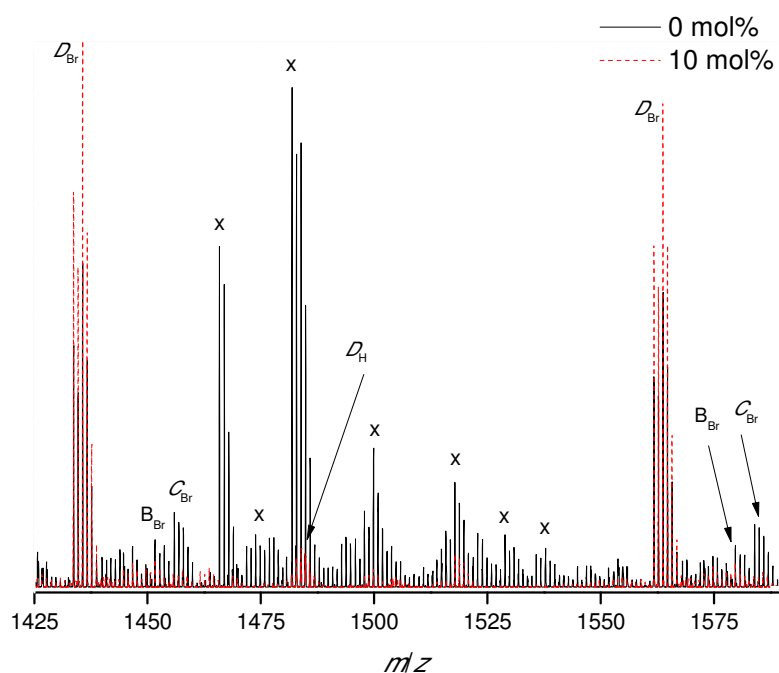
Fig. 7.2: ESI/MS spectrum of the PBA-maleimide [2+2] cycloaddition product from flow reaction with 10 eq. octene under irradiation at 365 nm (400 W) with (10 mol%) and without the photosensitizer TXS for 1.1 min residence time at 4°C.

Table 7.3. Overview of the species detected in ESI/MS (see Fig. 7.2) for the photo-induced cycloaddition between PBA-maleimide and octene with and without TXS. The observed main product is given in bold.

Symbol	End group 1	End group 2	DP	Ion	m/z_{theory}	m/z_{exp}
B_{Br}	maleimide	Br	9	Na^+	1577.822	1577.822
B_H	maleimide	H	10	Na^+	1499.911	1499.916
B'_{Br}	maleimide	Br	8	$C_6H_9N_2O_2^+$	1567.815	1567.820
B'_H	maleimide	H	9	$C_6H_9N_2O_2^+$	1489.904	1489.909
C_{Br}	'dimer'	Br	8	Na^+	1589.797	1589.797
D_{Br}	**[2+2]**	**Br**	**8**	**Na^+**	**1433.780**	**1433.773**
D_H	[2+2]	H	9	Na^+	1483.953	1483.944
$E_{Br,Br}$	dimerization	Br,Br	7	Na^+	1467.566	-
$E_{Br,H}$	dimerization	Br,H	8	Na^+	1517.740	-
$E_{H,H}$	dimerization	H,H	9	Na^+	1567.912	-

7.3.4 Approaching equimolarity

In the tests with TXS, excesses of the alkene were still employed. While reaction outcomes were sufficient, it was of interest if the amount of alkene can be reduced to increase the economic efficiency of the reaction. In principle – if reactions could be carried out under equimolar conditions (as seen with small molecules in flow even in absence of TXS) – also polymer-polymer conjugation would become available for block-copolymers synthesis. Thus, the content of the secondary alkene was systematically varied in presence of 10 mol% of TXS under otherwise unchanged flow conditions. The amount of alkene was varied between 10 to 1 eq., see **Table 7.4**.

Table 7.4: Overview of the reaction yields as determined by ESI/MS for the photo-induced cycloaddition between pBA-maleimide and 2-methyl pentene under variation of the alkene content. The ESI/MS is not fully quantitative, but allows a reasonable assessment of reaction yields for end group modifications.

Entry	equiv. **1**	yield$_{[2+2]}$ / %
1	10	≥ 95
2	8	≥ 95
3	6	≥ 90
4	4	≥ 85
5	2	≥ 90
6	1	≥ 85

High conversions were observed in the full concentration range. However, a minimum excess of 6 eq. is required to reach truly complete conversion, virtually showing no residues of the starting material. Therefore, all further experiments were performed with at least 5 equivalents of alkene to assure the quantitative conversion of the maleimide-functional polymer. Under equimolar conditions, maleimide conversions above 80% were obtained. While this efficiency was not sufficient to reach polymer-polymer conjugation, it is still in good agreement with methods such as UV-induced radical thiol-ene reactions.[37] The maleimide alkene-enone photocycloaddition represents a highly efficient conjugation method that is certainly applicable in side-chain modifications, grafting-to or cross-linking reactions. Studies focusing on these aspects are currently under the way in our laboratories.

7.3.5 [2+2] UV-cycloadditions with functional alkenes in flow
Neither octene nor 2-methly pentene carry a dedicated functional group that are of interest in later application. Thus, alkenes bearing various functionalities were tested, see **Scheme 7.4** (Cyclooctene **3**, allylamine **4**, buten-3-ol **5**, allyl ethylether **6**, styrene **7** and triallyl cyanurate **8)**. Alkene **8** carries three functional alkene groups and can act as a potential cross linker or anchor point for further conjugation reactions. These alkenes represent a broad range of functionalities in order to test for functional group tolerance of the reaction.

All reactions with the alkenes given in **Scheme 7.4** were performed according to the conditions that were optimized with the alkenes **1** and **2**. For tabulated

results see **Table 7.5**. The cyclic alkene **3** allowed likewise yields of above 95% cycloadduct. Allylamine **4** seems not to undergo an alkene-enone cycloaddition; none of the peaks detected in ESI/MS could be assigned to a known species. Alkene **5**, an alcohol, is associated with a maximum yield of 85% while the ether-containing alkene **6**, allowed to reach yields above 90%. In both cases, quantitative conversion may be reached by increasing the equivalents of the reactant. Styrene **7** did not add to the maleimide in a sufficient rate. Only 24% of the expected [2+2] cycloadduct was formed. The 3-armed alkene **8** formed a [2+2] adduct ($\approx$ 80%) successfully with only one of the potential alkene groups being attached.[76,103] A possible double or triple addition of maleimide polymer was not detected in any significant quantity after irradiation. All alkenes **1** – **8** showed a slight increase of number average molecular weight from 1300 g·mol^{-1} to 1700 g·mol^{-1}. As noted above, this can be attributed to SEC calibration variation and to the increased mass of the chains is in the cycloaddition. All ESI/MS spectra for the polymers obtained are displayed in the work of Conradi *et al*.[174] Compared to our last study dealing with [2+2] cycloaddition,[76] between unbound maleimide and alkenes **1** – **8**, similar trends as described in here were observed regarding to the success of the individual reactions and its functional group tolerance.

Table 7.5: Yields of the photocycloaddition reaction in flow of pBA-maleimide with the functional alkenes given in Scheme 4 with c_{PBA} = 5·10[-4] mol·L^{-1} in presence of 0.1 equiv. photosensitizer TXS, irradiation at 365 nm (400 W) and a residence time of 1.1 min at 4°C.

Alkene	equiv. TXS	equiv. alkene	yield$_{[2+2]}$ / %
2-methyl pentene	0.1	4	$\geq$ 95
1-octene	0.1	5	$\geq$ 95
COE	0.1	5	$\geq$ 95
allylamine	0.1	5	--
buten-3-ol	0.1	5	$\geq$ 85
allyl ethylether	0.1	5	$\geq$ 90
styrene	0.1	5	24
triallyl cyanurate	0.1	1*	80

* 3 equiv. when number of functional groups is compared.

7.4 Conclusion

The successful implementation of UV-induced alkene-enone cycloaddition of alkenes with maleimide-functional polymers in a continuous flow reactor was demonstrated. Compared to previously studied batch reactions of similar type, a largely increased reaction efficiency is observed. Instead of reaction times lasting close to a day in batch, quantitative conversion of the starting material was observed after little over a minute reaction time.

Maleimide end-functional poly(butyl acrylate) was synthesized (in batch) via a novel pathway utilizing a NHS functional ATRP initiator. Via such initiator, NHS-functional PBA was obtained, which gives facile access to a maleimide functionality by exchange reaction of the activated ester.

[2+2] cycloadditions between the maleimide endgroup and unfunctionalized alkenes were performed in a custom made UV-flow reactor. After optimization of the reaction conditions, excellent end group conversions were observed when 10 mol% of the photosensitizer TXS were employed alongside a moderate excess of the alkene component. Reaction times are very short, allowing for complete conversion of the maleimide in roughly 1 min. Using the same methodology, also functional alkenes were introduced and conjugated to the polymers, allowing to ligate alcohols, ethers and multi-functional allyl-compounds in satisfactory yields.

Chapter 8
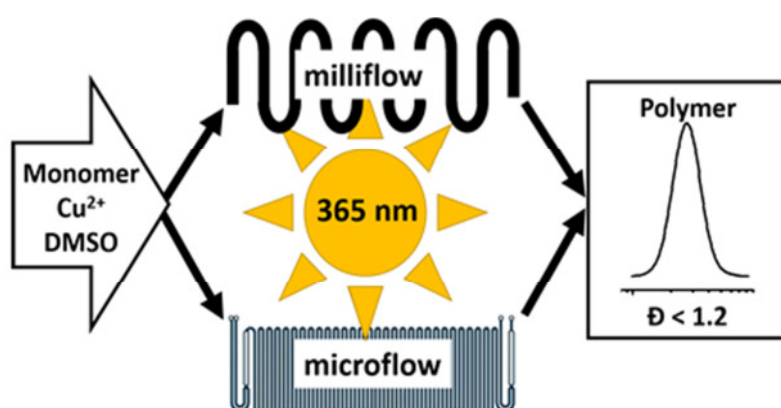
8. Photo-induced copper-mediated poly-merization of methyl acrylate in continuous flow reactors [††]

8.1 Abstract

Photo-induced copper-mediated radical polymerization of methyl acrylate (MA) was carried out in DMSO at 15°C in a tubular photo-flow reactor as well as in a glass-chip based microreactor. Polymerizations proceed rapidly to approximately 90 % monomer conversion within 20 minutes reactor residence time. Control of reactions is high as is evidenced by ideal polymerization kinetics, low dispersities of the obtained polymers (in the range of 1.1) and a linear evolution of number average molecular weights during polymerizations. PMA with average molecular weights between few hundred and ~5000 g·mol^{-1} were obtained under retention of pristine end group fidelity. Besides homopolymers, block-copolymerss can also be successfully synthesized and poly(methyl acrylate)-*b*-poly(butyl acrylate) block-copolymerss with a similar low dispersity are obtained. Reactions proceed under homogeneous reaction conditions. This feature allows for the reaction to be carried out in milli- and also in microflow devices. In both cases, equally good control is achieved with only minimal adaption of the reaction protocol, underpinning the simplicity and fast adaptability of the protocol to different flow reactors.

8.2 Introduction

Flow (micro)reactor technology (MRT) has recently drawn increasing attention by offering a wide range of new possibilities for academic research and industrial production in the polymer field.[179–182] Realizing flow reactions feature several advantages over batch processes. The high surface to volume ratio of the flow (micro)reactor technology avoids disadvantages of classical tubular or batch reactors, such as difficulties in the control of highly exothermic reactions or the formation of "hot spots" due to poor heat dissipation, it allows for uncomplicate heat exchange and constantly stable reaction conditions and also for thermal control in highly exothermic reactions.[77] The efficient thermal management in flow (micro)reactors can also be employed to avoid side reactions and accelerate slow reactions by increasing temperature and pressure.[78,79] This fact allows the use of a wide range of conventional solvents which cannot always be utilized in classical batch reactor processes under similar reaction conditions.[80] With MRT

good control and adjustment possibilities for reaction parameters including temperature, residence time, and reactant stoichiometry is provided. In the recent years the advantages of flow (micro)reactor technology were shown by different research groups, with most examples originating from organic and pharmaceutical research.[183] With respect to polymerization reactions, MRT also features distinct advantages. Application of (micro or milli) flow conditions to polymer reactions intrinsically allows for simple upscaling of processes and likewise acceleration of reactions in general. At the same time – and this is a distinct advantage of chain reactions – also materials of higher quality and overall yields can be obtained from MRT due to the higher stability that is offered by flow systems combined with the more defined reaction conditions can be achieved. Polymer materials with highly precise structures that are not easily matched by their batch reaction counterparts can be synthesized.[179] So far, polymers have been produced in laboratory flow reactors for a variety of reactions, including anionic polymerization, ring opening polymerization and diverse methods in the realm of controlled radical polymerization.[77] More recently, polymer *click* conjugations and *click*-like polymer modifications have been added to the available portfolio of flow reactions.[184]

Ligation of polyacrylates with other polymer counterparts via the copper catalyzed azide-alkyne conjugation (CuAAC) has been demonstrated on a flow chip reactor with high efficiency and comparatively fast reaction times.[185] A problem of such reaction is the use of certain copper species, which in this case tend to be only partially soluble. These inhomogeneities inevitably lead to blockages and fouling in the reactor channels, prohibiting stable flow conditions and eventual failure of the reactor setup. While these problems can be overcome by a careful choice of reaction conditions and by adjusting the physical parameters of the employed reactors, fewer possibilities exist to translate traditional copper-catalyzed reactions to flow. Within the realm of polymerizations, one of the most important copper-mediated processes is copper-mediated radical polymerization, namely atom-transfer radical polymerization (ATRP)[16,186–188] and single electron transfer – living radical polymerization (SET-LRP).[189–193] Both techniques require equilibrium between oxidation states of copper species which allows a reversible activation/deactivation of growing macroradicals and end-capping of the latter with a halide atom, typically bromine. Both ATRP and SET-LRP yield polymers of similar structure and the difference between both processes mostly stem from the choice of reaction conditions such as solvent polarity and temperature. For the distinct differences and specific reaction mechanisms of the two processes, the reader is referred to literature.[16,24,186–195] For both ATRP and SET-LRP flow reactions have been developed and in principle, production of polymers via these methodologies under continuous conditions is possible.[182,196,197] Yet, in all cases, the handling of the copper species and disproportionation of Cu(I) to solid Cu(0)

and often insoluble Cu(II) complexes as well as precipitation of copper salts and complexes makes the establishment of stable flow conditions challenging.[198]

Until recently, only a few transition metal mediated, controlled radical polymerizations could – unlike free-radical polymerizations – be efficiently initiated by UV-light.[199–202] Also reversible addition fragmentation radical transfer polymerization (RAFT)[203,204] could be initiated by the use of conventional UV-initiators. Still, these reactions are prone to side reactions due to the RAFT typical dithioester moieties acting as chromophores. Newer developments demonstrated that also development of UV-labile alkoxyamines could be used to perform UV-initiated nitroxide-mediated polymerizations (NMP).[70,71,74,205–207] Hawker and coworkers demonstrated that also ATRP can be directly initiated by UV-light if the copper catalyst is replaced by an iridium species.[70] Copper-mediated ATRP can be performed under UV-conditions by applying reverse ATRP conditions, thus making use of conventional initiators.[208–211] Moreover direct activation of the copper species via UV-light was reported, enabling a true UV-induced ATRP process comparable to the iridium system.[212] Also for a system closer to SET-LRP, photo-induced polymerization could be successfully carried out.[196] For copper-catalyzed azide-alkyne cycloadditions, photo-generation of the Cu(I) species was likewise reported.[213]

Herein, we focus on the photo-induced polymerization of methyl acrylate in polar solvents under reaction conditions typical for a SET-LRP reaction (or SARA-ATRP, supplemental activators and reducing agents – ATRP). Haddleton and coworkers have reported on the successful polymerization of a variety of monomers by this process and have demonstrated an efficient and fast light induced polymerization process. While photo-induced controlled polymerization is usually of highest interest for surface modification and surface patterning,[54,214] in this case the photo process might also be an interesting alternative for the synthesis of polymers by ATRP/SET-LRP on large scale in a solution process. From an economic point of view UV-irradiation is cheaper than thermal heating, UV-induced polymerization is not unproblematic. Reaction efficiencies depend largely on the nature of the light source and also on the reactor geometry. Light intensity gradients throughout a batch reactor are unavoidable due to absorption of light. As a consequence, such reactions can be difficult to scale up and reaction kinetics varies widely with the type of reaction vessel chosen. A possibility to overcome this problem is the application of MRT to the photo reactions. UV-flow reactors have been shown to be highly efficient and to accelerate several reactions to reach full conversion from reaction times of days to minutes by increasing the light intensity and efficiency.[50,76,152,154] While gaining more and more popularity in the field of organic chemistry synthesis, no

polymerization reactions have been reported for such lab-scale devices in homogeneous phase. This is a surprise, because reactors are comparatively cheap and easy to handle. In MRT flow reactors, channel widths and thus optical path-lengths are very small, allowing for very reproducible and easily upscalable reaction conditions. Employing UV-flow reactors does not only allow for continuous production of materials, but also for an increased efficiency of the reactions. Since residence times are usually short in micro- and milliflow reactors, interfering reactions stemming from degradation of materials from extended UV-illumination are generally avoided, leading to less side products and overall increased product quality.

Based on the novel photo-polymerization protocol introduced by Haddleton and coworkers, we demonstrate for the case of methyl acrylate, how the polymerization can be optimized for micro- and milliflow with high efficiency and short reaction times. This is the first report on a photo-induced controlled radical polymerization employing microreactors. The focus is put on a specific polymerization protocol, adaption of the described reactors to other (photo)polymerization methodologies is expected.

8.3 Results and discussion

Due to the rather low concentrations of copper that are required to mediate polymerization (in the present case about 0.02 equiv. compared to the initiator), strictly homogeneous reaction conditions are established and reaction blockage or fouling is eliminated. The reactor channel widths play no important role and the polymerization can be applied to micro- and milliflow conditions. For the work as described herein, we have chosen two different flow systems to compare: (i) a true microreactor glass-chip reactor (19.5 µL reactor volume, borosilicate) and (ii) a tubular UV-flow system with an internal volume of 11 mL. Each system features distinct advantages. The microflow setup is best suited for kinetic studies under very economic conditions, and - due to the very small channel width – can be used with UV-light sources of intermediate power. Here we applied a UV-light source with 100 W power, which was not used to full extent and usually attenuated to lower intensities. Conversely, the tubular reactor is less sophisticated (the reactor itself consists of transparent PFA tubing wrapped around an immersion well photo-reactor), but allows for synthesis of materials at significant scale due to the much higher internal volume. For the tubular reactor, a UV-light source with 400 W was chosen to achieve fast polymerizations. The peak wavelength in both cases was λ = 365 nm. The irradiation spectrum was relatively broad. In case of the microreactor, a conventional glass chip was used, thus optical transparency is limited at wavelengths below approximately 350 nm. For the present case study, we used

methyl acrylate as monomer and dimethyl sulfoxide as solvent. Good results were reported for this combination in batch processing. Thereby, the active copper species was generated from a Cu(II)Br$_2$ / tris(2 (dimethylamino)ethyl)amine (Me$_6$TREN) system (see **Scheme 8.1**). While the exact mechanism has not yet been elucidated, photo-activation of the Me$_6$TREN ligand followed by carbon-halogen bond breakage appears to be the dominant mechanism for chain initiation. In this process, initiator radicals are formed which are deactivated by the Cu(II) to yield the active Cu(I).[202]
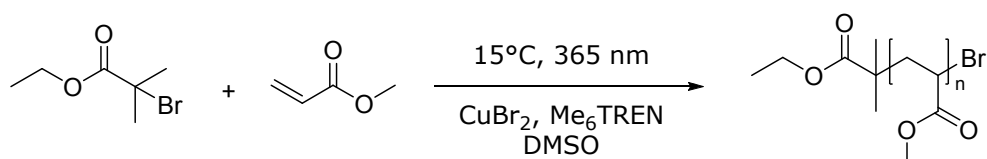
Scheme 8.1: UV-induced copper-mediated polymerization of methyl acrylate (MA) in DMSO using CuBr$_2$ and Me$_6$TREN as catalyst/ligand pair.

8.3.1 Polymerization in a tubular milli-flow reactor

Fig. 8.1 depicts the outcome of MA polymerizations at 15°C in the tubular reactor setup. Polymerization rates would be significantly higher at slightly elevated temperatures. Low reaction temperatures were chosen to underpin the photoinitiated character of the reactions. Additionally low temperatures help to avoid the formation of midchain radicals, as usually observed in any acrylate polymerization.[99,215] Midchain radicals inevitably lead to short chain and long chain polymer branching. Choosing low reaction temperatures allow synthesis of primarily linear chains with minimum branch points; giving additional value to this photo-polymerization process.

Three series of polymerizations were performed under variation of the target molecular weight, **Fig. 8.1**. Polymerizations were set to ideally reach 2000, 4000 and 9800 g·mol^{-1} at full conversion (with $c_{monomer}/c_{initiator}$ = 23, 47 and 116, respectively). No higher molecular weights have been target since this range covers already a broad range of materials typically synthesized via controlled polymerizations. Higher molecular weights will lead to increased viscosities, which was in the current study avoided in order to exclude complex viscosity effects. All polymerizations show a linear increase in M_n with respect to conversion. Very high conversions were reached in all cases in relatively short reaction time (maximum 20 minutes residence time, see discussion below). The reaction in flow is remarkably faster compared to all previously reported batch photo-polymerizations. The rate of reaction may be influenced by the choice of

light source. The rate increase may depend of two factors: the enhanced light efficiency of the flow reactor and usage of a more powerful UV-lamp.
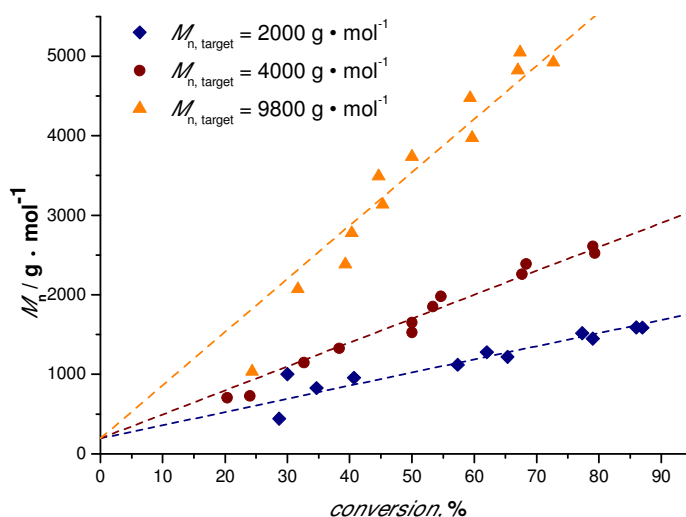
Fig. 8.1: Development of the M_n of a UV-initiated copper-mediated polymerization of MA, with targeted M_n = 2000 (♦), 4000 (•) and 9800 (▲) g·mol^{-1}, in a tubular milli-flow reactor. The dotted lines are best fits of the data, whereby the axis intercept was set to the molar mass of the initiator.

Conversion and the degree of polymerization in a flow reaction is influenced by variation of the residence time. With increasing flow rates, lower residence times are achieved. The data shown in **Fig. 8.1** were constructed from continuous polymerization under variation of the pump flow rate. At the same time, larger reactor volumes can be used at proportionally higher flow rates. For the here used reactor setup, a production of PMA of ≈ 60 g per day can be realized at a residence time of 20 min. Upscaling of the reaction is, as described, simple and can be realized by using a longer PFA tubing, wrapped around the light source.

The molecular weight evolution of the three polymerizations were fitted linearly. The slopes of all three reactions are slightly lower than the theoretical value (18, 31 and 67, respectively). The reason for the molecular weights remaining lower than expected remains unclear. Deviation from ideal behavior in controlled polymerization is often observed. The outcome of the reactions can be regarded to be within the usual limits of deviation.

In-line with the observation of a well-controlled polymerization, a decrease in the dispersity of the polymers was observed (see **Fig. 8.2**). With higher monomer conversion and longer reaction time, the dispersity indices decreased for all the targeted molecular masses (from roughly 1.2-1.3 to about 1.1). As expected, slightly higher initial dispersities were observed for increasing monomer to initiator ratios.
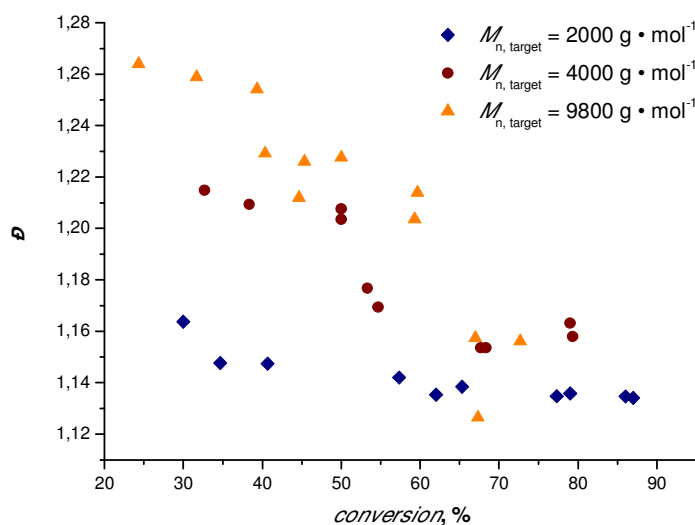
Fig. 8.2: Decrease of the dispersity with monomer conversion of MA polymerizations in a milli-flowreactor via UV-induced copper-mediated radical polymerization, with target number-average molecular weights of 2000 ($\blacklozenge$), 4000 ($\bullet$) and 9800 ($\blacktriangle$) g mol^{-1}.

To demonstrate that the reaction proceeds under high control, the first-order kinetic character of the polymerization was determined, **Fig. 8.3**. All reactions showed linearity indicating that the concentrations of the growing radicals remained nearly constant over the course of reactions. Small deviations from first order kinetics are seen for the highest target molecular weight reaction. Assuming, radical concentrations in all three polymerizations were of a similar order. In combination with the linear increase in average molecular weight and low dispersity of the polymers obtained it can be assumed that only little transfer and termination events disturb the livingness of the reactions. No inhibition period was observed and polymerization started already at low residence time. For accuracy, it is critical, dark containers were used for the

preparation of the reaction solution since natural light is also able to trigger polymerizations.
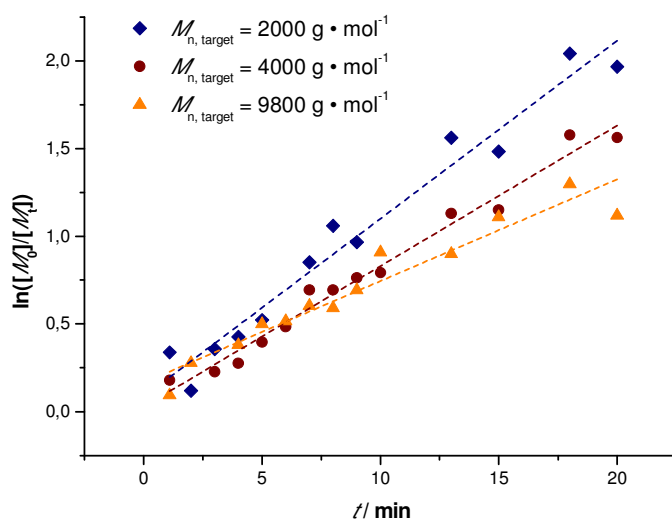
Fig. 8.3: First order kinetic plots of the MA polymerizations in a milli-flow reactor with targeted M_n = 2000 (◆), 4000 (●) and 9800 (▲) g mol^{-1}.

8.3.2 Polymerization in a chip micro-flow reactor

Besides the milli-flow reactor a micro-flow reactor was employed to carry out the UV SET-LRP polymerization to demonstrate that the reaction may be realized in a true microfluidic device. In the micro-flow reactor a reaction with a targeted M_n = 4000 g mol^{-1} was performed. A maximum conversion of 80% was reached after a residence time of 20 minutes in this specific reactor and light source combinations. The result is relatively comparable with the yields of the tubular flow reactor. Overall, the polymerizations in the micro-flow reactor feature the same characteristics as in milli-flow. Molecular weight evolution and dispersities are in the same range as in the polymerizations discussed above (as shown in **Fig. 8.4)**. **Fig. 8.4** displays the molecular weight distributions as obtained from SEC, scaled to monomer conversion of the respective samples. A clear shift of the distributions – also on the low-molecular weight side – was observed, which underpins that the reaction is easily applicable to different reactor setups and is highly interesting also for larger flow reactor systems in which kilogram (or higher) production of polymers can be achieved.
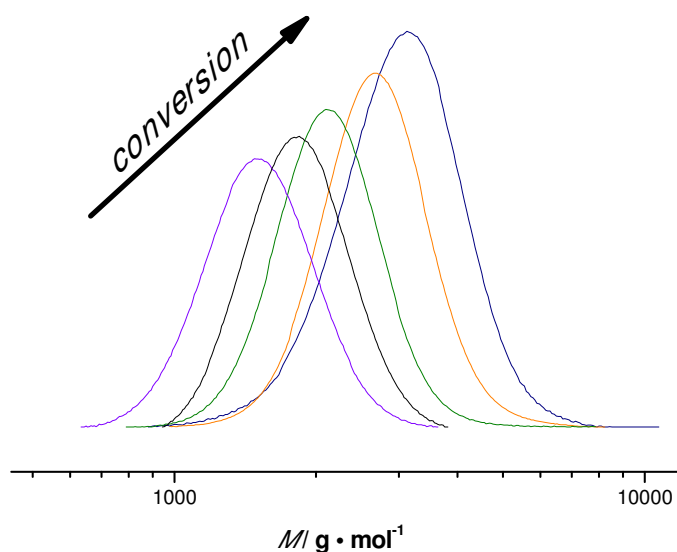
Fig. 8.4: Molecular weight distributions of PMA with increasing residence time in the microflow reactor synthesized via UV-initiated copper-mediated polymerization and with with targeted M_n of 4000 g·mol^{-1}. All distributions are scaled to monomer conversion.

The first order kinetic plot in micro- and milliflow reactions exhibit a good linearity, as seen in **Fig. 8.5**. There is a lower slope (■), indicating that radical concentrations in both reactions are slightly different. This is not surprising, since the reactor volume and reactor type had been changed and a light source of different intensity was used. The fit of the microreactor data indicate that at zero minutes residence time some polymerization had already taken place (the reactor is fed by light-transparent syringes, thus polymerization could already occur in the feed). This underlines the sensitivity of the reaction.
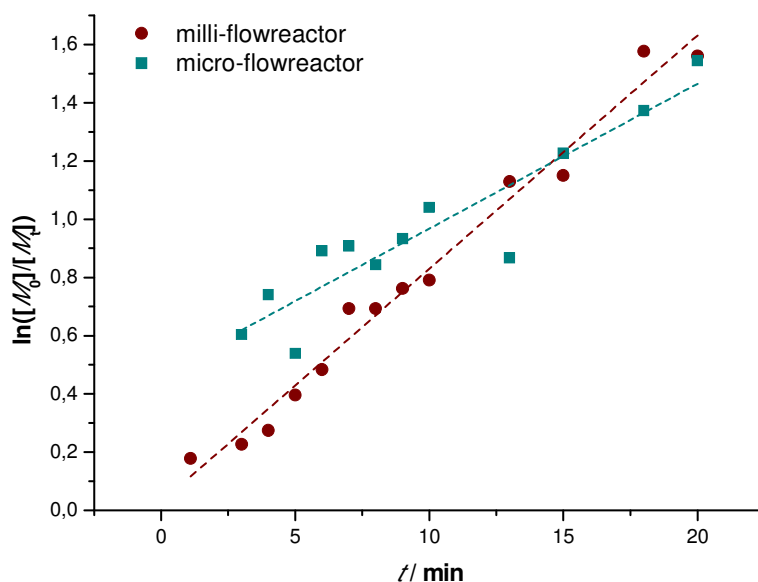
Fig. 8.5: Comparison of the kinetic first-order plots of a UV initiated copper-mediated polymerization of MA in a milli- (●) and a micro- (■) flow reactor.

8.3.3 End group fidelity

Finally, the quality of the polymers where analyzed by mapping the end group fidelity via electrospray ionization mass spectrometry (ESI/MS). Samples of polymers from the polymerization with a target M_n = 2000 g mol^{-1} after a reaction time of 10, 15 and 20 minutes were taken to check for the presence of termination products, which may decrease the livingness of the process. The polymer samples were associated with monomer conversion between 70 and 87%. All showed a very high degree of end group fidelity (see **Fig. 8.6** and

Table 8.1). The ESI/MS spectra display only one single-charged product species, this being the sodium adduct of the expected structure with the initiator group in α position and a bromine atom at the ω site, **Fig. 8.6**. With increasing reaction time, more double-charged polymers were observed, which is associated with the increase in overall chain length of the samples. Even though traces of side products were seen in the baseline of the spectra, absence of any significant amount of termination products (as given in the table for one of the disproportionation species) is clearly seen. The mass-spectrometric analysis confirmed the above made observation of excellent livingness of the process. UV-irradiation may cause several side products, ranging from self-initiated chains over crosslinking to polymer degradation. The practical absence of all such product species confirmed that the flow conditions only favor the desired product, but did not cause other processes as are often observed for UV-initiated batch reactions at similarly high light intensities. Some samples taken at even higher conversions were analyzed with virtually the same result.
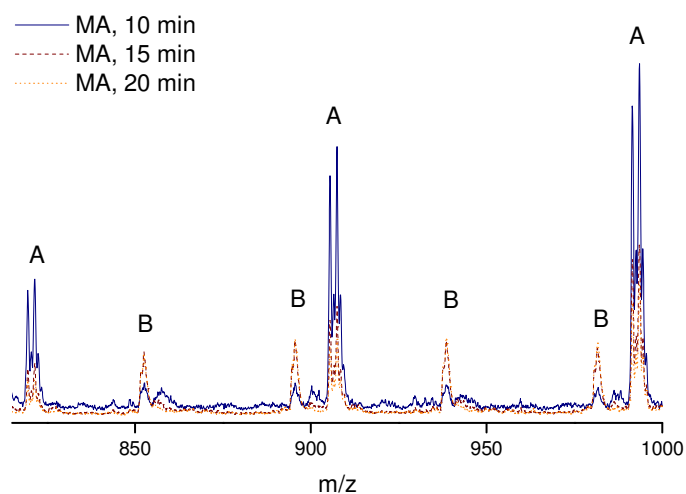
Fig. 8.6: Zoom into ESI/MS spectra of PMA obtained by UV-copper-mediated polymerization in flow reactors. The 15 and 20 min sample show higher relative intensities for double charged species due to their higher M_n which lies above the scan range of 2000 g mol^{-1}.

Table 8.1: Peak assignment of the ESI/MS spectra and the mass differences between experimental and theoretical m/z.

name	α end group	ω end group	units MA	ion	m/z_{exp}	m/z_{theo}	δ / Da
A	EBiB	Br	8	Na^+	905.50	905.28	0.22
B	EBiB	Br	18	Na^{2+}	894.67	894.32	0.35
C	EBiB	H	9	Na^+	--	913.46	--

8.3.4 Block-copolymers formation

Based on a PMA obtained from the tubular reactor, block-copolymerss were synthesized in the micro-flow reactor. For chain extensions, butyl acrylate (BA) was polymerized with a maximum reaction time of 20 minutes. Reaction conditions were chosen analogous to the homopolymerizations. PMA with an M_n = 3100 g mol^{-1} and a dispersity of 1.10 was chosen as the starting material. The targeted M_n of the block-copolymers was 7700 g mol^{-1} (at full BA conversion) and good control over the second block was also achieved, see **Fig. 8.7**. Polymerizations proceed to high conversions and feature low dispersities. For example, at a BA conversion of 51 %, a PMA-*b*-PBA polymer with a M_n = 4990 g mol^{-1} and a dispersity index of 1.16 was obtained (theoretical M_n at this conversion is 5400 g mol^{-1}). Block-copolymerizations can also easily be addressed in flow reactions, underpinning the versatility of the process, as well as the high livingness of the polymerizations.

It is important to test if other monomers can be polymerized in flow using the same protocol. Batch reactions showed that a relatively large variety of monomers can be controlled by photo-copper-mediated polymerization. However, fast polymerizing acrylates were used to stay within reasonable polymerization times to reach high conversions. In flow, several other monomers were also tested with mixed success. Styrene did not show significant polymerization of the timescale of the flow reactions (we chose 20 minutes as highest residence time as for the other reactions described in this work). In contrast, methyl methacrylate could well be polymerized by the protocol but reached only ≈ 35% conversion after 20 minutes (M_n = 2100 g mol^{-1}, Đ = 1.45). Thus, polymerization of such monomers might not be most favorable to produce homopolymers in an efficient manner in the current flow setups. Still, for block-copolymerizations, where reactions are often stopped prematurely to preserve end group fidelity, such reactions could be of significant interest for the future.
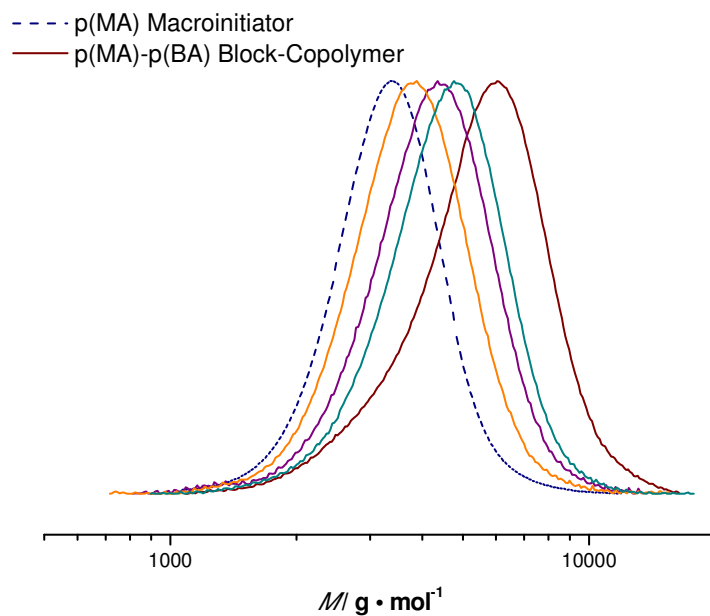
Fig. 8.7: Evolution of molecular weight distributions for the PMA-*b*-PBA block-copolymerss (solid line) obtained in flow microreactor and the distribution of the PMA macroinitiator (dashed line).

8.4 Conclusion

Photo-initiated copper-mediated radical polymerization offers intriguing features for the design and synthesis of complex materials. The translation of the batch process to flow chemistry offers to scale this reaction up for the production of significant amounts of complex material. This is in a batch is not directly possible due to light absorption profiles and insufficient penetration of light at increased optical path lengths. The good applicability of photo-copper-mediated polymerization of MA was demonstrated for both a commercial glass-chip microreactor (volume 19.5 µL) as well as a simple tubular milli-flow reactor (11 mL). Excellent control over polymerizations is in both cases realized. Reactions follow first order kinetics, number average molecular weight increases linearly with monomer conversion and low dispersities are reached for all polymers obtained. Reactions were particularly fast and conversions in the range of 90% were reached within 20 minutes reactor residence time. All polymers feature excellent end group fidelity and allow for efficient block-copolymersizations, as it was demonstrated by the synthesis of a series of PMA-*b*-PBA materials in the microreactor.

Overall, the described reactions give a further example for the increasing number of polymer reactions that benefit from microreactor application and flow chemistry. The methods described herein make use of comparatively simple and versatile flow reactors and do not required sophisticated instrumentation. Both the microflow and the tubular reactor are comparatively cheap, easy to set-up and of potential interest to the whole polymer community as a novel way to produce materials for a broad range of research projects. The novel photo-copper-mediated polymerization process solves the general problem of inhomogeneities that are commonly observed in thermal copper-mediated polymerizations in flow devices, making the photo-initiated process also from that point of view first choice for synthesis of materials from controlled polymerization.

Chapter 9

normal electron-demand

inverse electron-demand

H_2N-X

H_2O

new anchor point

+

[4+2]

X = aromate

X = surface
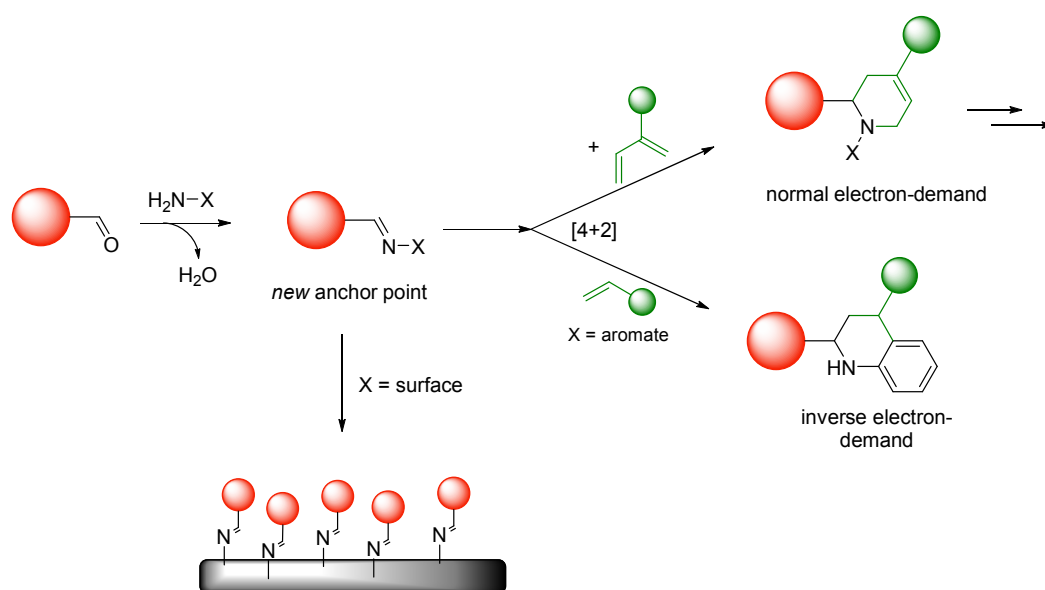
9. Irreversible Diels-Alder [4+2] cycloaddtion for polymer end group modification [‡‡]

9.1 Abstract

In the here presented work we demonstrated that the concept of an irreversible inverse electron-demand aza-Diels-Alder between electron-poor aldimines and a suitable diene like furan yielded an cycloadduct in a one-pot-synthesis with high yield for small molecules. Polymeric aldimine formation is well possible and proceeds with high yields with pure aniline. The aldimine formation is complementary to the oxime ligation. The eventually following inverse electron-demand HDA is not feasible. On the other hand the aldimine can be considered as a further anchor point for normal electron-demand HDA using electron-rich dienes, like *Danishefsky's* diene.

9.2 Introduction

The introduction of the *click* chemistry concept by *Kolb* et *al.*[26] in 2001 did undoubtedly have one of the largest impacts on organic, biochemical and polymer chemistry in the recent years.[30,31] Since this, several *click* type reactions were established, whereby the exact criteria of what makes a *click* reaction might vary with the field of research. In the polymer field, the atom efficient 1,3-dipolar cycloadditions and [4+2] Diels-Alder cycloadditions are with certainty the most prominent examples for reactions that are highly interesting for the conjugation of two oligomeric or polymeric building blocks.[216] Cycloadditions are generally a good choice for ligation; they yield no side products, which simplifies the work-up procedures after reaction. Also, they are – adhering Sharpless definition – spring-loaded to only one reaction trajectory. If the interacting HOMO/LUMO level fit well, the reactions are fast and have a high yield, leaving region- and stereoselectivity the only aspect of concern.[217]

The drawback of the competition between *endo* and *exo* products may partially be an issue for organic chemistry, but usually is of no concern in the field of polymers chemistry where the main goal is the formation of a stable $C-C$ bond.[161,218] Next to classical DA reactions between a diene and a dienophile, hetero-DA approaches have become increasingly popular, with the use of thio carbonyls as found in end groups of chains originating from reversible addition fragmentation chain transfer (RAFT) polymerization (RAFT-HDA), being a

---

prominent example.[88] On first glance, a disadvantage of DA chemistry is the intrinsic reversibility of the reactions (reverse Diels-Alder, rDA).[219] This reversibility can, however be used to develop reversibly switchable systems, as it had been demonstrated for RAFT-HDA.[220] Other advances towards non-reversible HDA reactions were made, with tetrazine systems being a prominent example (the DA is followed by loss of nitrogen, leading to the irreversibility of the reaction).[221]

In here, we perused similar routes to develop irreversible DA pathways for polymer modification and ligation. Based on polymeric aldimines that are obtained from aldehyde-functional materials with aniline-(derivates), such goal can be reached in two different reactions. At first, A reaction with a dienophile in an inverse electron-demand DA, making use of one of the double bonds of the former aniline, the other is a classical DA reaction with the so-called *Danishefky's* diene (*trans*-1-methoxy-3-trimethylsilyloxy-1,3-butadiene).[222] The inverse-electron demand HDA reaction is irreversible due to re-aromatization taking place after cycloaddition (see **Fig. 9.1**). The route via *Danishefky's* diene, a very electron-rich diene due to the trimethylsilyloxy-group, becomes irreversible due to cleavage of the TMS- and methoxy-group after reaction (see **Fig. 9.1**).

Aldimines are easily formed by condensation of aldehydes and amines. The preparation is straight forward enabling high yields within short reaction time. Aldehyde-functional polymers are easily available via atom transfer radical polymerization.[103] These polymers were initially developed in our laboratories for photochemical modification via [2+2] Paternò-Büchi cycloadditions of polymers and of nanoparticles.[76,125] Development of an alternative (thermally activated modification) reaction is thus interesting to broaden the use of such aldehyde-functional materials. Especially for photo patterning, the ability to switch between a thermal activation and a photochemical activation step of the same substrate would be highly intriguing. For polymer ligation purposes in thermal reactions, polymeric aldehydes have been so far exclusively used for oxime ligation.[34] Oximes are made by condensation of aldeyhdes and hydroxylamines. Surprisingly, oxime ligation has reached relative prominence, while aldimine formation – in principle it is simpler counterpart – has not been explored extensively. In comparison to amines, hydroxylamines are less accessible, as on the other hand amines are commercial available in broad variety or even directly accessible on surfaces (e.g. glass, silicon) by silanization (i.e. via (3-aminopropyl) trimethoxysilane). The study on aldimines as alternative pathway to the oxime ligation appears thus rewarding as it may allow for similar efficiencies, but simpler preparation procedures.

Fig. 9.1 depicts the polymeric aldimine formation as well as the two HDA reactions for further modifications. Aldehyde functional polymers were tested as well as modification of the resulting aldimine functional polymers with relatively simple counterparts. In this way, reactions can be tested in facile manner and easily traced by NMR and mass spectrometry. The principle of the reactions can later easily transferred to more complex systems carrying multiple aldehydes (or anilines) and to more complex enophiles and dienophiles. Regardless, the aldimine serves in the following as the actual reactive species in an HDA reaction. In the inverse-electron demand aza Diels-Alder cycloaddition[223,224] with an dieneophile, a non-aromatic intermediate is formed since a double bond of the aromatic ring is part of the diene. The concomitantly formed C=N double bond can in a fast subsequent reaction donate electrons and hence make the reaction irreversible by re-aromatization of the six-membered ring. Alternatively, (top part of **Fig. 9.1**) also *Danishefsky's* diene can react with the aldimine in a conventional HDA reaction. In here, no re-aromatization takes place to prevent the retro-reaction. Instead, the substituents of the diene can be split off, changing the reactivity of the diene in a way that the retro reaction is highly disfavored.
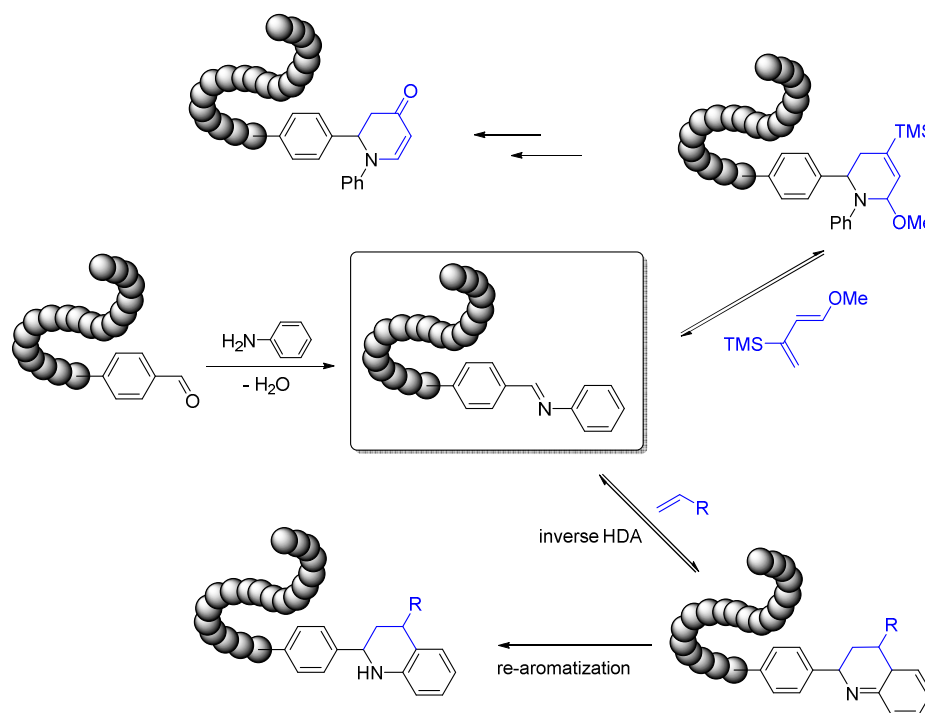
Fig. 9.1: Graphical concept of the two irreversible hetero Diels-Alder cycloadditions.

In principle the aldimine can be generated *in situ* for both reactions and the reaction can be conducted as a *one-pot* reaction. As shown before, such one-pot HDA strategy can be highly efficient when catalyzed by Lewis acids[225–229] or Brønsted acids are employed.[230,231] Until now both reaction routes are used for small molecules or nature product synthesis with a strong focus on stereochemistry. In this study, we aim to develop this reaction for polymer modification reactions.

The formation of the aldimine species was studied, followed by investigation of the HDA reactions. As later demonstrated, the concept of the inverse electron-demand HDA is suitable for small organic compounds, but does not reach sufficient efficiency for polymer systems. Nevertheless, aldimines are introduced as viable conjugation tool. Conjugation of the aldimine in an irreversible DA with *Danishefsky's* diene was successfully demonstrated, underpinning the general concept and giving access to aldimine HDA polymer modifications and to an alternative pathway for irreversible HDA modifications.

9.3 Results and discussion

9.3.1 Hetero Diels-Alder reactions between small model compounds

9.3.1.1 Aldimine formation
In order to achieve Diels-Alder conjugations, first the formation efficiency of the intermediate aldimine was investigated. Tests were carried out with small model compounds to elucidate the conditions of the condensation reaction proceeding to high conversion under equimolar use of reactants. While equimolar conditions are generally favored, also higher equivalents can be used since the aldimine displays only an intermediate.

Reactions were carried out with two model aldehydes, one being 4-hydroxy benzaldehyde, the other being a 4-hydroxybenzaldehyde-based ATRP initiator (FPBP) that mimics the structure of the later employed polyacrylate polymer.[103] Aldimine formation was then optimized on the basis of these two aldehydes with either aniline or *p*-nitroaniline (**Fig. 9.2**), which were selected based on literature studies where aromatic amines were considered as most effective for the targeted HDA reactions.[231–234]
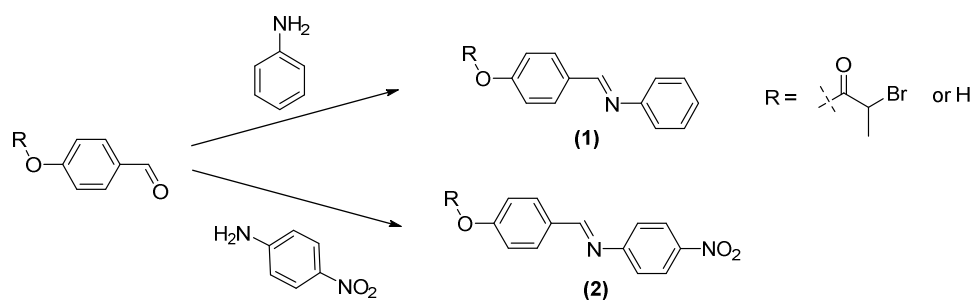
Fig. 9.2: Reaction scheme for the aldimine condensation yielding (**1**) and (**2**).

The aldehydes were mixed with the aromatic amines in dry THF. $MgSO_4$ was added to bind the residual water and to shift the condensation equilibrium to the product side. Results (with yields based on NMR characterization) are collated in **Table 9.1**. Tracing of the reaction progress is carried out by observation of the disappearance of the characteristic CHO signal (δ = 9.88 ppm) and the appearance of the aldimine proton signal (-C**H**=N-) at δ = 8.38 ppm. The yield was calculated by comparison of the two integrals.

Table 9.1: Overview of the yields of the aldimine condensation reaction. All reactions were performed at RT for 18 hours under continuous stirring.

Entry	Equivalents				V_{THF} / mL	$yield_{NMR}$ / %
	FPBP	4-hydroxy-BA	Aniline	p-nitro aniline		
1	1		1		10	64
2	1		2		10	17
3	1			1	10	17
4	1			1.5	10	15
5		1	1		25	93
6		1	1.5		25	92
7		1	2		25	0
8		1		1	25	< 1
9		1		1.5	25	< 1
10		1		2	25	< 1

The reactions between the ATRP-initiator and unsubstituted aniline yielded the desired aldimine (*yield* = 64%) when using one equiv. of aniline. Increasing amine concentration did not increase the yield of the reaction as one would expect (entry 2).On the contrary, excesses of amine seemed to favor side product formation as indicated by unidentified peaks arising in the ^{1}H-NMR spectra. Reactions of FPBP with *p*-nitroaniline yielded low amounts of the desired aldimine. The lower yield may be explained by the fact that the nitro-group is an electron-withdrawing group, which reduces the nucleophilicity of the amine and slows down the reaction.[235,236] Nevertheless, *p*-nitroaniline was still an interesting reaction partner since the nitro-group was able to promote the HDA reaction and was still beneficial for the complete reaction (see below). Full conversion of the aldehyde into the aldimine was not necessarily required since the HDA reaction removed aldimine from the reaction mixture and could shift the condensation equilibrium to the product side.

Nevertheless, best results on the model system were obtained for the reactions between 4-hydroxy-benzaldehyde and aniline with yields of 93% and 92%, respectively (**Table 9.1**, entry 5 & 6). Interestingly, in this reaction the yield drops dramatically when an excess of aniline was employed (entry 2 & 7).

The combination of *p*-hydroxy benzaldehyde and *p*-nitro aniline, entry 8, 9 & 10 showed no product formation at all (yield < 1%). The reason for this lack of reactivity was not directly evident, but exemplifies that the amine as well as the aldehyde component must be chosen with care for the aldimine formation. Regardless, from all reactions it can be well seen that using excess of the amine did not promote higher aldehyde conversions, at least not to the desired product, which is an important information for the following reactions on polymer systems to take into account.

9.3.1.2 Conversion of aldimines dienes in HDA cycloaddition

In a next step, the reactivity of the aldimines was tested in a HDA cycloaddition. Furan and cyclopentadiene (Cp) were used as dienophiles, see **Fig. 9.3**. The choice of a diene as enophile was not directly evident. Yet, both furan and Cp were both suitable to act as enophiles, and the presence of two enes in the molecule in principle allowed faster reaction since two equivalents of functional groups were available per equivalent of enophile.
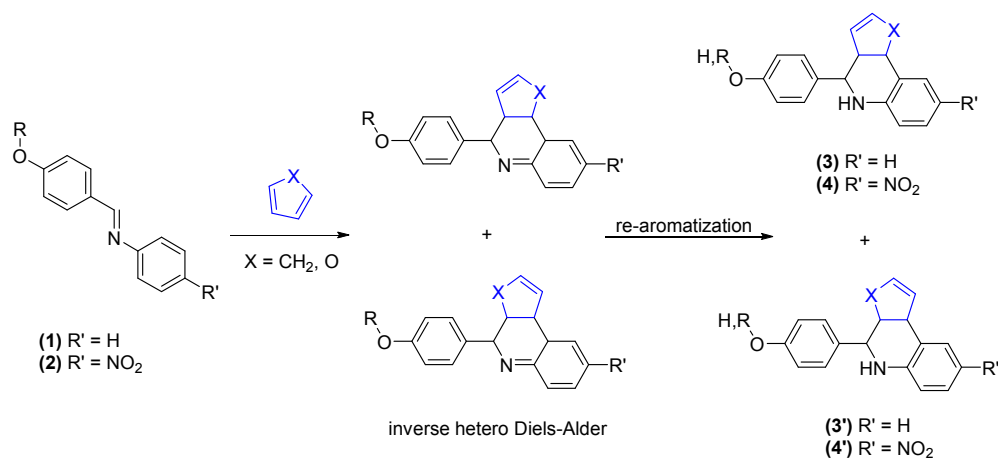
Fig. 9.3: Reaction pathway of the aldimine HDA with furan or Cp acting as dienophile in an inverse HDA leading to two regioisomers (**3** & **3'**) and (**4** & **4'**).

In the following experiments, the HDA reactions were directly performed as one-pot reactions – likewise demonstrated in literature.[237] For all reactions given in

Table 9.2 the aldimine was not isolated. To catalyze the HDA, lewis acids (LA, BF$_3$, Yb(OTf) or ZnCl) were added to the reaction mixtures.[226–231]

Table 9.2: Overview of the HDA cycloadditions carried out on a small molecule model system.

Entry	Equivalent						T / °C	t / h	Lewis acid / equiv.	conv / %
	FPBP	4-OH-BA	anilin	nitro-anilin	Cp	furan				
1	1			1.1	1		60	18	BF$_3$·Et$_2$O: 0.1	3
2	1			1.1		1	60	18	BF$_3$·Et$_2$O: 0.1	13
3	1			1.1		1	64	72	BF$_3$·Et$_2$O: 0.25	15
4	1			1.1		1	64	72	BF$_3$·Et$_2$O: 0.5	44
5	1			1.1		1	64	72	BF$_3$·Et$_2$O: 1	86
6	1			1.1		1	64	18	BF$_3$·Et$_2$O: 1.5	100
7	1			1.1		1	64	18	Yb(OTf)$_3$: 0.5	96
8	1			1.1		1	64	18	Yb(OTf)$_3$: 1	75
9	1			1.1		1	64	18	Yb(OTf)$_3$: 1.5	78
10		1	1.1		1		RT	18	ZnCl$_2$: 0.1	0.50
11		1	1.1		1		RT	18	BF$_3$·Et$_2$O: 0.1	0.50
12		1	1.1			1	RT	18	ZnCl$_2$: 0.1	0.50
13		1	1.1			1	RT	18	BF$_3$·Et$_2$O: 0.1	0.50
14		1		1.1	1		RT	18	ZnCl$_2$: 0.1	4
15		1		1.1	1		RT	18	BF$_3$·Et$_2$O: 0.1	5
16		1		1.1	1		60	18	BF$_3$·Et$_2$O: 0.1	14
17		1		1.1	1		64	72	BF$_3$·Et$_2$O: 0.25	33
18		1		1.1	1		64	72	BF$_3$·Et$_2$O: 0.5	29
19		1		1.1	1		64	72	BF$_3$·Et$_2$O: 1	75
20		1		1.1	1		64	18	BF$_3$·Et$_2$O: 1.5	51
21		1		1.1		1	RT	18	ZnCl$_2$: 0.1	3
22		1		1.1		1	RT	18	BF$_3$·Et$_2$O: 0.1	5
23		1		1.1		1	60	18	BF$_3$·Et$_2$O: 0.1	8

*Conv. determined by ^{1}H-NMR.

Again, ^{1}H-NMR-spectroscopy was used to determine the reaction yields (in **Table 9.2** based on aldehyde peak disappearance with concomitant absence of characteristic aldimine peaks). In a successful reaction, no peak deriving from the aldehyde or the aldimine should be visible while corresponding peaks from the Diels-Alder product should be clearly visible. Since several regioisomers are formed, the NMR spectra of the products are quite complex, so disappearance of the aldehyde and aldimine peak was used to determine start material conversions rather than product yields. In all reactions, slight excesses of the amine (1.1 equiv.) were employed to make sure that the reaction can proceed to completion.

The reaction (**Table 9.2**, entry 1) between the ATRP-initiator, *p*-nitroaniline and Cp showed rather low aldehyde conversions (3%). Furan as enophile (entry 2) resulted in low, but yet increased conversion of 13%. High conversions can be reached with the same system (entry 2-9), when using different lewis acid calatysts. The highest reaction efficiency was detected when 1.5 eq. of BF_3 were employed, after 18 h reaction time (entry 6). The ^{1}H-NMR spectrum of the associated product is depicted in **Fig. 9.4** (in comparison to a non-full conversion reaction; **Table 9.1**, entry 4). In the product spectrum, neither the peaks from the aldehyde nor the aldimine are seen. The peaks from the Diels-Alder product, on the other hand, are clearly visible. In the area δ = 8.0-6.5 ppm the peaks from the aromatic structures were found. The peaks from the heterocyclic six-membered ring (piperidine) and the heterocyclic five-membered ring (dihydrofuran, DHF) were found at δ = 5.0-3.0 ppm. The results are highly encouraging since in the pure aldimine formation, rather low yields were seen. As postulated, the aza Diels-Alder reaction shifts the equilibrium to the product side and allows the system to undergo full conversion. Based on the variations made, the best reaction condition for the ATRP-initiator as substrate to achieve the consecutive aldimine formation/HDA reaction is at 64°C for 18 h (overnight). The most favorable Lewis acid for this cycloaddition is $BF_3 \cdot Et_2O$. Generally, an increase in Lewis acid concentration promotes the HDA and directly leads to higher yields. When looking at the results for 4-hydroxy benzaldehyde, only low conversions were observed in all instances. Only in combination with *p*-nitroaniline and Cp, reasonable reaction outcomes can be achieved (entry 19 and 20). As mentioned above, the nitro-group has an inhibiting effect on the aldimine formation, yet is beneficial for the HDA reaction since its attachment lowers the LUMO level of the dienephile. *p*-Nitroaniline can be generally seen as a better choice for the desired reaction.
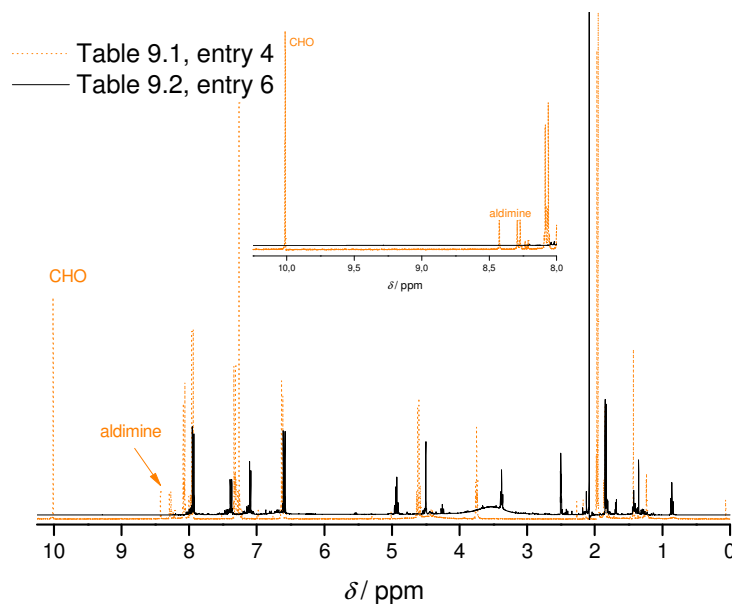
Fig. 9.4: ¹H-NMR spectrum depicts the test of aldimine formation (**Table 9.1**, entry 4; dotted orange line) which shows the formed aldimine and residual aldehyde. The tested HDA reaction (**Table 9.2**, entry 6; solid black line) verified by loss of both signals, due to the formation of the cycloadduct.

For further reactions with polymer substrates (see **section 9.3.2**), the reaction conditions of **Table 9.2**, entry 6 were chosen (FPBP/*p*-nitroaniline/furan/BF$_3$ = 1/1.1/1/1.5 at 64°C). This reaction gave the highest yields of all tested HDA reactions. Additionally, the FPBP constitutes an ATRP-initiator and is a structural mimic of an ATRP (acrylate) polymer, allowing extrapolation of the reaction conditions to polymer reactions.

9.3.2 Transfer of the optimized HDA conditions towards polymers modification

The polymer substrate was obtained via conventional ATRP polymerization[17] using BuA, CuBr, PMDETA and FPBP (equiv. = 75 / 1 / 2 / 1). Polymerizations proceeded with high efficiency as was shown by NMR, SEC and ESI/MS characterization. The polymer is associated with an of M_n = 2200 g mol^{-1}, $Đ$ = 1.25 and a high end group fidelity (> 95%) as proven by mass spectrometry

(see **Fig. 9.5**). Before transferring the one-pot HDA reaction, the aldimine condensation was examined in detail to test if the optimal reaction conditions for the small molecule reaction were applicable to the polymer system.

Polymeric aldimine formation was probed with unsubstituted aniline and the nitro-derivative at different equivalents, temperatures and concentrations (see **Table 9.3**). On the polymer system, ESI/MS was consequently employed to determine reaction yields (from comparing end group distribution patters). This approach is very straight forward and allows tracing even small changes in the reaction outcome. The results are in the following given as yields rather than start-compound conversion. Unlike NMR, ESI/MS is not sensitive to region- and stereoisomers, since the various potential products are all isobaric. Stereochemistry plays no important role for polymer modification in most cases and can thus be neglected.

Table 9.3: Tuning the aldimine formation for polymers (M_n = 2200 g mol^{-1}; c = 1.14 mmol L^{-1}).

Entry	Equivalent			T / °C	t / h	THF / mL	$yield_{ESI/MS}$ / %
	ATRP-polymer	p-nitro aniline	Aniline				
1	1	10		64	18	10	0
2	1	20		64	18	10	0
3	1		50	RT	18	5	90
4	1		50	64	18	5	80
5	1		50	0	18	5	90

As seen from **Table 9.3**, entry 1 & 2, reaction between the ATRP-polymer and *p*-nitroaniline resulted in no significant formation of any aldimine. The ESI/MS spectrum showed only the peaks of the substrate ATRP polymer. Increasing the amine concentration did not shift reaction to the product side. The result is some contradiction to the tests discussed above (**Table 9.1**, entry 3 & 4), where at least 17 % of product was observed. This clearly shows that this particular reaction is more hindered when performed on a polymers.

The aldimine formation was also tested between the ATRP-polymer and aniline (**Table 9.3**, entry 3-5). The condensation was tested at 0°C, room temperature

and 64°C. The three reactions gave product yields of 90% (entry 3), 80% (entry 4) and 90% (entry 5), respectively. The ESI/MS spectrum of entry 3 is shown in **Fig. 9.5**. As seen, a clear shift of the peaks was observed, marking the successful formation of the aldimine. The theoretical molecular mass of an aldimine end capped polymer with nine units of monomer (butyl acrylate) is 1634.84 Da, while the mass found in the spectrum is 1634.83 Da, which matches the experimentally observed *m/z*.

To the best of our knowledge, this is the first time the aldimine formation in a macromolecular system is reported. By using aromatic amines, the aldimine may also be called as *Schiff* base. The aldimine formation was performed in a high yield (90%) and within a reasonable timespan (18 h). By further investigations, the needed reaction time can be probably reduced to a few hours. At the moment, there is only one comparable reaction, the oxime ligation. The oxime ligation also starts with an aldehyde which reacts with hydroxylamine, yielding via a condensation reaction to an oxime. For instance, one polymer application of the oxime ligation deals with surface patterning. The required aldehyde is generated by a photochemical reaction and the following oxime formation takes place at the formerly irradiated sites.[34] The aldimine formation is comparable towards yield and reaction time. An advantage is the easy available starting material (here aniline), since the hydroxylamine for the oxime ligation has to be synthesized prior to use. This can happen either via oxidation of amines or reduction of nitroxides. Therefore, preparing an aldimine is one step faster. The aldimine ligation is a good opportunity for surface grafting. Glass and other silicium based networks can be functionalized with amines using silans like (3-aminopropyl) trimethoxysilan.[238] Depending on the substituents of the aldimine, both oxime and aldimine tend to behave similar towards hydrolysis under acidic conditions.[239] Hence, both ligation pathways complement each other and are equal in application variety.
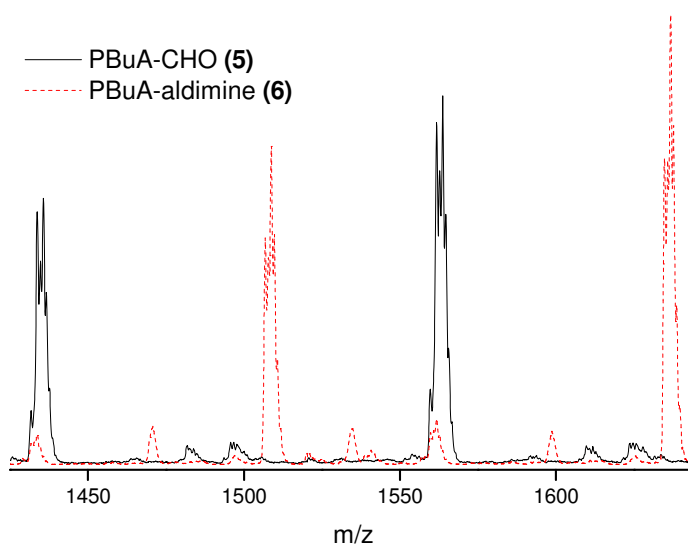
Fig. 9.5: End group modification of aldehyde functionalized PBuA via condensation.

The one-pot aldimine-formation followed by HDA reactions showed no success for polymer end group modification. Hence, the above described aniline-based polymer aldimine was further used to test the HDA reactions (see **Table 9.4**). Even though this particular reaction product did not carry an activating nitro-group, some reaction was expected when comparing the outcome of the HDA reactions given in **Table 9.3**. Yet, each tested reaction was completely unsuccessful, indicating that the obtained aldimine is generally not reactive in an HDA reaction.

Table 9.4: Hetero Diels-Alder [4+2] polymer cycloaddition of a polymer. The reaction were performed in 5 mL dry THF for 18 hours at room temperature at continuously stirring (M_n = 2200 g mol^{-1}; c = 1.14 mmol L^{-1}).

| Entry | Equivalent | | | | | Lewis acid / equiv. | $yield_{ESI/MS}$ / % |
	ATRP-polymer	aldimine polymer	Aniline	Furan	Cp		
1		1		50		BF$_3$·Et$_2$O: 2	< 1
2		1			50	BF$_3$·Et$_2$O: 2	0
3	1		50	50		BF$_3$·Et$_2$O: 2	0
4	1		50		50	BF$_3$·Et$_2$O: 2	< 1
5		1	50		50	Diphenyl phosphate: 2	0

9.3.3 Danishefsky's diene as an alternative for HDA reactions in normal electron demand DA

The previous results showed that the concept of the irreversible HDA is possible for small molecules but the transfer to polymers fails entirely due to the mismatch of reactivities required for the aldimine formation and the HDA cycloaddition, respectively. Yet, being able to synthesize aldimines as endgroups is by itself interesting as the concept and very similar to the oxime ligation that is often used in polymer conjugation.

For the conjugation, we focused on the second HDA route via *Danishefsky's* diene. A specific reaction scheme is given in **Fig. 9.6**.

Fig. 9.6: Mechanism of a Diels-Alder [4+2] cycloaddition using *Danishefsky's* diene.
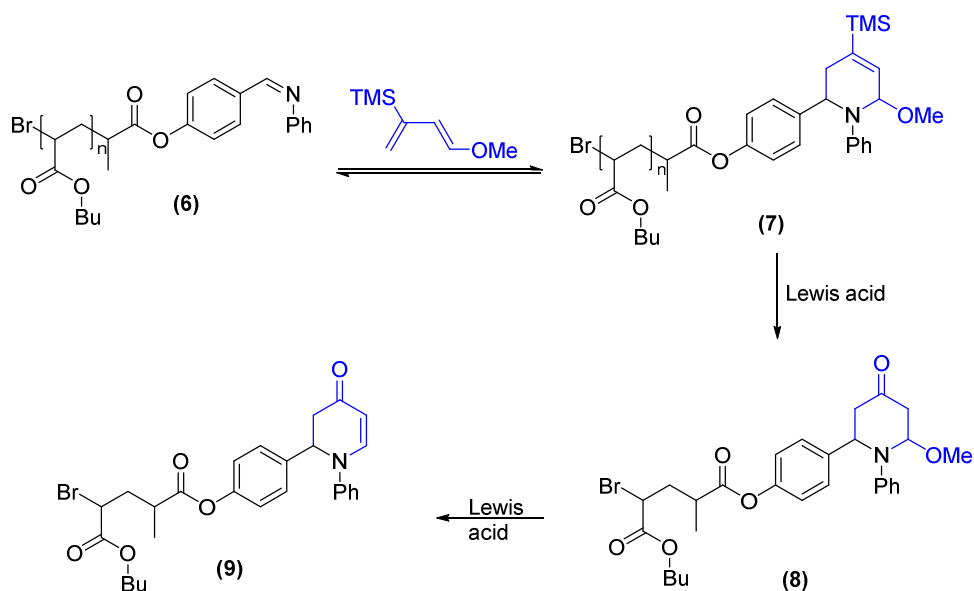
Table 9.5: Overview of the reactions between aldehyde functionalized polymers and *Danishefsky's* diene. The reaction were carried out in solution of 5 mL dry THF (M_n = 2200 g mol^{-1}; c = 1.14 mmol L^{-1}).

Entry	Equivalent		T / °C	t / h	Lewis acid / equiv.	yield$_{ESI/MS}$ / %
	aldimine polymer	Danishefsky's diene				
1	1	50	RT	18	BF$_3$·Et$_2$O: 2	20$_{(8)}$ + 80$_{(9)}$
2	1	50	RT	5 days	BF$_3$·Et$_2$O: 2	32$_{(8)}$ + 48$_{(9)}$
3	1	50	RT	5 days	BF$_3$·Et$_2$O: 5	16$_{(8)}$ + 65$_{(9)}$
4	1	50	RT	5 days	Yb(OTf)$_3$: 5	50$_{(9)}$

Table 9.5 gives the outcome of the HDA of the polymeric aldimine with the *Danishefsky's* diene, using an excess of the diene, 100 % yield can be reach within 18 h at room temperature. Compared to the reaction with Cp or furan, a much higher driving force for the HDA reaction to occur is postulated, which can be easily explained by the rise in the HOMO-level and subsequent better orbital overlap with the aldimine. The reaction must be differentiated between two

different product species. After HDA reaction, the employed Lewis acid promotes the cleavage of the TMS group, effectively making the reaction irreversible. In a second step, also the methoxy group originally attached to the diene, can be cleaved, giving rise to the second product. Both products (**8**) and (**9**) were identified via ESI/MS (see **Fig. 9.7**). Product (**7**), which is in principle capable of an rDA was not detected in ESI/MS. The theoretical molecular weights of the cycloadducts; e.g. (theo$_{(8)}$ = 1574.79 Da) match the measured m/z values (exp$_{(8)}$ = 1574.83 Da).
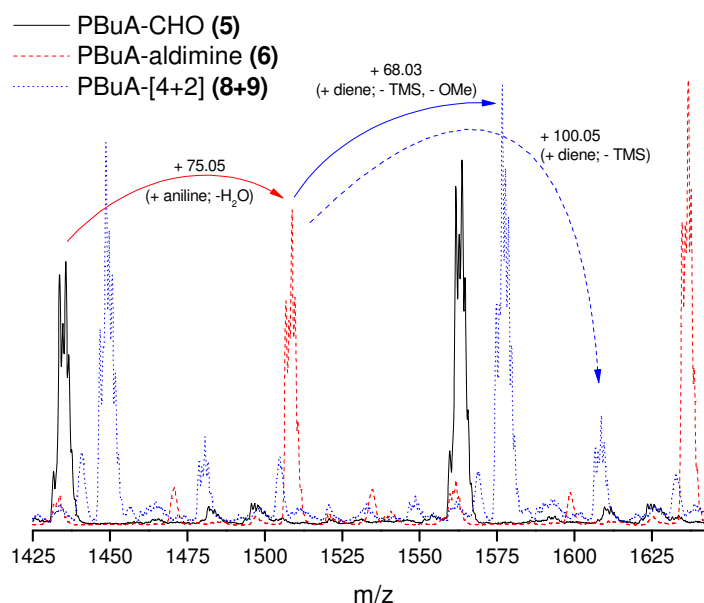
Fig. 9.7: Zoom into one repeating unit of the ESI/MS [4+2] cycloaddition using *Danishefsky's* diene.

Table 9.5, entry 2-4 shows that a prolonged reaction did not increase the yield. Longer reaction times (entry 2) and higher amounts of Lewis acid (entry 3, 5 equiv.) decrease the yield, most likely due to degradation or competitive side reactions. Also the choice of Lewis acid has a considerable impact. While good results are obtained with $BF_3 \cdot Et_2O$, only moderate yields are observed in reactions with $Yb(OTf)_3$.

9.4 Conclusions

It was shown that the concept of an irreversible inverse electron-demand aza-Diels-Alder between electron-poor aldimines and a suitable diene like furan yielded an cycloadduct in a one-pot-synthesis with high yield (100%, see **Table 9.2**) for small molecules. Transfer of this reaction strategy towards a polymeric system fails and leads to a mismatch of reactivities for the HDA reaction and aldimine formation. Polymeric aldimine formation proceeds with high yields with pure aniline, yet, this substrate shows no reactivity towards the HDA reaction in an inverse electron-demand reaction. On the other hand, it was demonstrated that a reaction between the highly electron rich *Danishefsky's* diene and the aldimine proceeds well with very high efficiency.

Chapter 10

10. Experimental section

10.1 Analytical equipment

Electro spray ionization mass spectrometry (ESI/MS). The spectra were recorded on an LCQ mass spectrometer (Finigian MAT) equipped with an atmospheric pressure ionization source operating in the nebulizer assisted electro spray mode. The instrument was calibrated in the m/z range 220-2000 using a standard solution containing caffeine, MRFA and Ultramark 1621. A constant spray voltage of 4.5 kV was used and nitrogen at a dimensionless auxiliary gas flow-rate of 10 and a dimensionless sheath gas flow-rate of 60 were applied. The capillary voltage, the tube lens offset voltage and the capillary temperature were set to 34 V, 10 V and 270°C, respectively. A 250 µL aliquot of a polymer solution with concentration of 10 µg mL^{-1} was injected. A mixture of either THF and methanol (THF:MeOH = 3:2) or dichloromethane and methanol (DCM:MeOH = 1:3), all HPLC grade, were used as solvent.

Electrospray ionization mass spectrometry (ESI/MS) was performed on an LTQ Orbitrap Velos Pro mass spectrometer (Thermo Fischer Scientific) equipped with an atmospheric pressure ionization source operating in the nebulizer-assisted electrospray mode. The instrument was calibrated in the m/z range 220-2000 using a standard solution containing caffeine; MRFA, and Ultramark 1621. A constant spray voltage of 5 kV was used, and nitrogen at a dimensionless auxiliary gas flow rate of 3 and a dimensionless sheath gas flow rate of 3 were applied. The capillary voltage, the tube lens offset voltage, and the capillary temperature were set to 25 V, 120 V, and 275°C, respectively. A 250 µL aliquot of polymer solution with a concentration of 10 µg ml^{-1} was injected. A mixture of THF and methanol (THF:MeOH = 3:2), all HPLC grade, were used as solvent.

THF size exclusion chromatography (THF-SEC). Analysis of the MWDs of the polymer samples were performed on a Polymer Laboratories Spectra Series (P100, AS100, Shodex RI-71), comprising an autosampler, a PLgel 5.0 µm guard column (50 × 7.5 mm), followed by three PLgel 5 µm Mixed-C columns (300 × 7.5 mm) and a differential refractive index detector using THF as the eluent at 40°C with a flow rate of 1 mL min^{-1}.

Analytical SEC (Size Exclusion Chromatography) was performed on a Tosoh EcoSEC HLC-8320 GPC, comprising an autosampler, a PSS guard column SDV (50 x 7.5 mm), followed by three PSS SDV analytical linear XL (5 µm, 300 x 7.5 mm) columns thermostated at 40°C (column molecular weight range: 1×10^{2} – 1×10^{6} g mol^{-1}), and a differential refractive index detector (Tosoh EcoSEC RI) using THF as the eluent at with a flow rate of 1 mL·min^{-1}.

The SEC system was calibrated using linear narrow polystyrene standards ranging from 474 to 7.5×10^6 g mol^{-1} (PS (K = 14.1×10^{-5} dLg^{-1} and α = 0.70), PiBoA (K = 5.0×10^{-5} dLg^{-1} and α = 0.745), PMMA (K = 9.44×10^{-5} dLg^{-1} and α = 0.719)), BA (α = 0.74, K = 10.2×10^{-5} dL g^{-1}, THF 30°C)[99] and NIPAAM (α = 0.54, K = 24.9×10^{-5} dL g^{-1}, THF 20°C)[240] and toluene as a flow marker.

Nuclear magnetic resonance spectroscopy. ^{1}H-NMR spectra were recorded in deuterated chloroform, D_2O and $DMSO_{D6}$ applying a pulse delay of 12 s with two NMR spectrometer (300 and 400 MHz) from Oxford Instruments Ltd. using a Varian probe (9 mm-4-nucleus AutoSWPFG).

Transmission electron microscopy (TEM). The particle size and the morphology of the polyDVB nanoparticles were studied using a Transmission Electron Microscope (TEM) (FEI Tecnai G2 Spirit Twin) operated at 120 kV.

Scanning electron microscopy (SEM). The characterization of the nanoparticles were carried out using an FEI Quanta 200FEG-SEM instrument.

Dynamic light scattering (DLS). The average hydrodynamic diameter and the polydispersity index of the nanoparticles were determined using a ZetaPALS equipment (Brookhaven Instruments Cooperation).

Infrared spectroscopy. Infrared spectra were recorded using an attenuated total reflectance infrared (ATR-IR) from BRUKER, Tensor-27, ATR probe Pike MIRacle 19993.

Elemental analysis. Analysis was carried out with a FlashEA 1112 Elemental Analyzer (Thermo Electron Corporation) and using BBOT (2,5-bis(5-tert-butyl-benzoxazol-2-yl)thiophene – $C_{26}H_{26}N_2O_2S$) as an internal standard in order to monitor the progress of the functionalization at each step and to calculate the grafting density based on the oxygen content.

Photoemission spectroscopy. All photoemission spectra were measured using a commercial Physical Electronics PHI-5600LS photoelectron spectrometer. Core-level spectra were acquired using monochromatized Al-K$_\alpha$ X-rays (photon energy 1486.6 eV). The spot size of the beam was about 1 mm^2, and the overall energy resolution (photons and photoelectrons) was adjusted to < 0.5 eV (FWHM). The binding energy scale was calibrated by means of an independent Au reference sample setting the Au 4f$_{7/2}$ core level position to 84.00 eV.

Contact angle measuremnet. The contact angle measurement (sessile drop methode) was performed on a DataPhysics OCA-15 plus with distilled H_2O.

Gas chromatography/ mass spectrometry. GC/MS were measure with a Thermo Scientific Trace GC Ultra, a DSQ II iontrap equipped with an autoinjector AI 3000.

10.2 Other equipment

Continuous tubular reactor setup. The tube flow UV-reactor consists of a HPLC pump (Knauer BlueShadow 20P), a quartz cooling mantle (Photochemical Reactors Ltd., UK) which was wrapped tightly by a 25 m fluorinated gastight transparent PFA tubing (VICI, 1/16" × 0.75 mm, 25 m, V_{tubing} = 11 mL). A 16 W low pressure lamp (λ_{max} = 254 nm) or a 400 W medium pressure UV-lamp (λ_{max} = 365 nm). The whole tubing is irradiated homogeneously by the UV-lamp. The reaction temperature (T = 4°C) was controlled by a cryostat (Grant LTD6/20) filled with water. Furthermore, the irradiation source and reactor is mounted in a closed box for safety reasons.[76] Only in **Ch. 6** a peristaltic pump (Heidolph Pumpdrive 5001, SP quick) was used.

Microreactor setup. The microreaction was performed in the Labtrix® Start R2.2 system (Chemtrix BV, NL), fitted with a glass microreactor (3227, reactor volume = 19.5 µL) containing an SOR-2 static micromixer. Reactant solutions were introduced into the reactor through two 1 mL gas-tight syringes (SGE) capable of delivering two solutions at flow rates between 0.1 and 25 µL min^{-1}. The flow rates were controlled via a syringe pump (Chemyx) and the reactor temperature was controlled via a thermoelectric cooler temperature controller MTTC1410 (Melcor Thermal Solutions, temperature range −15–195°C). The same setup was used by Vandenbergh *et al*. for thermal polymerizations.[179] An OMNICURE Series 1000 system was used as UV-light source. The OMNICURE system was equipped with a 100 W high pressure mercury vapor short arc lamp (320–500 nm) at an iris setting of 50 %.

Solvent drying machine. Dry solvents (DCM, THF, DMF, CHCl$_3$, and toluene) were obtained via a Braun MB SPS-800 solvent purification system.

10.3 Experimental part for Ch. 3 - Photoinduced conjugation of aldehyde functional polymers with olefins via [2+2] cycloaddition

Materials. Isobornyl acrylate (iBoA, Aldrich, tech.), styrene (Sty, Aldrich, 99%), methyl methacrylate (MMA, Aldrich, 99%) monomers were de-inhibited over a column of activated basic alumina. Copper (I) Bromide (Cu(I)Br, Sigma-Aldrich, 98%) was washed with acetic acid at 80 °C for 18 h to remove any soluble oxidized species before being filtered, washed with absolute ethanol, to pH 7, then washed with ethyl ether, and then dried under vacuum. 4-Hydroxybenzaldehyde (Aldrich, 98%), 2-bromopropanoyl bromide (Aldrich, 97%), triethylamine (TEA, Sigma-Aldrich, 99%), 1-octene (Aldrich, 98%), 2-methylpentene (Aldrich, 98%), allylamine (Aldrich, 98%), 3-buten-1-ol (Aldrich, 96%), trimethylolpropane allyl ether (Aldrich, 98%), triallyl cyanurate (Aldrich, 97%) were used as received.

Synthesis of 4-formylphenyl-2-bromopropanoate (FPBP). The compound 4-hydroxybenzaldehyde (9.327 g, 0.076 mol), 200 mL THF and TEA (9.754 g, 0.096 mol) were placed into a 250 mL three-necked round bottom flask fitted with a condenser, a magnetic stirrer, a nitrogen inlet-outlet, and an addition funnel containing a mixture of 2-bromopropanoyl bromide (20 g, 0.096 mol) and 50 mL THF. The flask was placed into an ice-water bath. The solution of 2-bromopropionyl bromide was added dropwise over a period of 0.5 h under inert conditions. Subsequently, the mixture was allowed to reach room temperature and left stirring overnight. A white precipitate was filtered off. The solvent was removed and the crude product was dissolved in dichloromethane. The solution was washed three times with 1 M HCl and twice with water. Finally, the solution was dried with $MgSO_4$, and the solvent was removed in vacuo. Further purification by column chromatography, using hexane and ethyl acetate (hex: EtOAc = 5:1–3:1) as eluents, yielded 15.16 g (77.3 %) yellowish liquid product.

^{1}H NMR (300 MHz, $CDCl_3$): δ = 9.96 (s, 1H, CHO), 7.92-7.88 (m, 2H, ortho to CHO), 7.30-7.23 (m, 2H, meta to CHO), 4.61-4.54 (q, 1H, CHBr, J = 6.86 Hz) and 1.92 (d, 3H, CH3, J = 6.86 Hz).

General ATRP polymerization. The purified Cu(I)Br (0.75 mmol, 108 mg, 1.5 eq.) was added under inert atmosphere into a sealed schlenk tube. A mixture of 0.076 mol (16 mL, 150 eq.) of the monomer iBoA and 1.13 mmol (235 µL, 2.2 eq.) of PMDETA was purged with nitrogen for 0.5 h to remove residual oxygen followed by addition to the reaction flask via a degassed syringe. EtOAc, 25 vol % was treated likewise and the reaction mixture was heated up to 75°C in an oil bath. Subsequently, the polymerization was started by adding 0.5 mmol (128 mg, 1 eq.) of degassed initiator. After the desired reaction time was reached,

polymerization was stopped by cooling in liquid nitrogen and a NMR sample was taken for conversion determination. The polymer/monomer mixture was dissolved in THF and the copper catalyst was removed by passing the diluted reaction mixture over silica. After evaporating of the excess solvent, the polymer was precipitated into a mixture of ice cold methanol:water (4:1; 10-fold excess) yielding 5.32 g of polymer with M_n = 3200 g mol^{-1} and $Đ$ = 1.16 (by THF-SEC).

Procedure for [2+2] cycloaddition. A typical procedure is given; 55 mg (0.02 mmol, 1 eq.) of aldehyde functional polymer (M_n = 3200 g mol^{-1}, Đ = 1.16) was mixed with 140 μL 1-octene (0.885 mmol, 50 eq.) and dissolved in 1.25 mL toluene. The flask was sealed and flushed for 10 min with N_2 and later stirred for 48 h at room temperature while irradiated with UV-light using a Multilamp Reactor MLU 18 from Photochemical Reactor Ltd. After reaction, the solvent and remaining olefin was removed in vacuo.

10.4 Experimental part for Ch. 4 – UV-induced functionalization of poly (divinylbenzene) nanoparticles via efficient [2+2] photocycloaddition

Materials. Sodium dodecyl sulfate (SDS, Merck), hexadecane (Sigma Aldrich) and 2,2'-Azodi(2-methylbutyronitrile) (Wako Chemicals, V59) were used as received and without further purification. Divinylbenzene (DVB, Sigma Aldrich, 80%) and butyl acrylate (BuA, Sigma Aldrich, 99%) monomers were passed through a basic alumina column to remove the inhibitor. Copper bromide (CuBr, Sigma Aldrich, 98%) was purified by successively washing with acetic acid, absolute ethanol and ethyl ether and dried under vacuum. Goat Anti-Mouse IgG (H+L) with 40 nm gold label was obtained from Kirkegaard & Perry Laboratories, Inc. (KPL).

Synthesis of polydivinylbenzene nanoparticles. Polydivinyl benzene (polyDVB) nanoparticles were prepared via radical polymerization using the miniemulsion technique. The oil phase consisting of 3 g of divinylbenzene monomer, 0.125 mg hexadecane and 50 mg initiator V59 was mixed and emulsified in the continue phase comprising of 12 g deionized water and 36 mg of the ionic SDS surfactant. After an hour of premulsification via stirring at 1000 rpm, the miniemulsion was prepared by ultrasonication for 3 minutes at 65% intensity (Branson 450W sonifier, 1/4 inch tip) in a pulse regime (30 seconds sonication, 20 seconds pause) at 0°C to avoid polymerization of the monomer. The polymerization was done at 72°C while stirring for 30 minutes. The polyDVB nanoparticles were extensively washed with deionized water and ethanol by repetitive centrifugation and redispersion in order to remove the surfactant and the unreacted monomer. Finally, the nanoparticles were isolated and freeze-dried to remove all solvents.

[2+2] cycloaddition with ATRP initiator. An aldehyde functionalized ATRP initiator 4-Formylphenyl 2-bromopropanoate (FPBP) was used for the [2+2] cycloaddition. The synthesis of this initiator is described elsewhere.[103] For the surface functionalization of the polyDVB particles with the ATRP initiator, 25 mg of polyDVB particles were mixed with 25 ml of dichloromethane and treated with ultrasound for 10 minutes to prevent clustering of the polymer particles. 250 mg of 4-formylphenyl 2-bromopropanoate was added to the flask, sealed and flushed with N_2 for 30 min. This was followed by 48 h of UV-light irradiation at room temperature while being stirred. After the reaction, the solvent was removed by evaporation and the nanoparticles were washed thoroughly with toluene by centrifugation and redispersion to remove the remaining initiator.

ATRP polymerization. 10 mg of polyDVB particles, which are surface functionalized with the ATRP initiator, 5 mg (0.035 mmol) CuBr and 1 mL of

toluene were added into a sealed Schlenk tube, degassed and treated with ultrasound for 10 minutes. A mixture of 500 µL (3.5 mmol) of the monomer BuA and 15 µL (0.07 mmol) PMDETA was flushed with N_2 for 30 minutes followed by addition to the Schlenk tube via a degassed syringe. The reaction mixture was heated in an oil bath for 24 h at 65°C and polymerization was stopped by cooling in ice bath. The particles were washed extensively with deionized water and THF to remove the copper catalyst and the non-grafted polymer chains.

Synthesis of N-succinimidyl-*p*-formylbenzoate. In a 3-necked 250 mL flask, 4-formyl benzoic acid (5 g, 33.3 mmol), N-hydroxysuccinimide (NHS) (11.5 g, 99.9 mmol), and 50 mL dry tetrahydrofuran were mixed and cooled in an ice bath. N,N'-dicyclohexylcarbodiimide (DCC) (7.56 g, 36.6 mmol) was dissolved in 20 mL dichloromethane; 4-Dimethylaminopyridine (DMAP) (0.41 g, 3.33 mmol, 0.1 eq.) was dissolved in 10 mL dichloromethane and both added slowly over a period of 10 minutes to the mixture. Urea formed immediately upon first drop of DMAP addition. The mixture was kept in an ice bath for an hour and stirred for 48 h at room temperature. The mixture was filtered to remove the urea. After addition of ~50 mL diethylether, a white precipitate was formed immediately. The precipitate was washed with distilled water and the water phase with white precipitate was filtered. The filtrate was washed with ethyl acetate and dried with $MgSO_4$. After evaporation of the solvent a white powder is obtained. Yield was 60%. ^{1}H-NMR, $CDCl_3$: δ = 10.15 (-CHO, s, 1H), 8.33-8.30 (ortho to CHO, d, 2H), 8.05-8.03 (meta to CHO, d, 2H), 2.95 (-CH2, s, 4 H).

Coupling of gold labelled biomolecules. For the coupling of gold labeled biomolecules to the polyDVB nanoparticles, NHS group was first incorporated to the particle surface by an UV-induced [2+2] cycloaddition on the polyDVB particles with an aldehyde functionalized NHS-ester. 25 mg of polyDVB particles were mixed with 25 mL of THF and treated with ultrasound for 10 minutes to prevent clustering of the polymer particles. 250 mg of N-succinimidyl-*p*-formylbenzoate was added to the flask, sealed and flushed with N_2 for 30 min. This was followed by 48 h of UV-light irradiation at room temperature while being stirred. After the reaction, the solvent was removed by evaporation and the nanoparticles were washed thoroughly with THF by multiple centrifugation and redispersion to remove the remaining starting products. In order to couple the biomolecules, the NHS-ester functionalized particles were dispersed in MES buffer (10 mM; pH 8.5) to reach a solid content of 0.5%. 50 µL gold-labelled goat Anti-Mouse IgG were added and mixed for 3h. Afterwards, the samples were washed with 0.1 mM MES buffer by centrifugation and redispersion.

10.5 Experimental part for Ch. 5 – Application of the [2+2] Paternò-Büchi cycloaddition for cellulose surface modification

Materials. Following products were used: VWR filter paper (No. 516-0813), Whatman filterpaper (No. 5), *p*-toluenesulfonyl chloride acid (Aldrich, 99%), 4-hydroxybenzaldehyde (Acros, 99%), sodium hydroxide (NaOH, Vel), pyridine (Acros, 99+%, dried over molsieve), DBU (1,8-Diazabicycloundec-7-ene, Acros, 99%), N-isopropylacrylamide (NIPAAM, Acros, 99%), DMF (dimethylformamide, VWR Prolabo, 99.8%), allyl chloroacetate (Acros, 98%), trimethylolpropane allyl ether (TMPEA, Aldrich, 98%), 2,4,6-trilallyloxy-1,3,5-triazine (triallylcyanurate, Aldrich, 97%), DoPAT (2-(dodecylthiocarbonothioylthio)propionic acid), AIBN (Acros, 98%), EtOAc, (VWR Prolabo 99.5%), DCM (VWR Prolabo, 99+%), 3-butenol (Aldrich, >98%) and dioxane (VWR Prolabo, 98%). The photosensitizer thioxanthen-9-one (TXS, 97%, Aldrich). DoPAT was prepared as described elsewhere.[241] BA and NIPAAM were passed over a silica column prior to use. AIBN was recrystallized twice before usage.

Pretreatment for activation of cellulose. The cellulose (VWR filter paper No 516-0813 and Whatman No 5) was cut into squares of approximately 0.5 × 0.5 cm. The cellulose (cel-OH) was shaked in 10% NaOH overnight. Afterwards the activated cellulose (cel-OH*) was repeatedly washed with absolute ethanol and was directly used.

Tosylation of cellulose. Cel-OH* (0.2 g) was mixed with an excess of *p*-toluene sulfonic acid chloride (2.35 g, 0.0123 mol) in dry pyridine (7.5 mL, 0.2 g cel-OH*). The mixture was stirred for approximately 24 h. To stop the reaction 15 mL of ice-cold H_2O/aceton (1:1, v/v) was slowly added. The toslyated cellulose (cel-OTs) can be subsequently washed with H_2O and then stored in THF. v_{max}(ATR)/cm^{-1}: 2950 – 2850, 1380 (-CH$_3$); 3100 – 3000, 1700 – 1500, 840 – 810 (C=C), 860 – 680 (=CH) and 1420 – 1330, 1200 – 1145 (-SO$_2$O-).

Cellulose-aldehyde adapted nucleophilic substitution via Williamson ether synthesis. 10 pieces of cel-OTs were mixed with *p*-hydroxybenzaldehyde (0.61 g, 5 mmol) and DBU (1,8-Diazabicycloundec-7-ene, 1.5 mL, 10 mmol) in 100 mL DMF. NaOH (0.2 g, 5 mmol) dissolved in 1 mL water was added. The reaction was placed on an orbital shaker for 7 days at RT and showed a new signal. ATR-IR, v_{max}(ATR)/cm^{-1}: 1685 (CHO).

Preparation of allyl functionalized DoPAT. The reaction was performed in flame-dried glassware. DOPAT (1 eq., 8.56 mmol, 3 g), 3-butenol (1.1 eq., 0.678 mmol, 0.809 mL) and 200 mL dry DCM were mixed in a three-neck flask under inert atmosphere. The mixture was cooled down to 0°C. Then a solution of

100 mL dry DCM containing DCC (1.2 eq., 10.3 mmol, 2.13 g) and DMAP (0.1 eq., 0.86 mmol, 0.11 g) was added dropwise. The solution turned immediately orange. The reaction mixture was allowed to reach r.t. and was stirred overnight. The white precipitate, urea, was removed by filtration over celite, washed with THF (3 x). The solvent was removed in vacuo and 100 mL water was added. The product was extracted three times with DCM, dried over $MgSO_4$, yielding of 3.79 g crude product. The crude product was purified via column chromatography (2:5 = EtOAc:PE), yielding 2.98 g (86.2%).

Preparation of allyl end group functionalized polymers. The synthesized RAFT agent allylDoPAT (1 eq., 0.69 mmol, 279 mg), BA (100 eq., 69.4 mmol, 10 mL), AIBN (0.05 eq., 0.035 mmol, 5.7 mg) and 5 mL EtOAc were added into a Schlenk flask. The mixture was deoxygenized via three freeze-pump-thaw cycles and then placed in a pre-heated oil bath (65°C). After 140 min, polymerization was stopped by cooling in ice water. After evaporating of the excess solvent and monomer, the polymer was characterized; yielding 4.3 g (48.2% *conv*.) of polymer with M_n = 6990 g mol^{-1} and $Đ$ = 1.12 (by THF-SEC).

The synthesized RAFT agent allylDoPAT (1 eq., 0.35 mmol, 143 mg), NiPAAM (75 eq., 26.5 mmol, 3.00 g), AIBN (0.1 eq., 0.035 mmol, 5.7 mg) and 10 mL dioxane were added into a Schlenk flask. It was deoxygenized via three freeze-pump-thaw cycles. The reaction mixture was placed in a pre-heated oil bath (80°C). After 60 min, polymerization was stopped by cooling in ice water. The polymer/monomer mixture was precipitated into petrol ether (three times). After evaporating of the solvent the polymer was characterized; yielding 1.68 g (56.4% *conv*.) of polymer with M_n = 9500 g mol^{-1} and $Đ$ = 1.16 (by THF-SEC).

Cycloaddition between the aldehyde-cellulose and allyl-functionalized polymer. One piece of cel-CHO (0.5 cm × 0.5 cm) was mixed with 25 mg polymer (either PBA or PNIPAAM), 0.1 mg TXS and 10 mL acetonitrile. The flask was sealed, flushed for 10 min with N_2 and later stirred for 48 h at room temperature while irradiated with UV-light using a Multilamp Reactor MLU 18 (12 × 15 W, λ_{max} = 254 nm) from Photochemical Reactor Ltd. After reaction the solvent and remaining polymer was washed with THF three times. Showing a new signal in infrared; v_{max}(ATR)/cm^{-1}: 1731 (C=O).

10.6 Experimental part for Ch. 6 – Efficient [2+2] photocycloadditions under equimolar conditions by employing a continuous UV-flow reactor

Materials. Maleimide (Sigma-Aldrich, 98%), 1-octene (Aldrich, 98%), 2-methyl-1-pentene (Aldrich, 98%), allylamine (Aldrich, 98%), 3-buten-1-ol (Aldrich, 96%), allyl ethyl ether (Sigma-Aldrich, 95%) and triallyl cyanurate (Aldrich, 97%) were used as received. The two solvent ethyl acetate and acetonitrile were of analytical grade (Prolabo, VWR).

General procedure for the [2+2] cycloaddition under batch conditions. A 0.104 M maleimide solution (1 equiv., 0.52 mmol, 50 mg) was mixed with 1-octene (10 equiv., 1.04 mmol, 0.163 mL) and filled up to a volume of 5 mL ethyl acetate ($0.1 \ \text{mol} \cdot \text{L}^{-1}$ solution with respect to maleimide). The solution was purged with nitrogen for 5 min to remove residual oxygen. Later, the solution was irradiated for 24 h in the Multilamp reactor MLU 18 under continuous stirring. The solvent and residual volatile alkene was removed under reduced pressure yielding the cycloadduct, 6-hexyl-3-azabicyclo [3.2.0]heptane-2,4-dione. Borosilicate glass containers were used as reaction vessel, thus a material with a UV cut-off close to the excitation wavelength of maleimide. Tests with fused silica containers demonstrated that the borosilicate vials gave comparable results in the used reactor/light source setup.

General procedure for the [2+2] cycloaddition under flow conditions. 0.01 M Maleimide (1 eq., 1 mmol, 97.1 mg) was mixed with 1-octene (1 eq., 1 mmol, 0.157 mL) and filled up to a volume of 100 mL with ethyl acetate (EtOAc). The solution was purged with nitrogen for 20 min to remove residual oxygen. Later the solution was pumped through the UV-reactor equipped with UV-transparent PFA tubing as the residence unit with a residence time of 2.5 min. The solvent and residual volatile alkene was removed under reduced pressure yielding the cycloadduct, 6-hexyl-3-azabicyclo [3.2.0]heptane-2,4-dione (The detailed flow reactor description and spectra e.g. NMR and FTIR can be found in the Supporting Information[76]).

^{1}H-NMR (CDCl$_3$, 300 MHz): δ = 8.01 (br s, 1H, NH), 3.5-2.5 (m, 2H, C$_{H \ \text{next to} \ \text{carbonyl}}$), 2.5-1.7 (m, 3H, CH & CH$_2$ ring), 1.7-1.4 (m, 2H, CH$_2$), 1.4-1.2 (m, 8H, CH$_2$), 0.88 (m, 3H, CH$_3$).[76]

v_{max}(film)/cm^{-1}: 3217, 3074, 2957, 2924, 2760, 2854, 1765, 1709, 1462, 1377, 1342, 1294, 1261, 1236, 1171, 1030, 972, 841, 800.

From integration of the NMR spectrum, the diastereomeric ratio can be determined to roughly 7:3 (GC analysis) for product *anti*-1 to *syn*-1 (**Ch. 6**, **Scheme 6.1**).

10.7 Experimental part for Ch. 7 – Fast and efficient photoinduced alkene-enone cycloaddition for polymer modification by applying UV-flow reactor technology

Materials. Ethanolamine (> 99%, Sigma Aldrich), Boc-anhydride (97%, Acros), THF (tech., Prolabo), maleimide (99% Aldrich), diisopropyl azodicarboxylate (DIAD 98%, Aldrich), triphenylphosphin (99%, Acros), TFA (99%, Acros), N-hydroxysuccinimide (NHS 98%, Aldrich), 2-bromopropionyl bromide (97%, Aldrich), 2-bromo-2-methylpropionyl bromide (98%, Aldrich), (99%, DCM (tech. Prolabo), pyridine (99+%, Acros), butyl acrylate (BA 99+%, Acros), CuBr (98%, Sigma Aldrich), PMDETA (99%, Aldrich), ethyl acetate (EtOAC tech., Prolabo), triethyl amine, thioxanthen-9-one (TXS 97%, Aldrich). 2-Methyl pentene (99%, Acros), 1-octene (98%, Aldrich), cyclooctene (95% COE, Fluka), allyl amine (98%, Aldrich), buten-3-ol (96%, Aldrich), allyl ethylether (95%, Aldrich), styrene (99.5%, Acros) and triallyl cycanurate (97%, Aldrich). The BA was deinhibited over a column of basic alumina, prior to use. Copper(I) bromide was first washed with acetic acid, later ethanol then diethyl ether (tech.) and dried in vacuo. All other compounds were used as received.

Synthesis of NHS modified ATRP initiators: a) 2,5-dioxopyrrolidin-1-yl 2-bromo-2-methylpropanoate and b) 2,5-dioxopyrrolidin-1-yl 2-bromopropanoate. Both initiators were synthesized following modified literature procedures.[242] NHS (6 g, 1.2 eq., 52.1 mmol), 100 mL dry DCM and pyridine (3.86 g, 1.1 eq., 47.8 mmol) were placed into a 250 mL three-necked round bottom flask fitted with a condenser, a magnetic stirrer, a nitrogen inlet, and an addition funnel containing a mixture of the corresponding acid bromide [a) 2-bromopropionyl bromide (9.38 g, 1 eq., 43.4 mmol) and b) 2-bromo-2-methylpropionyl bromide (10.00 g, 1 eq., 43.4 mmol)] and 50 mL DCM. The flask was placed into an ice-water bath. The solution of the acid bromide was added dropwise over a period of 0.5 h under nitrogen. Then the mixture was stirred at room temperature overnight, after which 100 mL DCM was added. The solution was washed three times with 1 M HCl, once with 150 mL H_2O and with brine (150 mL). Finally, the organic phase was dried with $MgSO_4$, and the solvent was removed, yielding fine white crystals. Yield: a) 7.82 g (72%) and b) 8.72 (76%) Further purification was performed via column chromatography (silica) using hexane:EtOAc = 3:1, v/v. a) secondary NHS-ester initiator: ^{1}H-NMR (300 MHz, $CDCl_3$) = 4.45-4.36 (q, 1H, CHBr, J = 7 Hz), 2.76 (s, 4H, CH_2), 1.84 (d, 3H, CH_3, J = 7 Hz). b) tertiary NHS-ester initiator: ^{1}H-NMR (300 MHz, $CDCl_3$) = 2.85 (s, 4H, CH_2), 2.06 (s, 6H, CH_3).

Preparation of Boc-protected ethanolamine.[243] Ethanolamine (1 eq., 1.4 g, 22.91 mmol) was dissolved in 50 mL dry THF and cooled down to 0°C. Boc-anhydride (1 eq. 5.0 g, 22.91 mmol) was added and a white precipitate was

formed immediately but disappeared again. The reaction mixture was allowed to reach room temperature and stirred for 4-5 h. Then the solvent was removed and the remaining clear oil was dissolved in DCM. The organic layer was consecutively washed with 25 mL $NaHCO_3$ solution, 25 mL water and 25 mL brine and dried over $MgSO_4$. The solvent was removed in vacuo, yielding a clear oil as product (3.05 g, 83%). ^{1}H-NMR ($CDCl_3$, 300 MHz): 5.02 ppm (br s, 1H, NH), 3.69 (t, 2H, CH_2), 3.06 (t, 2H, CH_2), 2.97 (br s, 1H, OH), 1.43 (s, 9H, CH_3).

Preparation and deprotection of 1-(2-aminoethyl)-1*H*-pyrrole-2,5-dione trifluoroacetate.[244] Ph_3P (1 eq, 11.74 g, 44.79 mmol) and DIAD (1 eq, 8.79 mL, 1.03 g cm^{-3}, 44.79 mmol) was dissolved in 250 mL dry THF at 0°C and stirred for 20 min, yielding a yellow cloudy mixture. Then the Boc-protected aminoethanol (1 eq, 7.22 g, 44.79 mmol), dissolved in 100 mL dry THF was added at 0°C and stirred for 20 min. When the maleimide (1.2 eq, 5.22 g, 53.75 mmol) was added, the solution changed color quickly to orange. The reaction was then stirred at room temperature for 2 days. The solvent was removed and the orange oil was washed twice with hexane:Et_2O (1:1, v/v) to remove $Ph_3P=O$ residues. The product was purified via column chromatography with petrol ether:EtOAc (5:2->2:1, v/v); The product was obtained as white powder (7.04 g, 65.4%). ^{1}H-NMR ($CDCl_3$, 300 MHz): δ = 6.71 (s, 2H, H_{ring}), 4.72 (br s, 1H, NH), 3.66 (m, 2H, CH_2), 3.33 (m, 2H, CH_2NH), 1.40 (s, 9H, CH_3).

Deprotection was carried out with 40% TFA solution in DCM at 0°C and stirring for 2-3 h.[245] The solvent and excessive TFA was removed under reduced pressure. The residue was dissolved in 5 mL MeOH and precipitated into 50 mL Et_2O, yielding the ammonia trifluoroacetate salt as a fine fluffy powder (4.38 g, 86.6%). ^{1}H-NMR (D_2O, 400 MHz): δ = 6.86 (s, 2H, H_{ring}), 3.80 (m, 2H, CH_2), 3.19 (m, 2H, $CH_2NH_3^+$).

Exchange of NHS-group by maleimide ammonia trifluoroacetate. NHS-functional poly(butyl acrylate) (1 eq., 1.31 g, 1.08 mmol, 1200 g mol^{-1}) was mixed with ammonia trifluoroacetate salt (2.2 eq., 605 mg, 2.38 mmol) and triethylamine (TEA) (2.2 eq, 790 µL, 0.7255 g cm^{-3}, 2.38 mmol) in solution of 10 mL dry THF. The mixture was stirred for 2 days at 30°C in the dark. The excess of TFA-salt and amine was removed via passing the solution through a 3-4 cm thick layer of silica, for three times (1.28 g, 98%). ESI/MS (3 THF: 2 MeOH, positive mode): $C_{79}H_{131}N_2O_{23}BrNa^+$; theory: 1577.822 g mol^{-1}; found: 1577.8 g mol^{-1}.

General procedure for ATRP polymerization. The purified Cu(I)Br (1 eq., 1.38 mmol, 198 mg), BA (75 eq., 104.13 mmol 15 mL) and PMDETA (2 eq., 2.75 mmol, 575 µL) was added into a sealed Schlenk tube. A second Schlenk tube with 2,5-dioxopyrrolidin-1-yl 2-bromopropanoate (1 eq., 1.38 mmol, 348 mg) and 1 mL EtOAc was prepared. Both tubes were deoxygenized via three

freeze-pump-thaw cycles. The initiator solution was then added via a degassed needle to the monomer solution and the reaction mixture was placed in a pre-heated oil bath (65°C). After 30 min, polymerization was stopped by cooling in liquid nitrogen and a NMR sample was taken for conversion determination. The polymer/monomer mixture was dissolved in THF and the copper catalyst was removed by passing the diluted reaction mixture over silica. After evaporating of the excess solvent and monomer, the polymer was characterized; yielding 1.3 g (9.8% *conv*.) of polymer with M_n = 1300 g mol^{-1} and $Đ$ = 1.18 (by THF-SEC).

10.8 Experimental part for Ch. 8 – Photo-induced copper-mediated polymerization of methyl acrylate in continuous flow reactors

Materials. Ethyl 2-bromoisobutyrate (EBiB, Alfa Aesar, 98+%), copper(II) bromide (CuBr2, Sigma-Aldrich, 99%), dimethyl sulfoxid (DMSO, Merck, pro analysis) were all used as received. Tri(2 (dimethylamino)ethyl)amine (Me$_6$TREN) was synthesized according to literature procedure[246]. Methyl acrylate (MA, Acros, 99%) and butyl acrylate (BA, Acros, 99%) was deinhibited over a column of activated basic alumina, prior to use.

General procedure for the synthesis of PMA using the continuous tubular flow reactor. Methyl acrylate (23.723 g, 47 eq., 275.29 mmol), EBiB (1.165 g, 1 eq., 5.90 mmol), CuBr$_2$ (0.025 g, 0.02 eq., 0.11 mmol) and Me$_6$TREN (0.157 g, 0.12 eq., 0.69 mmol) were mixed in a 250 mL volumetric flask and filled up to a volume of 250 mL with DMSO. The polymerization targeted a number average molecular weight (M_n) of 4000 g mol^{-1}. The mixture was poured into a 250 mL brown laboratory bottle with a GL-45 screw cap and purged with nitrogen for approximately 45 min before starting the polymerization. Polymerizations with other target molecular weights were carried out accordingly under adjustment of concentrations.

Procedure for the synthesis of PMA using the microreactor setup. Methyl acrylate (0.415 g, 44 eq., 4.82 mmol), EBiB (0.021 g, 1 eq., 0.11 mmol), CuBr$_2$ (0.001 g, 0.02 eq., 0.01 mmol) and Me$_6$TREN (0.003 g, 0.12 eq., 0.01 mmol) were mixed in a 5 mL volumetric flask and filled up to a volume of 5 mL with DMSO. The polymerization targeted a number average molecular weight (M_n) of 3800 g mol^{-1}. Prior to use the mixture was purged with nitrogen for 3 min and then transferred into two 1 mL gas tight syringes and inserted into the syringe pump.

10.9 Experimental part for Ch. 9 – Irreversible Diels-Alder [4+2] cycloaddition for polymer end group modification

Materials. Butyl acrylate (BuA, Sigma Aldrich, 99%) was passed through a basic alumina column to remove the inhibitor. Copper bromide (CuBr, Sigma Aldrich, 98%) was purified by successively washing with acetic acid then absolute ethanol (EtOH) followed by diethyl ether (Et$_2$O) and dried under vacuum. 4-Hydroxybenzaldehyde (Aldrich, 98%), 2-bromopropanoyl bromide (Aldrich, 97%), triethylamine (TEA, Sigma-Aldrich, 99%), aniline (Sigma Aldrich, 99.5%), 4-nitroaniline (Sigma Aldrich, 99%), dicyclopentadiene (DiCp, Sigma Aldrich, 95%), furan (Acros, 98%), boron trifluoride etherate (BF$_3$·Et$_2$O in THF, Acros, 48%), ZnCl$_2$ anhydrous (Sigma Aldrich, 99.99%), ytterbium(III) trifluoromethanesulfonate (Yb(OTf)$_3$, Sigma Aldrich, 99.99%), diphenyl phosphate (Sigma Aldrich, 99%), *Danishefsky's* diene (trans-1-methoxy-3-trimethylsiloxy-1,3-butadiene, Sigma Aldrich, 95%) were used as received. THF was dried and purified via a Braun MB SPS-800 solvent purification system. The other solvents were purchased from Prolabo VWR in the required grades (i.e. HPLC grade for MS and SEC) and used without further purification.

ATRP polymerization. The initiator, 4-formylphenyl-2-bromopropanoate (FPBP), was synthesized as described elsewhere.[103] Two different solutions were made. One solution contained BuA (75 equiv., 104.13 mmol, 15 mL), Cu(I)Br (1 equiv., 1.375 mmol, 198 mg) and FPBP (1 equiv., 1.375 mmol, 353.5mg). The second solution contained PMDETA (2 equiv., 2.75 mmol, 0.575 mL) and 10 vol% EtOAc (1.5 mL). Both solutions were degassed via three cycles of freeze-pump-thaw and then mixed in a glove box. The polymerization was carried out at 65°C for 30 min, yielding 3.47 g (conv = 26%) with M_n = 2216 g mol^{-1}, DP_n = 17.3 and $Đ$ = 1.25.

Dicyclopentadiene preparation. Cyclopentadiene (Cp) was freshly obtained via retro Diels-Alder of diCp by distillation (oil bath T = 160°C.

General procedure aldimine formation. 4-Hydroxybenzaldehyde or FPBP (either 1 equiv.) was mixed with 1-2 equiv. of amine (either aniline or 4-nitroanilie) in dry THF. A spoonful of MgSO$_4$ was added to all samples to bind formed water. The reaction mixture was stirred at ambient temperature overnight.

General Diels-Alder reaction. The one-pot reactions were carried out as followed 4-hydroxybenzaldeyhde or FPBP (1 equiv.) was mixed with 1-2 equiv. of amine (either aniline or 4-nitroanilie), dienophil (freshly cracked Cp or furan; 1 equiv.) and 0.1-5 equiv. catalyst in 10 mL dry THF. For the reactions between

ATRP polymers (25 mg) and small molecules significant higher equivalent were tested (up to 50 equiv.). A spoonful of $MgSO_4$ was added to all samples to bind formed water. The reaction mixture was stirred at ambient temperature overnight.

Chapter 11

11. General conclusion

11.1 Summary

Modern synthetic photochemistry was developed in the middle of the last century. Mainly academics show interest in the field, particularly in the preparation of organic compounds.[170,171] Photochemistry has many advantages like spatial control. Reactions often require no further reagents than the compounds themselves and the solvents. In downstream processes, the product can be purified if necessary by conventional means. Up to now, only few research work was done by polymer chemists testing the utility of photochemistry for polymer modification. The here presented dissertation focused on the research of polymer modification. Photochemistry, mainly [2+2] cycloaddition was tested for its scope to modify polymer end groups, surfaces and particles. The research work consisted of two main tasks:

1. To search for and subsequently optimize an adequate photoreaction with high yields, high reaction rates, and functional group tolerance.
2. To improve this reaction by testing several photo-reactors and comparing different reactor techniques, i.e. batch *vs*. continuous flow mode.

The flow photochemistry technology was tested and applied as a synthetic mean for the preparation of well-defined polyacrylates and of block-copolymers. Additionally, alternatives for a photochemical modification were sought and resulted in the use of the established route for aldehyde end group functionalized polymers. These two chemical different modification routes provided true orthogonality.

The first photoreaction which was examined in this work and used for polymer end group modifications was the so-called Paternò-Büchi cycloaddition. This is a [2+2] addition between an aldehyde and an alkene. Therefore, functionalized polyacrylates were synthesized using an ATRP initiator carrying a carbonyl functionality. The reaction was carried out in a Multilamp ("Rayonet") reactor. After irradiation the bromine functionality was unharmed and could be used for a post-polymerization chain extension. By applying the Multilamp reactor, the reaction time needed for complete conversion was 48 h with a 50-fold excess of alkenes compared to the polymer end group. A drawback of the reaction is the relatively long reaction time and the required excess of quencher alkene. On the other hand, the reaction showed no side-product formation. The only observed product was the expected cycloadduct with the bromine end group. Moremore,

the reaction is tolerant towards a variety of functionalities like alcohols, ethers, multifunctional alkenes and can be applied as well for internal alkenes like cyclooctene.

The approach applying the Paternò-Büchi cycloaddition was used to surface graft nanoparticles made by mini-emulsion polymerization of divinylbenzene (DVB). The particle surface presented free alkenes which could be reacted in the formerly adapted [2+2] photo-addition with an ATRP initiator. In the following step, the initiator was used to grow polymer on top of the DVB particle. Via surface analytic techniques (EDX & XPS) the structure of the hairy nano-spheres and a high grafting density of 4 to 5 molecules per nm^2 were confirmed. The topology of the to-be modified structure does not play a significant role, because three-dimensional spheres and later on two-dimensional cellulose sheets were modified successfully.

Beside a surface patterning of nanoparticles by the alkenes-aldehyde cycloaddition, the developed reaction was also able to modify cellulose sheets with a thermo-responsive poly acrylamide. Thus, the cellulose was activated and surface modified. At first small molecules were coupled to the cellulose surface, as confirmed by ATR-IR. Afterwards, thermoresponsive PNIPAAM was photo-grafted to the natural substrate. In temperature-depending contact angle measurements, the substrate showed the typical switch from hydrophilic to hydrophobic behavior at temperatures above 32°C.

The lack of acceptable reaction rates was completely solved by switching over to a different [2+2] reaction, here alkene-enone system, in combination with the use of the flow chemistry technology. In the beginning, this process was tested only with small molecules. Maleimide served as an enone source. In batch mode, the reaction was faster than using aldehydes. The excess of alkenes could be reduced to 10-times and the reaction time was decrease to 8 h. Beside the reaction change, the reactor itself was changed from a batch to a continuous photo flow-reactor. With this setup change, the light efficiency of the UV-lamp exciting the enone functionality increased significantly. This effect mainly bases on the Lambert-Beer-law, due to the close distance between the light-arc and the reaction solution. The alkene excess could be lowered down to equimolarity and the reaction times were decreased to 5 minutes. Equimolarity of the reactants is an important condition, if the reaction shall fulfill the strict *click* reaction criteria for polymers.[31] For example, it is essential for the preparation of block-copolymers.

The alkene-enone photoreaction, performed in a UV-flow reactor, was transferred to a polymer system. A well-controlled P(BA) with an N-hydroxysuccinimide (NHS) end group was synthesized. The maleimide was subsequently introduced via exchanging the NHS-ester. By adding an aromatic ketone as a photosensitizer, the reaction was completed within one minute and degradation of polymer backbone due to high UV-irradiation (400 W) was suppressed. One weakness for polymeric systems was the loss of equimolarity. 5 equivalent of alkene are necessary to shift the reaction completely to the product side. Hence, a highly efficient polymer conjugation method was developed which is tolerant towards many different functionalities, as there are alcohols, ethers and multifunctional alkenes. The cycloaddition occurs faster for secondary and internal alkenes, thus broadening the application range.

Within the current research work, it was not possible to perform true *click* conditions. Beside this drawback, a powerful polymer modification reaction was established. The polymer modification reaction has two possible fields of application. The alkene-enone reaction can be used to modify two-dimensional surfaces. Only photochemical reactions allow a spatial control over the modification. The other application can be the coupling of small molecules, like linker/ anchor points to (nano)particles or a *grafting to* approach of pre-synthesized polymers to three-dimensional substrates. The newly developed photo-modification can be used for the creation of thermo-responsive substrates (e.g. using P(NIPAAM)), biosensor applications or drug-delivery particles. The alkene-enone cycloaddition is comparable to the photo-activated thiol-ene.[247] Both reactions need an excess of one of the reactants. On the other hand, they are both fast and versatile in application. In the future, both reactions can complete each other in the field of molecular chemistry.

In cooperation with the group of D. M. Haddelton a *photo*SET-LRP (photo single electron transfer – living radical polymerization) was invented using the developed meso-flow UV-photoreactor to produced polyacrylate of good molecular weight control and narrow dispersity ($\approx$ 1.1). The reaction mixture does not contain any photosensitive initiator, like benzoylperoxide or azo-compounds. The proposed catalytic species is a photo-activated amine-ligand, here Me_6TREN, acting as a co-initiator and chelating ligand for the insoluble copper(II)bromide. The controlled character of polymerization was underlined by polymerizing a second different monomer to the first block, yielding in a PMA-*b*-PBA polymer.

By the invention of a fairly cheap custom-made photo flowreactor, a new method of polymer modification and polymerization setup was established. The reactor can be made with easy means by almost everyone and offers a continuous tubular reactor which is capable of producing kilos of advanced materials with little effort within a few days. Furthermore, by applying the flow reactor technology scale up to pilot plants or even industrial scale is eased. This recent progress shows that classical 'glass flask batch' chemistry evolves into a new state of automated and parallelized way of synthesis. As a long-term impact it will settle down in academic research enabling better reproducibility of reactions. Hopefully, the photo flow technology awoke the long sleep of photochemistry and places it as a practical alternative for heat-induced reaction in industry and science.[171]

Beside the previous described polymer modification techniques based on UV–irradiation, an alternative modification was developed. The modification based on the aldimine ligation technique formed by condensation of aldehyde functionalized polymers with aromatic amines. This reaction was highly efficient and fast. It is complement to the oxime ligation,[118] which is often referred to as a *click* reaction for polymer modification. The formed aldimine can be used as an anchor point for further conjugation reactions. Two routes were tested based on irreversible DA cycloadditions: 1) An inverse electron-demand imino DA, followed by re-aromatization. 2) A normal electron-demand aza DA using the *Danishefsky's* diene, followed by loss of TMS and later methoxy group. By doing so, we tested and introduced an alternative pathway that is orthogonal to photoreactions.

11.2 Outlook

The here presented work started in the beginning with an inefficient and slow [2+2] cycloaddition. Within the period of this thesis, this reaction was optimized to become highly efficient, fast and functional group tolerant towards polymer conjugation reactions. The reaction can be used for polymer modification and as well for grafting application on various substrates.

The next step of this reaction is utilizing the advantage of spatial control given by photochemistry. Surfaces could be modified site-specific by using a mask or pattern while illumination. For example, thermo-responsive material could be grafted in a specific pattern to a surface, enabling a reversible cell attachment or detachment.

Beside the reaction, the UV-flow-reactor itself could be improved. The 400 W lamp could be exchange by a weaker lamp (e.g. 125 W) with the same emission spectrum to lower the chance of photochemical degradation. It could be tested if the alkene-enone cycloaddition could be performed at lowered temperatures (e.g. -30°C – 0°C) to suppress byproduct formation. Furthermore, it can be examined if the application of light filters (e.g. filter solution, pyrex glass) support the cycloaddition.

The use of the photosensitizer TXS demonstrated the advantage of catalysts or chromophores. Compared to the work of Du et al. (2009) and Ischay et al. (2010) Ruthenium catylsyts might change the required wavelength from UV to visible light.

It is worth to investigate more time in the discovered *photo*SET-LRP since it offers an route for photo-induced CRP techniques. In addition, the one-pot preparation of block-copolymers in a tubular reactor using two pumps with different monomers is worth to investigate. It could lead the path to semi-automated block-copolymer synthesis. Bock copolymers are interesting because they can form via microphase separation micelles or nano-substructures. These phenomena would create new material abilities like high-impact PMMA or nanoreactors.[248]

Chapter 12

12. Publications and conferences

12.1 List of publications

- *Photoinduced conjugation of aldehyde functional polymers with olefins via [2+2]-cycloaddition*, M. Conradi, T. Junkers, *Macromolecules* **2011**, *44*, 7969-7976.
- *Synthesis of star and H-shape polymers via a combination of cobalt-mediated radical polymerization and nitrone-mediated radical coupling reactions*, C. Detrembleur, A. Debuigne, O. Altintas, M. Conradi, E. H. H. Wong, C. Jérôme, C. Barner-Kowollik and T. Junkers, *Polym*. *Chem*. **2012**, 135-147.
- *Enhanced spin capturing polymerization and radical coupling mediated by cyclic nitrones*, K. L. Ranieri, M. Conradi, P.-Y. Chavant, V. Blandin, C. Barner-Kowollik and T. Junkers, *Aust*. *J. Chem*. **2012**, *65*, 1110-1116.
- *Efficient [2+2] photocycloadditions under equimolar conditions by employing a continuous UV-flow reactor*, M. Conradi and T. Junkers, *J. Photochem*. *Photobiol*. *A: Chem*. **2013**, *259*, 41-46.
- *UV-induced functionalization of poly(divinylbenzene) nanoparticles via efficient [2+2] photocycloadditions*, A. Ethirajan, L. Baeten, M. Conradi, K. Ranieri, B. Conings, H.-G. Boyen and T. Junkers, *Polym*. *Chem*. **2013**, *4*, 4010-4016.
- *Photo-induced copper-mediated polymerization of methyl acrylate in continuous flow reactors*, B. Wenn, M. Conradi, A. D. Carreiras, D. M. Haddleton, T. Junkers, *Polym*. *Chem*. **2014**, *136*, accepted.
- *Irreversible diels-alder [4+2] cycloaddtion for polymer end group modification*, M. Conradi, D. Decoutere and T. Junkers, *Polymers* **2014**, submitted.
- *Fast and efficient photoinduced alkene-enone cycloaddition for polymer modification by applying UV-flow reactor technology*, M. Conradi and T. Junkers, *Macromolecules* **2014**, submitted.

12.2 List of conference presentations

12.2.1 List of oral presentations

- *Photoinduced conjugation of aldehyde functional polymers with olefins via [2+2]-cycloaddition*, M. Conradi and T. Junkers, *IUAP meeting* **2011**, September 29, Gent, Belgium.

12.2.2 List of poster presentations

- *Photoinduced conjugation of aldehyde functional polymers via [2+2] cycloaddition with olefines*, M. Conradi and T. Junkers, *Belgian Polymer Group Meeting (BPG)* **2011,** May 12-13, Houffalize, Belgium.
- *Photoinduced conjugation of aldehyde functional polymers via [2+2] cycloadditions with* furan derivatives, M. Conradi and T. Junkers, *Belgian Polymer Group Meeting (BPG)* **2012,** May 10-11, Blankenberge, Belgium.
- *Rapid accerleration of a photoinduced [2+2] cycloaddition by usage of flow chemistry*, M. Conradi and T. Junkers, *Belgian German (Macro)-molecular meeting (BeGe)* **2012**, December 3-4, Hoffalize, Belgium.
- *High resolution two mass spectrometry for polymer end group analysis*, M. Conradi and T. Junkers, *6th international symposium on the separation and characterization of natural and synthetic macromolecules (SCM-6)* **2013**, February 6-8, Dresden, Germany.
- *Development of a photoinitiated polymer conjugation reaction based on [2+2] cycloaddition of maleimide derivatives*, M. Conradi and T. Junkers, *Belgian Polymer Group Meeting (BPG)* **2013,** May 16-17, Houffalize, Belgium.
- Photoinitiated polymer conjugations based on [2+2] cycloaddition of maleimide derivatives, M. Conradi and T. Junkers, *IAP meeting* **2013**, June 14, Gent, Belgium.

Chapter 13

13. Acknowledgment

Finally it is over. "I am done! Ik ben klar! Ich hab es geschafft!" Over the whole period of my PhD research I had a lot of help of many people. Without these people it would be impossible for me to finish this thesis. First of all, the UHasselt provided me with a doctoral fund. Then I got the opportunity to help building up a prosperous research group with my promoter Thomas Junkers starting from scratch. Within the first years, we installed all important lab techniques and equipment.

Nevertheless, I have to thank my promoter Thomas Junkers for the help and support during the last four years. It was not always the easiest time but the results were good. Thank you for the opportunity of working in your group and the trust you had in me. Always, you had an open ear for the PhD student and their problems/concerns.

Furthermore, I have to thank all my colleges from PRD, DSOS, NMR and the MIP guys. You made my working days more exciting and brighten up some dull days. Besides nice colleges I also meet great people and found new friends. I like to mention the professor and the scientific discussion on the fumehood bord. Neomy gefeliciteerd voor het GPC toestel. Veel plezier. Kayte, thanks for the neverending supply of excellent baking goods. Benjamin, you are a good sparring partner. Einen Marathon bin ich schon gelaufen. Wiebke viel Erfolg bei deiner eigenen Verteidigung!

At last I like to point out the help of my family. Without my parents I would not be here. They supported me during all my life and still abroad, far from home. Mama und Papa, ihr habt versucht mir alle Möglichkeiten im Leben zu geben. Dank euch konnte ich studieren und mich auf meinen eigenen Weg begeben. Stephan as a little brother I do not want to miss you. If I mention my family I also have to talk about my "bonus" family in Diepholz. As I married Jana they became a new part of mine. Liebe Heeder und Wehrkamper, es ist wirklich schön euch zu haben.

Jana, it is hard for me to put it into words. Without you I would be too afraid of going to Belgium. You supported me in good and bad times. Together we can master the coming up issues in our life. Wie soll ich es sagen, Du machst mein Leben vollständig.

Thank you all very much! Hartelijk bedankt! Vielen Dank für eure Hilfe, Unterstützung und einfach, dass ihr da seid!

Chapter 14

14. References

(1) Staudinger, H. *Berichte Dtsch. Chem. Ges. B Ser.* **1920**, *53*, 1073–1085.
(2) Loy, W. *Chemiefasern für technische Textilproduke*; Edition Textiltechnik; 2. grundlegende überarbeitete und erweiterte Auflage.; Deutscher Fachverlag: Frankfurt am Main, 2008.
(3) Elias, H.-G. *Macromolecules: Volume 3: Physical Structures and Properties*; 1. Edition.; Wiley-VCH Verlag GmbH & Co. KGaA, 2008.
(4) Mülhaupt, R. *Macromol. Chem. Phys.* **2003**, *204*, 289–327.
(5) Böhm, L. L. *Angew. Chem.* **2003**, *115*, 5162–5183.
(6) Elias, H.-G. *Macromolecules: Volume 4: Applications of Polymers*; 1. Edition.; Wiley-VCH Verlag GmbH & Co. KGaA, 2009.
(7) Elias, H.-G. *Macromolecules: Volume 1: Chemical Structures and Syntheses*; 1. Edition.; Wiley-VCH, 2005.
(8) Yuan, H. G.; Kalfas, G.; Ray, W. H. *J. Macromol. Sci. Part C Polym. Rev.* **1991**, *31*, 215–299.
(9) Vivaldo-Lima, E.; Wood, P. E.; Hamielec, A. E.; Penlidis, A. *Ind. Eng. Chem. Res.* **1997**, *36*, 939–965.
(10) Gardon, J. L. *J. Polym. Sci. [A1]* **1968**, *6*, 643–664.
(11) Elias, H.-G. *Macromolecules: Volume 2: Industrial Polymers and Syntheses*; 1. Edition.; Wiley-VCH, 2006.
(12) Jenkins, A. D.; Kratochvíl, P.; Stepto, R. F. T.; Suter, U. W. *Pure Appl. Chem.* **1996**, *68*, 2287–2311.
(13) Matyjaszewski, K.; Davis, T. P. *Handbook of Radical Polymerization*; Wiley-IEEE, 2003.
(14) Moad, G.; Rizzardo, E. *Macromolecules* **1995**, *28*, 8722–8728.
(15) Chiefari, J.; Chong, Y. K. (Bill); Ercole, F.; Krstina, J.; Jeffery, J.; Le, T. P. T.; Mayadunne, R. T. A.; Meijs, G. F.; Moad, C. L.; Moad, G.; Rizzardo, E.; Thang, S. H. *Macromolecules* **1998**, *31*, 5559–5562.
(16) Matyjaszewski, K.; Xia, J. *Chem. Rev.* **2001**, *101*, 2921–2990.
(17) Matyjaszewski, K. *Macromolecules* **2012**, *45*, 4015–4039.
(18) Fischer, H. *Macromolecules* **1997**, *30*, 5666–5672.
(19) Goto, A.; Fukuda, T. *Prog. Polym. Sci.* **2004**, *29*, 329–385.
(20) Jenkins, A. D.; Jones, R. G.; Moad, G. *Pure Appl. Chem.* **2010**, *82*, 483–491.
(21) Klok, H.-A. *Macromolecules* **2009**, *42*, 7990–8000.
(22) Sumerlin, B. S.; Vogt, A. P. *Macromolecules* **2010**, *43*, 1–13.
(23) Liu, S.; Maheshwari, R.; Kiick, K. L. *Macromolecules* **2009**, *42*, 3–13.
(24) Konkolewicz, D.; Monteiro, M. J.; Perrier, S. *Macromolecules* **2011**, *44*, 7067–7087.
(25) Charleux, B.; Delaittre, G.; Rieger, J.; D'Agosto, F. *Macromolecules* **2012**, *45*, 6753–6765.
(26) Kolb, H. C.; Finn, M. G.; Sharpless, K. B. *Angew. Chem. Int. Ed.* **2001**, *40*, 2004–2021.
(27) Huisgen, R. *Proc. Chem. Soc.* **1961**, 357–396.
(28) Huisgen, R.; Szeimies, G.; Möbius, L. *Chem. Ber.* **1967**, *100*, 2494–2507.
(29) Azide-alkyne Huisgen cycloaddition. *Wikipedia, the free encyclopedia*, 2013.
(30) Barner-Kowollik, C.; Inglis, A. J. *Macromol. Chem. Phys.* **2009**, *210*, 987–992.

(31) Barner-Kowollik, C.; Du Prez, F. E.; Espeel, P.; Hawker, C. J.; Junkers, T.; Schlaad, H.; Van Camp, W. *Angew. Chem. Int. Ed.* **2011**, *50*, 60–62.
(32) Detrembleur, C.; Debuigne, A.; Altintas, O.; Conradi, M.; Wong, E. H. H.; Jérôme, C.; Barner-Kowollik, C.; Junkers, T. *Polym. Chem.* **2012**, *3*, 135–147.
(33) Meldal, M. *Macromol. Rapid Commun.* **2008**, *29*, 1016–1051.
(34) Pauloehrl, T.; Delaittre, G.; Bruns, M.; Meißler, M.; Börner, H. G.; Bastmeyer, M.; Barner-Kowollik, C. *Angew. Chem. Int. Ed.* **2012**, *51*, 9181–9184.
(35) Inglis, A. J.; Sinnwell, S.; Stenzel, M. H.; Barner-Kowollik, C. *Angew. Chem. Int. Ed.* **2009**, *48*, 2411–2414.
(36) Gruendling, T.; Oehlenschlaeger, K. K.; Frick, E.; Glassner, M.; Schmid, C.; Barner-Kowollik, C. *Macromol. Rapid Commun.* **2011**, *32*, 807–812.
(37) Koo, S. P. S.; Stamenović, M. M.; Prasath, R. A.; Inglis, A. J.; Du Prez, F. E.; Barner-Kowollik, C.; Van Camp, W.; Junkers, T. *J. Polym. Sci. Part Polym. Chem.* **2010**, *48*, 1699–1713.
(38) Fukui, K.; Yonezawa, T.; Shingu, H. *J. Chem. Phys.* **1952**, *20*, 722–725.
(39) Fukui, K. *Science* **1982**, *218*, 747–754.
(40) Woodward, R. B.; Hoffmann, R. *J. Am. Chem. Soc.* **1965**, *87*, 395–397.
(41) Woodward, R. B.; Hoffmann, R. *Angew. Chem. Int. Ed. Engl.* **1969**, *8*, 781–853.
(42) Geerlings, P.; Ayers, P. W.; Toro-Labbé, A.; Chattaraj, P. K.; De Proft, F. *Acc. Chem. Res.* **2012**, *45*, 683–695.
(43) Intersystem crossing. *Wikipedia, the free encyclopedia*, 2013.
(44) In *IUPAC Compendium of Chemical Terminology*; Nič, M.; Jirát, J.; Košata, B.; Jenkins, A.; McNaught, A., Eds.; IUPAC: Research Triangle Park, NC.
(45) Hammond, G. S.; Turro, N. J.; Liu, R. S. H. *J. Org. Chem.* **1963**, *28*, 3297–3303.
(46) Turro, N. J.; Wriede, P. A.; Dalton, J. C.; Arnold, D. R.; Glick, A. H. *J. Am. Chem. Soc.* **1967**, *89*, 3950–3952.
(47) Turro, N. J. *Modern molecular photochemistry*; University Science Books, 1991.
(48) Bach, T.; Hehn, J. P. *Angew. Chem. Int. Ed.* **2011**, *50*, 1000–1045.
(49) *CRC Handbook of Organic Photochemistry and Photobiology, Third Edition - Two Volume Set - CRC Press Book*.
(50) Hook, B. D. A.; Dohle, W.; Hirst, P. R.; Pickworth, M.; Berry, M. B.; Booker-Milburn, K. I. *J Org Chem* **2005**, *70*, 7558–7564.
(51) Terao, K.; Nishiyama, Y.; Tanimoto, H.; Tsumoru, M.; Oelgemöller, M.; Kakiuchi, K. *J. Flow Chem.* **2012**, *35*, 1144–1152.
(52) Du, J.; Yoon, T. P. *J. Am. Chem. Soc.* **2009**, *131*, 14604–14605.
(53) Kronfeld, K.-P.; Timpe, H.-J. *J. Für Prakt. Chem.* **1988**, *330*, 571–584.
(54) Yagci, Y.; Jockusch, S.; Turro, N. J. *Macromolecules* **2010**, *43*, 6245–6260.
(55) Cardenas-Daw, C.; Kroeger, A.; Schaertl, W.; Froimowicz, P.; Landfester, K. *Macromol. Chem. Phys.* **2012**, *213*, 144–156.
(56) Büchi, G.; Inman, C. G.; Lipinsky, E. S. *J. Am. Chem. Soc.* **1954**, *76*, 4327–4331.
(57) Döpp, D.; Memarian, H. R.; Fischer, M. A.; Eijk, A. M. J. V.; Varma, C. A. G. O. *Chem. Ber.* **1992**, *125*, 983–984.
(58) Bach, T. *Liebigs Ann.* **1997**, *1997*, 1627–1634.

(59) Yurteri, S.; Cianga, I.; Yagci, Y. *Macromol. Chem. Phys.* **2003**, *204*, 1771–1783.

(60) Crimmins, M. T.; Reinhold, T. L. In *Organic Reactions*; John Wiley & Sons, Inc., 2004.

(61) Griesbeck, A. G.; Stadtmüller, S. *Chem. Ber.* **1990**, *123*, 357–362.

(62) Griesbeck, A. G.; Bondock, S. *Aust J Chem* **2008**, *61*, 573–580.

(63) Oelgemoeller, M. *Chem. Eng. Technol.* **2012**, *35*, 1144–1152.

(64) Ischay, M. A.; Lu, Z.; Yoon, T. P. *J Am Chem Soc* **2010**, *132*, 8572–8574.

(65) Gruendling, T.; Kaupp, M.; Blinco, J. P.; Barner-Kowollik, C. *Macromolecules* **2011**, *44*, 166–174.

(66) Winkler, M.; Mueller, J. O.; Oehlenschlaeger, K. K.; Montero de Espinosa, L.; Meier, M. A. R.; Barner-Kowollik, C. *Macromolecules* **2012**, *45*, 5012–5019.

(67) Oehlenschlaeger, K. K.; Mueller, J. O.; Heine, N. B.; Glassner, M.; Guimard, N. K.; Delaittre, G.; Schmidt, F. G.; Barner-Kowollik, C. *Angew. Chem. Int. Ed.* **2013**, *52*, 762–766.

(68) Fouassier, J.-P. *Photoinitiation, photopolymerization, and photocuring: fundamental and applications*; Hanser Publisher: New York, 1995.

(69) Fouassier, J.-P. *Photochemistry and UV curing: new trends*; Research Signpost: Trivandum, India, 2006.

(70) Fors, B. P.; Hawker, C. J. *Angew. Chem. Int. Ed.* **2012**, *51*, 8850–8853.

(71) Guillaneuf, Y.; Bertin, D.; Gigmes, D.; Versace, D.-L.; Lalevée, J.; Fouassier, J.-P. *Macromolecules* **2010**, *43*, 2204–2212.

(72) Versace, D.-L.; Guillaneuf, Y.; Bertin, D.; Fouassier, J. P.; Lalevée, J.; Gigmes, D. *Org. Biomol. Chem.* **2011**, *9*, 2892–2898.

(73) Guillaneuf, Y.; Versace, D.-L.; Bertin, D.; Lalevée, J.; Gigmes, D.; Fouassier, J.-P. *Macromol. Rapid Commun.* **2010**, *31*, 1909–1913.

(74) Nicolas, J.; Guillaneuf, Y.; Lefay, C.; Bertin, D.; Gigmes, D.; Charleux, B. *Prog. Polym. Sci.* **2013**, *38*, 63–235.

(75) Wang, H.; Li, Q.; Dai, J.; Du, F.; Zheng, H.; Bai, R. *Macromolecules* **2013**, *46*, 2576–2582.

(76) Conradi, M.; Junkers, T. *J. Photochem. Photobiol. Chem.* **2013**, *259*, 41–46.

(77) Tonhauser, C.; Natalello, A.; Löwe, H.; Frey, H. *Macromolecules* **2012**, *45*, 9551–9570.

(78) Bally, F.; Serra, C. A.; Hessel, V.; Hadziioannou, G. *Chem. Eng. Sci.* **2011**, *66*, 1449–1462.

(79) Wilms, D.; Klos, J.; Frey, H. *Macromol. Chem. Phys.* **2008**, *209*, 343–356.

(80) Hessel, V. *Chem. Eng. Technol.* **2009**, *32*, 1655–1681.

(81) Flow Chemistry | Chemtrix BV - Flow Chemistry Equipment and Flow Chemistry Servi http://www.chemtrix.com/ (accessed Nov 6, 2013).

(82) Tasdelen, M. A.; Kahveci, M. U.; Yagci, Y. *Prog. Polym. Sci.* **2011**, *36*, 455–567.

(83) Mansfeld, U.; Pietsch, C.; Hoogenboom, R.; Becer, C. R.; Schubert, U. S. *Polym. Chem.* **2010**, *1*, 1560–1598.

(84) Lutz, J.-F. *Angew. Chem. Int. Ed.* **2007**, *46*, 1018–1025.

(85) Iha, R. K.; Wooley, K. L.; Nyström, A. M.; Burke, D. J.; Kade, M. J.; Hawker, C. J. *Chem. Rev.* **2009**, *109*, 5620–5686.

(86) Lutz, J.-F.; Schlaad, H. *Polymer* **2008**, *49*, 817–824.

(87) Lowe, A. B. *Polym. Chem.* **2010**, *1*, 17–36.

(88) Sinnwell, S.; Inglis, A. J.; Davis, T. P.; Stenzel, M. H.; Barner-Kowollik, C. *Chem. Commun.* **2008**, 2052–2054.

(89) Gress, A.; Völkel, A.; Schlaad, H. *Macromolecules* **2007**, *40*, 7928–7933.

(90) Adzima, B. J.; Tao, Y.; Kloxin, C. J.; DeForest, C. A.; Anseth, K. S.; Bowman, C. N. *Nat. Chem.* **2011**, *3*, 256–259.

(91) Bach, T. *Synthesis* **1998**, 683–703.

(92) Nehrings, A.; Scharf, H.-D.; Runsink, J. *Angew. Chem. Int. Ed. Engl.* **1985**, *24*, 877–878.

(93) Adam, W.; Stegmann, V. R. *Synthesis* **2001**, *2001*, 1203–1214.

(94) Caldwell, R. A.; Sovocool, G. W.; Gajewski, R. P. *J. Am. Chem. Soc.* **1973**, *95*, 2549–2557.

(95) Dalton, J. C.; Wriede, P. A.; Turro, N. J. *J. Am. Chem. Soc.* **1970**, *92*, 1318–1326.

(96) D'Auria, M.; Racioppi, R. *Curr. Org. Chem.* **2009**, *13*, 939–954.

(97) Bach, T.; Bergmann, H.; Brummerhop, H.; Lewis, W.; Harms, K. *Chem. - Eur. J.* **2001**, *7*, 4512–4521.

(98) Hammaecher, C.; Portella, C. *Chem. Commun.* **2008**, 5833.

(99) Junkers, T.; Barner-Kowollik, C. *J. Polym. Sci. Part Polym. Chem.* **2008**, *46*, 7585–7605.

(100) Tsarevsky, N. V.; Bencherif, S. A.; Matyjaszewski, K. *Macromolecules* **2007**, *40*, 4439–4445.

(101) Koo, S. P. S.; Junkers, T.; Barner-Kowollik, C. *Macromolecules* **2009**, *42*, 62–69.

(102) Gruendling, T.; Hart-Smith, G.; Davis, T. P.; Stenzel, M. H.; Barner-Kowollik, C. *Macromolecules* **2008**, *41*, 1966–1971.

(103) Conradi, M.; Junkers, T. *Macromolecules* **2011**, *44*, 7969–7976.

(104) Sailor, M. J.; Park, J.-H. *Adv. Mater.* **2012**, *24*, 3779–3802.

(105) Thanh, N. T. K.; Green, L. A. W. *Nano Today* **2010**, *5*, 213–230.

(106) Lu, Z.; Yin, Y. *Chem. Soc. Rev.* **2012**, *41*, 6874–6887.

(107) Fleige, E.; Quadir, M. A.; Haag, R. *Adv. Drug Deliv. Rev.* **2012**, *64*, 866–884.

(108) Landfester, K.; Musyanovych, A.; Mailänder, V. *J. Polym. Sci. Part Polym. Chem.* **2010**, *48*, 493–515.

(109) Zeller, A.; Musyanovych, A.; Kappl, M.; Ethirajan, A.; Dass, M.; Markova, D.; Klapper, M.; Landfester, K. *ACS Appl. Mater. Interfaces* **2010**, *2*, 2421–2428.

(110) Ethirajan, A.; Landfester, K. *Chem. – Eur. J.* **2010**, *16*, 9398–9412.

(111) Landfester, K. *Angew. Chem. Int. Ed.* **2009**, *48*, 4488–4507.

(112) Arumugam, S.; Popik, V. V. *J. Am. Chem. Soc.* **2011**, *133*, 5573–5579.

(113) Arumugam, S.; Popik, V. V. *J. Am. Chem. Soc.* **2011**, *133*, 15730–15736.

(114) Arumugam, S.; Popik, V. V. *J. Am. Chem. Soc.* **2012**, *134*, 8408–8411.

(115) Orski, S. V.; Poloukhtine, A. A.; Arumugam, S.; Mao, L.; Popik, V. V.; Locklin, J. *J. Am. Chem. Soc.* **2010**, *132*, 11024–11026.

(116) Dietrich, M.; Delaittre, G.; Blinco, J. P.; Inglis, A. J.; Bruns, M.; Barner-Kowollik, C. *Adv. Funct. Mater.* **2012**, *22*, 304–312.

(117) Pauloehrl, T.; Delaittre, G.; Winkler, V.; Welle, A.; Bruns, M.; Börner, H. G.; Greiner, A. M.; Bastmeyer, M.; Barner-Kowollik, C. *Angew. Chem. Int. Ed.* **2012**, *51*, 1071–1074.

(118)   Pauloehrl, T.; Delaittre, G.; Bruns, M.; Meißler, M.; Börner, H. G.; Bastmeyer, M.; Barner-Kowollik, C. *Angew. Chem. Int. Ed.* **2012**, *51*, 9181–9184.

(119)   Choi, E. C.; Jin, S. M.; Park, Y. J.; Kim, Y. *J. Chin. Inst. Chem. Eng.* **2008**, *39*, 483–488.

(120)   Downey, J. S.; Frank, R. S.; Li, W.-H.; Stöver, H. D. H. *Macromolecules* **1999**, *32*, 2838–2844.

(121)   Joso, R.; Reinicke, S.; Walther, A.; Schmalz, H.; Müller, A. H. E.; Barner, L. *Macromol. Rapid Commun.* **2009**, *30*, 1009–1014.

(122)   Manuszak Guerrini, M.; Charleux, B.; Vairon, J.-P. *Macromol. Rapid Commun.* **2000**, *21*, 669–674.

(123)   Barsbay, M.; Güven, O.; Stenzel, M. H.; Davis, T. P.; Barner-Kowollik, C.; Barner, L. *Macromolecules* **2007**, *40*, 7140–7147.

(124)   Nebhani, L.; Schmiedl, D.; Barner, L.; Barner-Kowollik, C. *Adv. Funct. Mater.* **2010**, *20*, 2010–2020.

(125)   Ethirajan, A.; Baeten, L.; Conradi, M.; Ranieri, K.; Conings, B.; Boyen, H.-G.; Junkers, T. *Angew. Chem. Int. Ed.* **2012**, *submitted*.

(126)   Gardella, J. A.; Ferguson, S. A.; Chin, R. L. *J. Appl. Spectrosc.* **1986**, *40*, 224–232.

(127)   Chastain, J. *Handbook of X-Ray Photoelectron Spectroscopy*; Physical Electronics Diviion: Eden Prairie, MN, 1992.

(128)   Ethirajan, A.; Ziener, U.; Landfester, K. *Chem. Mater.* **2009**, *21*, 2218–2225.

(129)   Baier, G.; Siebert, J. M.; Landfester, K.; Musyanovych, A. *Macromolecules* **2012**, *45*, 3419–3427.

(130)   Schmaljohann, D.; Oswald, J.; Jørgensen, B.; Nitschke, M.; Beyerlein, D.; Werner, C. *Biomacromolecules* **2003**, *4*, 1733–1739.

(131)   Da Silva, R. M. P.; Mano, J. F.; Reis, R. L. *Trends Biotechnol.* **2007**, *25*, 577–583.

(132)   Janes, K. A.; Calvo, P.; Alonso, M. J. *Adv. Drug Deliv. Rev.* **2001**, *47*, 83–97.

(133)   Sinha, V. R.; Kumria, R. *Int. J. Pharm.* **2001**, *224*, 19–38.

(134)   Maeda, T.; Kanda, T.; Yonekura, Y.; Yamamoto, K.; Aoyagi, T. *Biomacromolecules* **2006**, *7*, 545–549.

(135)   Rimmer, S.; Soutar, I.; Swanson, L. *Polym. Int.* **2009**, *58*, 273–278.

(136)   Chung, J. E.; Yokoyama, M.; Yamato, M.; Aoyagi, T.; Sakurai, Y.; Okano, T. *J. Controlled Release* **1999**, *62*, 115–127.

(137)   Heinze, T.; Liebert, T. *Prog. Polym. Sci.* **2001**, *26*, 1689–1762.

(138)   Goldmann, A. S.; Tischer, T.; Barner, L.; Bruns, M.; Barner-Kowollik, C. *Biomacromolecules* **2011**, *12*, 1137–1145.

(139)   Malmström, E.; Carlmark, A. *Polym. Chem.* **2012**, *3*, 1702.

(140)   Ethirajan, A.; Baeten, L.; Conradi, M.; Ranieri, K.; Conings, B.; Boyen, H.-G.; Junkers, T. *Polym. Chem.* **2013**, *4*, 4010–4016.

(141)   Böhm, A.; Gattermayer, M.; Trieb, C.; Schabel, S.; Fiedler, D.; Miletzky, F.; Biesalski, M. *Cellulose* **2013**, *20*, 467–483.

(142)   Hong, K. H.; Liu, N.; Sun, G. *Eur. Polym. J.* **2009**, *45*, 2443–2449.

(143)   Delaittre, G.; Dietrich, M.; Blinco, J. P.; Hirschbiel, A.; Bruns, M.; Barner, L.; Barner-Kowollik, C. *Biomacromolecules* **2012**, *13*, 1700–1705.

(144)   Hoffmann, N. *Chem Rev* **2008**, *108*, 1052–1103.

(145)   Lainchbury, M. D.; Medley, M. I.; Taylor, P. M.; Hirst, P.; Dohle, W.; Booker-Milburn, K. I. *J. Org. Chem.* **2008**, *73*, 6497–6505.

(146)   Hegedus, L. S.; Holden, M. S.; McKearin, J. M. *Org. Synth.* **1990**, *Coll. Vol. 7*, 501.

(147)   Sugimoto, A.; Fukuyama, T.; Sumino, Y.; Takagi, M.; Ryu, I. *Tetrahedron* **2009**, *65*, 1593–1598.

(148)   Shvydkiv, O.; Yavorskyy, A.; Tan, S. B.; Nolan, K.; Hoffmann, N.; Youssef, A.; Oelgemöller, M. *Photochem. Photobiol. Sci.* **2011**, *10*, 1399–1404.

(149)   Loutfy, R. O.; Mayo, P. D. *Can. J. Chem.* **1972**, *50*, 3465–3471.

(150)   Griesbeck, A. G. *Synlett* **2003**, 0451–0472.

(151)   Schmeling, N.; Hunger, K.; Engler, G.; Breiten, B.; Rölling, P.; Mixa, A.; Staudt, C.; Kleinermanns, K. *Polym. Int.* **2009**, *58*, 720–727.

(152)   Schwalbe, T.; Autze, V.; Hohmann, M.; Stirner, W. *Org. Process Res. Dev.* **2004**, *8*, 440–454.

(153)   Wiles, C.; Watts, P. *Eur. J. Org. Chem.* **2008**, *2008*, 1655–1671.

(154)   Lévesque, F.; Seeberger, P. H. *Org Lett* **2011**, *13*, 5008–5011.

(155)   Coyle, E. E.; Oelgemöller, M. *Photochem. Photobiol. Sci.* **2008**, *7*, 1313–1322.

(156)   Fukuyama, T.; Hino, Y.; Kamata, N.; Ryu, I. *Chem. Lett.* **2004**, *33*, 1430–1431.

(157)   Tsutsumi, K.; Terao, K.; Yamaguchi, H.; Yoshimura, S.; Morimoto, T.; Kakiuchi, K.; Fukuyama, T.; Ryu, I. *Chem. Lett.* **2010**, *39*, 828–829.

(158)   Jähnisch, K.; Hessel, V.; Löwe, H.; Baerns, M. *Angew. Chem. Int. Ed.* **2004**, *43*, 406–446.

(159)   Diels, O.; Alder, K. *Justus Liebigs Ann. Chem.* **1928**, *460*, 98–122.

(160)   Ahrendt, K. A.; Borths, C. J.; MacMillan, D. W. C. *J. Am. Chem. Soc.* **2000**, *122*, 4243–4244.

(161)   Nicolaou, K. C.; Snyder, S. A.; Montagnon, T.; Vassilikogiannakis, G. *Angew. Chem. Int. Ed.* **2002**, *41*, 1668–1698.

(162)   Bräse, S.; Gil, C.; Knepper, K.; Zimmermann, V. *Angew. Chem. Int. Ed.* **2005**, *44*, 5188–5240.

(163)   Durmaz, H.; Dag, A.; Altintas, O.; Erdogan, T.; Hizal, G.; Tunca, U. *Macromolecules* **2007**, *40*, 191–198.

(164)   Horie, T.; Sumino, M.; Tanaka, T.; Matsushita, Y.; Ichimura, T.; Yoshida, J. *Org Process Res Dev* **2010**, *14*, 405–410.

(165)   Booker-Milburn, K. I.; Cowell, J. K.; Sharpe, A.; Jiménez, F. D. *Chem. Commun.* **1996**, 249–251.

(166)   Booker-Milburn, K. I.; Cowell, J. K.; Delgado Jiménez, F.; Sharpe, A.; White, A. J. *Tetrahedron* **1999**, *55*, 5875–5888.

(167)   Sinnwell, S.; Inglis, A. J.; Stenzel, M. H.; Barner-Kowollik, C. *Macromol. Rapid Commun.* **2008**, *29*, 1090–1096.

(168)   Hall, D. J.; Van Den Berghe, H. M.; Dove, A. P. *Polym. Int.* **2011**, *60*, 1149–1157.

(169)   Malkoch, M.; Thibault, R. J.; Drockenmuller, E.; Messerschmidt, M.; Voit, B.; Russell, T. P.; Hawker, C. J. *J. Am. Chem. Soc.* **2005**, *127*, 14942–14949.

(170)   Oelgemöller, M.; Shvydkiv, O. *Molecules* **2011**, *16*, 7522–7550.

(171)   Knowles, J. P.; Elliott, L. D.; Booker-Milburn, K. I. *Beilstein J. Org. Chem.* **2012**, *8*, 2025–2052.

(172)   Wenn, B.; Conradi, M.; Carreiras, A.; Haddleton, D.; Junkers, T. *Polym. Chem.* **2014**, *5*, 3053–3060.

(173)   Roth, P. J.; Kessler, D.; Zentel, R.; Theato, P. *J. Polym. Sci. Part Polym. Chem.* **2009**, *47*, 3118–3130.

(174)   Conradi, M.; Junkers, T. *Macromolecules* **2014**, *submitted*.

(175)   Zhang, Q.; Vanparijs, N.; Louage, B.; De Geest, B. G.; Hoogenboom, R. *Polym. Chem.* **2014**, *5*, 1140.

(176)   Zammarelli, N.; Luksin, M.; Raschke, H.; Hergenröder, R.; Weberskirch, R. *Langmuir* **2013**, *29*, 12834–12843.

(177)   Johnson, R. P.; John, J. V.; Kim, I. *Eur. Polym. J.* **2013**, *49*, 2925–2948.

(178)   Lecolley, F.; Tao, L.; Mantovani, G.; Durkin, I.; Lautru, S.; Haddleton, D. M. *Chem. Commun.* **2004**, 2026–2027.

(179)   Vandenbergh, J.; de Moraes Ogawa, T.; Junkers, T. *J. Polym. Sci. Part Polym. Chem.* **2013**, *51*, 2366–2374.

(180)   Nie, Z.; Xu, S.; Seo, M.; Lewis, P. C.; Kumacheva, E. *J. Am. Chem. Soc.* **2005**, *127*, 8058–8063.

(181)   Hornung, C. H.; Guerrero-Sanchez, C.; Brasholz, M.; Saubern, S.; Chiefari, J.; Moad, G.; Rizzardo, E.; Thang, S. H. *Org. Process Res. Dev.* **2011**, *15*, 593–601.

(182)   Noda, T.; Grice, A. J.; Levere, M. E.; Haddleton, D. M. *Eur. Polym. J.* **2007**, *43*, 2321–2330.

(183)   Bogdan, A. R.; Poe, S. L.; Kubis, D. C.; Broadwater, S. J.; McQuade, D. T. *Angew. Chem. Int. Ed.* **2009**, *48*, 8547–8550.

(184)   Vandenbergh, J.; Junkers, T. *Polym. Chem.* **2012**, *3*, 2739–2742.

(185)   Vandenbergh, J.; Tura, T.; Baeten, E.; Junkers, T. *J. Polym. Sci. Part Polym. Chem.* **2014**, n/a–n/a.

(186)   Kato, M.; Kamigaito, M.; Sawamoto, M.; Higashimura, T. *Macromolecules* **1995**, *28*, 1721–1723.

(187)   Matyjaszewski, K.; Patten, T. E.; Xia, J. *J. Am. Chem. Soc.* **1997**, *119*, 674–680.

(188)   Haddleton, D. M.; Crossman, M. C.; Hunt, K. H.; Topping, C.; Waterson, C.; Suddaby, K. G. *Macromolecules* **1997**, *30*, 3992–3998.

(189)   Percec, V.; Popov, A. V.; Ramirez-Castillo, E.; Monteiro, M.; Barboiu, B.; Weichold, O.; Asandei, A. D.; Mitchell, C. M. *J. Am. Chem. Soc.* **2002**, *124*, 4940–4941.

(190)   Percec, V.; Guliashvili, T.; Ladislaw, J. S.; Wistrand, A.; Stjerndahl, A.; Sienkowska, M. J.; Monteiro, M. J.; Sahoo, S. *J. Am. Chem. Soc.* **2006**, *128*, 14156–14165.

(191)   Rosen, B. M.; Percec, V. *Chem. Rev.* **2009**, *109*, 5069–5119.

(192)   Percec, V.; Popov, A. V.; Ramirez-Castillo, E.; Weichold, O. *J. Polym. Sci. Part Polym. Chem.* **2003**, *41*, 3283–3299.

(193)   Lligadas, G.; Rosen, B. M.; Monteiro, M. J.; Percec, V. *Macromolecules* **2008**, *41*, 8360–8364.

(194)   Haehnel, A. P.; Fleischmann, S.; Hesse, P.; Hungenberg, K.-D.; Barner-Kowollik, C. *Macromol. React. Eng.* **2013**, *7*, 8–23.

(195)   Anastasaki, A.; Waldron, C.; Wilson, P.; McHale, R.; Haddleton, D. M. *Polym. Chem.* **2013**, *4*, 2672–2675.

(196)   Burns, J. A.; Houben, C.; Anastasaki, A.; Waldron, C.; Lapkin, A. A.; Haddleton, D. M. *Polym. Chem.* **2013**, *4*, 4809–4813.

(197)   Shen, Y.; Zhu, S. *AIChE J.* **2002**, *48*, 2609–2619.

(198)   Chan, N.; Cunningham, M. F.; Hutchinson, R. A. *J. Polym. Sci. Part Polym. Chem.* **2013**, *51*, 3081–3096.

(199) Detrembleur, C.; Versace, D.-L.; Piette, Y.; Hurtgen, M.; Jérôme, C.; Lalevée, J.; Debuigne, A. *Polym. Chem.* **2012**, *3*, 1856–1866.

(200) Miao, X.; Zhu, W.; Zhang, Z.; Zhang, W.; Zhu, X.; Zhu, J. *Polym. Chem.* **2013**, *5*, 551–557.

(201) Arvanitopoulos, L. D.; Greuel, M. P.; Harwood, H. J. *Polym. Prepr.* **1994**, *35*, 549–550.

(202) Anastasaki, A.; Nikolaou, V.; Zhang, Q.; Burns, J.; Samanta, S.; Waldron, C.; Haddleton, A. J.; McHale, R.; Fox, D. J.; Percec, V.; Wilson, P.; Haddleton, D. M. *J. Am. Chem. Soc.* **2013**, *136*, 1141–1149.

(203) Quinn, J. F.; Barner, L.; Barner-Kowollik, C.; Rizzardo, E.; Davis, T. P. *Macromolecules* **2002**, *35*, 7620–7627.

(204) Muthukrishnan, S.; Pan, E. H.; Stenzel, M. H.; Barner-Kowollik, C.; Davis, T. P.; Lewis, D.; Barner, L. *Macromolecules* **2007**, *40*, 2978–2980.

(205) Versace, D.-L.; Lalevée, J.; Fouassier, J.-P.; Guillaneuf, Y.; Bertin, D.; Gigmes, D. *Macromol. Rapid Commun.* **2010**, *31*, 1383–1388.

(206) Guillaneuf, Y.; Gigmes, D.; Marque, S. R. A.; Astolfi, P.; Greci, L.; Tordo, P.; Bertin, D. *Macromolecules* **2007**, *40*, 3108–3114.

(207) Fukuyama, T.; Kajihara, Y.; Ryu, I.; Studer, A. *Synthesis* **2012**, *44*, 2555–2559.

(208) Tasdelen, M. A.; Uygun, M.; Yagci, Y. *Macromol. Chem. Phys.* **2011**, *212*, 2036–2042.

(209) Tasdelen, M. A.; Uygun, M.; Yagci, Y. *Macromol. Chem. Phys.* **2010**, *211*, 2271–2275.

(210) Tasdelen, M. A.; Ciftci, M.; Yagci, Y. *Macromol. Chem. Phys.* **2012**, *213*, 1391–1396.

(211) Taskin, O. S.; Yilmaz, G.; Tasdelen, M. A.; Yagci, Y. *Polym. Int.* **2013**, n/a–n/a.

(212) Konkolewicz, D.; Schröder, K.; Buback, J.; Bernhard, S.; Matyjaszewski, K. *ACS Macro Lett.* **2012**, *1*, 1219–1223.

(213) Alzahrani, A. A.; Erbse, A. H.; Bowman, C. N. *Polym. Chem.* **2014**, *5*, 1874–1882.

(214) Piletsky, S. A.; Matuschewski, H.; Schedler, U.; Wilpert, A.; Piletska, E. V.; Thiele, T. A.; Ulbricht, M. *Macromolecules* **2000**, *33*, 3092–3098.

(215) Barner-Kowollik, C.; Beuermann, S.; Buback, M.; Castignolles, P.; Charleux, B.; Coote, M. L.; Hutchinson, R. A.; Junkers, T.; Lacík, I.; Russell, G. T.; Stach, M.; Herk, A. M. van. *Polym. Chem.* **2014**, *5*, 204–212.

(216) Danishefsky, S.; Kitahara, T. *J. Am. Chem. Soc.* **1974**, *96*, 7807–7808.

(217) Spino, C.; Rezaei, H.; Dory, Y. L. *J Org Chem* **2004**, *69*, 757–764.

(218) Wijnen, J. W.; Zavarise, S.; Engberts, J. B. F. N.; Charton, M. *J. Org. Chem.* **1996**, *61*, 2001–2005.

(219) Rickborn, B. In *Organic Reactions*; John Wiley & Sons, Inc., 2004.

(220) Oehlenschlaeger, K. K.; Guimard, N. K.; Brandt, J.; Mueller, J. O.; Lin, C. Y.; Hilf, S.; Lederer, A.; Coote, M. L.; Schmidt, F. G.; Barner-Kowollik, C. *Polym. Chem.* **2013**, *4*, 4348–4355.

(221) Hansell, C. F.; Espeel, P.; Stamenović, M. M.; Barker, I. A.; Dove, A. P.; Du Prez, F. E.; O'Reilly, R. K. *J. Am. Chem. Soc.* **2011**, *133*, 13828–13831.

(222) Mięsowicz, S.; Chaładaj, W.; Jurczak, J. *Synlett* **2010**, *2010*, 1421–1425.

(223) Hedberg, C.; Pinho, P.; Roth, P.; Andersson, P. G. *J Org Chem* **2000**, *65*, 2810–2812.

(224) Jørgensen, K. A. *Angew. Chem. Int. Ed.* **2000**, *39*, 3558–3588.

(225) Aggarwal, V. K.; Vennall, G. P.; Davey, P. N.; Newman, C. *Tetrahedron Lett.* **1997**, *38*, 2569–2572.

(226) Babu, G.; Perumal, P. T. *Tetrahedron* **1998**, *54*, 1627–1638.

(227) Chavez, D. E.; Jacobsen, E. N. *Org. Lett.* **2003**, *5*, 2563–2565.

(228) Kobayashi, S.; Ishitani, H.; Nagayama, S. *Synthesis* **1995**, *1995*, 1195–1202.

(229) Juhl, K.; Jørgensen, K. A. *Angew. Chem. Int. Ed.* **2003**, *42*, 1498–1501.

(230) Akiyama, T.; Takaya, J.; Kagoshima, H. *Tetrahedron Lett.* **1999**, *40*, 7831–7834.

(231) Akiyama, T.; Morita, H.; Fuchibe, K. *J. Am. Chem. Soc.* **2006**, *128*, 13070–13071.

(232) Boger, D. L.; Corbett, W. L.; Curran, T. T.; Kasper, A. M. *J. Am. Chem. Soc.* **1991**, *113*, 1713–1729.

(233) Anniyappan, M.; Nagarajan, R.; Perumal, P. T. *Synth. Commun.* **2002**, *32*, 99–103.

(234) Nagarajan, R.; Chitra, S.; Perumal, P. T. *Tetrahedron* **2001**, *57*, 3419–3423.

(235) Phan, T. B.; Breugst, M.; Mayr, H. *Angew. Chem. Int. Ed.* **2006**, *45*, 3869–3874.

(236) Vollhardt, K. P. C.; Schore, N. E.; Butenschön, H. *Organische Chemie*; 5th ed.; Wiley-VCH: Weinheim, 2011.

(237) Wabnitz, T. C.; Saaby, S.; Anker Jørgensen, K. *Org. Biomol. Chem.* **2004**, *2*, 828.

(238) Schiestel, T.; Brunner, H.; Tovar, G. E. M. *J. Nanosci. Nanotechnol.* **2004**, *4*, 504–511.

(239) Kalia, J.; Raines, R. T. *Angew. Chem. Int. Ed Engl.* **2008**, *47*, 7523–7526.

(240) Zhou, S.; Fan, S.; Au-yeung Steve C. F.; Wu, C. *Polymer* **1995**, *36*, 1341–1346.

(241) Ferguson, C. J.; Hughes, R. J.; Nguyen, D.; Pham, B. T. T.; Gilbert, R. G.; Serelis, A. K.; Such, C. H.; Hawkett, B. S. *Macromolecules* **2005**, *38*, 2191–2204.

(242) Gao, W.; Xu, D.; Lim, D. W.; Craig, S. L.; Chilkoti, A. *Polym Chem* **2011**, *2*, 1561–1566.

(243) Boeckler, C.; Frisch, B.; Schuber, F. *Bioorg. Med. Chem. Lett.* **1998**, *8*, 2055–2058.

(244) Walker, M. A. *Tetrahedron Lett.* **1994**, *35*, 665–668.

(245) Liu, F.; Soh Yan Ni, A.; Lim, Y.; Mohanram, H.; Bhattacharjya, S.; Xing, B. *Bioconjug. Chem.* **2012**, *23*, 1639–1647.

(246) Feng, L.; Hu, J.; Liu, Z.; Zhao, F.; Liu, G. *Polymer* **2007**, *48*, 3616–3623.

(247) Kade, M. J.; Burke, D. J.; Hawker, C. J. *J. Polym. Sci. Part Polym. Chem.* **2010**, *48*, 743–750.

(248) Gazit, O.; Khalfin, R.; Cohen, Y.; Tannenbaum, R. *J. Phys. Chem. C* **2009**, *113*, 576–583.